INTERACTIONS OF HIGH VOLTAGE ATMOSPHERIC COLD PLASMA WITH MICROORGANISM AND PROTEIN IN FOOD SYSTEMS
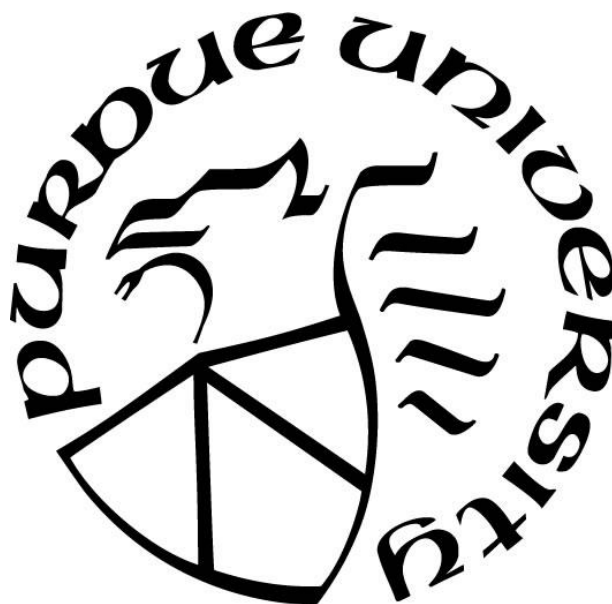
by

Lei Xu

A Dissertation

Submitted to the Faculty of Purdue University

In Partial Fulfillment of the Requirements for the degree of

Doctor of Philosophy

Department of Food Science

West Lafayette, Indiana

December 2018

THE PURDUE UNIVERSITY GRADUATE SCHOOL
STATEMENT OF COMMITTEE APPROVAL

Dr. Bernard Tao, Chair

    School of Agricultural & Biological Engineering

Dr. Allen L. Garner

    School of Nuclear Engineering

Dr. Brian Farkas

    Department of Food Science

Dr. Kevin M. Keener

    Department of Food Science and Human Nutrition, Iowa State University

Dr. Bruce Applegate

    Department of Food Science

Approved by:

    Dr. Carlos M. Corvalan

        Head of the Graduate Program

「信就是所望之事的實底，是未見之事的確據。」

– *希伯來書 11:1*

'*Now faith is the substance of things hoped for, the evidence of things not seen.*'

– *Hebrews 11:1*

ACKNOWLEDGMENTS

I earnestly express my profound gratitude to my supervisor Dr. Tao for without his significant supervisorial input this study wouldn't have been possible. I benefited greatly from his guidance and insight with regard to interpreting all the research data, guidance in innovative thoughts, as well as his great mentorship for career development. I am blessed to have you be my advisor to teach me mass transfer or reactions kinetics, as well as leadership development to achieve a career success.

Many thanks to Dr. Garner for his patience and kind assistance in revising manuscripts, equations developing, and experimental design. Thank you for inviting me to join your lab meeting every semester which I learned a lot during the meeting. I would also like to express my gratitude to Dr. Applegates, Dr. Keener, Dr. Farkas for all your time and effort during my Ph.D. study. I would like to acknowledge all your advice and encouragement, with what promote me to encounter all the challenges in this research.

I would like to thank Malithi Wickramathilaka, Felicia Hall, Yiwen Bao, Chumin Zhang, Dr. Connie Bonham, Dr. Hu Hou, Collin Felten, Dr. Jen-Y Huang, Dongdong Ma, Yazmin Munoz, Russell Brayfield, Dr. Hu Shi, Jean Jensen, Feifei Zhao, for your experimental assistance and technical support. Many thanks to all my friends here at Purdue: Fang Fang, Jin Sha, Dongqi Liu, Yezhi Fu, Xingjian Bai, Ying Xie, Xiaowei Zhang, Xingyun Peng, Lilin Cheng, Ying Xie, Yuan Lyv, Tianming Yao, Jingfan Chen, Yizhe Zhang, Fei Jia, Yuanyuan Ji, Joy and Mike, whose support went deeper than they realized.

Special thanks and uncompromised appreciations go to my loving parents (*贾宝秀&徐德星*) and families in Tsingtao. I do not have enough words to thank for all the effort put into my education and personal development, for giving me all their love, guidance and support during my whole life I will never be able to finish to thank them. My dear love, Dr. Xin Su, I am blessed to be your wife and have your unwavering love and support.

I owe many people appreciation, all of whom might not be acknowledged here, but I am in no doubt there will be opportunities outside the printed page to assure them of my deepest appreciation for their support.

TABLE OF CONTENTS

LIST OF TABLES

LIST OF FIGURES

ABBREVIATIONS

AA	Ascorbic Acid
AC	Alternating Current
ACP	Atmospheric Cold Plasma
ACPJ	Atmospheric Cold Plasma Jet
Agar	Agarose
ANOVA	Analysis of Variance
APGD	Atmospheric Pressure Glow Discharge
BSA	Bovine Serum Albumin
CD	Far-UV-Circular Dichroism
CDC	Center for Disease Control and Prevention
CFU	Colony Forming Units
DBD	Dielectric Barrier Discharge
DC	Direct Current
DHAA	Dehydroascorbic Acid
DSM film	Soybean Meal-based Edible film
EPA	Environmental Protection Agency
FCS	Food Contact Substance
FDA	Food and Drug Administration
FTIR	Fourier-transform Infrared Spectroscopy
GLM	General Linear Model
HPLC	High Performance Liquid Chromatography
HPP	High Pressure Processing
HTP	High Temperature Plasmas
HVACP	High Voltage Atmospheric Cold Plasma
LTP	Low Temperature Plasmas
MA65	Modified Air
MS	Mass Spectrometry
MS/MS	Tandem Mass Spectrometry
NTSB	2-nitro-5-thiosulfobenzoate
OAS	Optical Absorption Spectroscopy
OES	Optical Emission Spectroscopy
OJ	Orange Juice
PEF	Pulsed Electric Fields
PME	Pectin Methylesterase
PMEu	PME units
RF	Radio Frequency
RGS	Reactive Gas Species

RNS	Reactive Nitrogen Species
ROS	Reactive Oxygen Species
RS	Reactive Species
RTD	Ready-To-Drink
S. enterica	*Salmonella enterica* serovar Typhimurium
SDS-	Sodium Dodecyl Sulfate-Polyacrylamide Gel
PAGE	Electrophoresis
SH	Sulfhydryl, or Thiol Groups
S–S	Disulfide Bonds
TSA	Tryptic Soy Agar
TSB	Tryptic Soy Broth
USDA	United States Department of Agriculture
USDA-	US Department of Agriculture's Food Safety
FSIS	Inspection Service
UV	Ultraviolet
UV-Vis	UV-visible
XLD	Xylose Lysine Deoxycholate

ABSTRACT

Author: Xu, Lei. PhD
Institution: Purdue University
Degree Received: December 2018
Title: Interaction of High Voltage Atmospheric Cold Plasma with Microorganism and Protein in Food System
Committee Chair: Bernard Tao

Multiple studies have demonstrated atmospheric cold plasma (ACP) as an effective non-thermal technology for microbial decontamination, surface modification, and functionality alteration in food processing and packaging. ACP constitutes charged particles, such as positive and negative ions, electrons, quanta of electromagnetic radiation, and excited and non-excited molecules, which corresponds to its predominant reactive properties. However, in many of these applications, the interactions between plasma and the components in food matrix are not well-understood. The **overall goals** of this dissertation were to 1) evaluate the interactions between high voltage atmospheric cold plasma (HVACP) and microbes in liquid and semi-solid food; 2) investigate plasma transfer into semi-solid foods and determine the relationship between microbial inactivation and plasma transfer; 3) explore the interactions between plasma and proteins.

The first study explored the microbial (*Salmonella enterica* serovar Typhimurium, *S. enterica*) inactivation efficacy of HVACP. The physicochemical interactions between HVACP and biomolecules, including an enzyme (pectin methylesterase, PME), vitamin C and other components in orange juice (OJ) under different conditions was also evaluated. Both direct and indirect HVACP treatment of 25 mL OJ induced greater than a 5 log reduction in *S. enterica* following 30 s of treatment with air and MA65 gas with no storage. For 50 mL OJ, 120 s of direct HVACP treatment followed by 24 h storage achieved *S. enterica* reductions of 2.9 log in air and 4.7 log in MA65 gas. An indirect HVACP treatment of 120 s followed by 24 hours storage resulted in a 2.2 log reduction in air and a 3.8 log reduction in MA65. No significant ($P < 0.05$) Brix or pH change occurred following 120 s HVACP treatment. HVACP direct treatment reduced vitamin C content by 56% in air and PME activity by 74% in air and 82% in MA65. These results demonstrated that HVACP can significantly reduce *Salmonella* in OJ with minimal quality degradation.

The second study in this dissertation examined the penetration process of plasma into semi-solid food and the resulting microbial inactivation efficacy. Agar gels of various densities (0.25, 0.5, 1.0, and 2%) with a pH indicator were inoculated with *S. enterica* (10^7>CFU) and exposed directly (between the electrode) or indirectly (adjacent to the plasma field created between the two electrodes) to 90 kV at 60 Hz for up to 1.5 h. A long treatment time (1.5 h) caused sample temperature to increase 5~10 °C. The microbial analysis indicated a greater than 6 $\log_{10}$ (CFU) reduction (both with air and MA65) in the zone with a pH change. Inactivation of bioluminescence cells in the plasma penetrated zone confirmed that the plasma, and its generated reactive species, inactivate microbial as it penetrates into the gel. A two-minute HVACP direct treatment with air at 90 kV induced greater than 5 $\log_{10}$ (CFU) *S. enterica* reduction in applesauce.

The third study investigated the interactions between HVACP and protein, using bovine serum albumin (BSA) as a model protein. The physicochemical and structural alteration of BSA and its reaction mechanism, when subjected to HVACP, were investigated. After treating 10 mL of BSA solution (50 mg/mL) at 90 kV for 20, 40, or 60 min, we characterized structural alteration and side-group modification. FTIR spectroscopy, Raman spectroscopy, and circular dichroism analysis indicated protein unfolding and decreased secondary structure (25 % loss of α-helix, 12% loss of β-sheet) in HVACP treated BSA. Average particle size in the protein solutions increased from 10 nm to 113 µm, with a broader distribution after 60 min HVACP treatment indicating protein aggregation. SDS-PAGE and mass spectrometer analysis observed a formation of new peptides of 1 to 10 kDa, indicating that the plasma triggered peptide bond cleavage. Chemical analysis and mass spectrometer results confirmed the plasma modifications on the side chains of amino acids. This study reveals that HVACP treatment may effectively introduce structural alteration, protein aggregation, peptide cleavage, and side-group modification to proteins in aqueous conditions, through several physicochemical interactions between plasma reactive species (reactive oxygen species and reactive nitrogen species) and the proteins. This finding can be readily applied to other plasma-protein studies or applications in the food system, such as enzyme inactivation or protein-based film modifications.

CHAPTER 1.   INTRODUCTION

1.1   Atmospheric Cold Plasma (ACP)

1.1.1   Definition

Plasma, the fourth state of matter, is an ionized gas, consisting of various ions, electrons, and uncharged particles, photons, free radicals, and atoms [3]. From solid, liquid, gas and to plasma, the energy of the four states of matters increases progressively during state transition. Sufficient applied energy ionize gas molecules, generating plasma [4]. The free electric charges (electrons and ions) in the plasma contribute to the electrical conductivity of plasma when exposed to electromagnetic fields. Plasmas can be found broadly in the environment, such as in ionospheres, neon-lights, and gas-discharge tubes. The diverse characteristics of the plasma, including the temperatures, densities and ionization degree, varies significantly [5]. Based on electron density and temperature, plasmas are classified as either high-temperature or low-temperature plasmas. And the low-temperature plasmas include non-thermal plasma and thermal plasma [6, 7]. Table 1.1 is a summary of the general classification of plasmas and their main characteristics.

Table 1.1 Plasma classification [8].

Plasma	Characteristics	Example
High temperature plasma (equilibrium plasma)	$T_e \approx T_{ion} \approx T_{gas} = 10^6 - 10^8 K$	Fusion plasma
Low-temperature plasma		
Thermal plasma (local equilibrium plasma)	$T_e \approx T_{ion} \approx T_{gas} \leq 2 \times 10^4 K$	Arc plasma, plasma torches
Non-thermal plasma (non-equilibrium plasma)	$T_e \gg T_{ion}$ $T_e \leq 10^5 K (\approx 10eV) \ T_{ion} \approx T_{gas} \approx 300 - 10^3 K$ *Cold plasma ($T_{gas} \approx$ Room temperature)*	Glow discharge, corona, barrier discharge

Note: T_e: electron temperature, T_{ion}: ion temperature, T_{gas}: gas temperature.

Through excitation, ionization, elastic collisions, and dissociation of molecules, energy is transferred from free electrons to the heavy neutral particles. For atomic gases, the energy is transferred from the electrons to the heavy particles through elastic collisions [9]. However, in molecular gases, the energy transfer process is dominated by the vibrational excitation [10]. The gas temperature is significantly lower than the electrons temperature, since the collisional energy transfer between electrons and heavy particles is less efficient than the energy transfer from the electric field to the electrons. In addition, the difference in mass between the electrons and neutrals (the mass of electrons is much smaller than neutrals), leads to inefficient energy transfer [9, 10].

In high-temperature plasma, the generated plasma species are in a thermal equilibrium state; this means the temperature of electrons and heavy ions is both very high. In low-temperature plasmas, heavy particles consume the majority energy of electrons, increases its temperature. There is a local thermodynamic equilibrium between electrons and heavy particles in the low-thermal plasmas. However, in non-thermal plasma, the electrons temperature is much higher than the temperature of ions and neutral gas, due to the difference in collision rate between the electrons among themselves and with heavy particles [7, 8]. This small kinetic transfer between electrons and heavy particles leads to a high remaining energy among electrons [11]. It is common to interpret generating non-thermal plasmas as that to apply the electric field where the electrical energy is mainly used for generating henergetic electrons without increasing the temperature of the gas medium [7].

Atmospheric cold plasma (ACP), is a non-thermal plasma, with the temperature remains close or at room temperature, as shown in Table 1.1 [7]. With regards to the differences in neutral gas temperatures, thermal plasmas are widely applied for application where thermal treatment is required, such as welding, cutting, or spraying [7, 10]. ACPs are prevalent in processing thermal sensitive targets, such as surface treatment of skin or ready to eat foods [12-14].

1.1.2   Generation Sources

Various electric power sources have been developed to generate plasma, including corona discharge, DBD, atmospheric pressure plasma jet, electron beams, the plasma needle, microwave discharges, operating under alternating current (AC) or pulsed [1, 7, 15-19]. The various geometrical shapes of experimental arrangements among the different types of gas discharges,

provide the feasibility of plasma into large-scale applications [20]. The focus of this study is ACP, which is usually generated by dielectric barrier discharge (DBD), cold plasma jet or corona discharge.

   Corona discharge. In the corona discharge setup, ionized gas is generated in the surrounding of a conductor, normally coupled with secondary electron emission [20]. The electrified is normally sharp, non-uniform and very strong, compared with the surrounding gas, to accelerate the generation of ionized gas. Therefore corona discharges typically use sharp points, edges or thin wires as the electrodes, to treat living or non-living materials [20-22]. The electrode geometry is typically a sharp, curved electrode arranged in counterpart to a flat one [22], which is demonstrated in Figure 1.1. Corona discharges are adaptable for various industrial applications, such as generate ozone species for water disinfection [23], or surface treatment [22, 24], to remove volatile organic compounds [25].
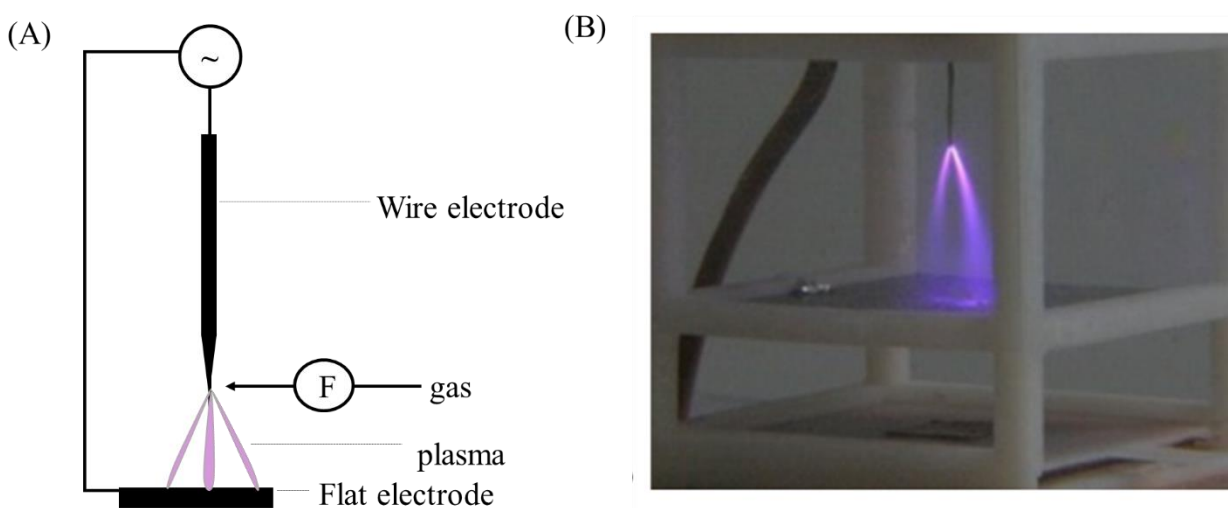
Figure 1.1 Setups for corona discharge. (a) The principle of corona discharge: point-to-plate setup, (b) photo of corona discharge [26].

   Dielectric barrier discharge (DBD). In the setup, the dielectric barriers are located between two metal electrodes, or at least one of the metal electrodes is covered by a thin layer of dielectric or highly resistive material, using ceramic, glass, quartz, polymers or other materials [7, 27]. These materials have a low dielectric loss or high breakdown strength, which can limit the DC current in the inter-electrode gap space and prevent arc transition [28]. DBDs typically use two electrodes to generate plasma (in the kHz range), known as 'barrier discharges'. There are two

basic configurations of DBDs: the volume DBD and the surface DBD [29]. In the volume DBD, the treated object serves as the second electrode. In the surface DBDs, two electrodes in direct contact with the dielectric will be used to generate plasma around the electrodes [7, 30]. DBD mostly generates micro-discharges (filamentary mode), which appear randomly between the electrodes. The DBD is also referred to as the "silent discharge" because it does not generate sparks, characterized as the local overheating or local shock waves/noise [7, 27]. DBDs come in various configurations, such as planar DBDs, volume discharge, coplanar DBDs and surface DBD, [31] as depicted in Figure 1.2. Additionally, operation types can also be categorized based on the operation time scale: the continuous alternating current operation DBD and the pulsed nanosecond operation DBD.
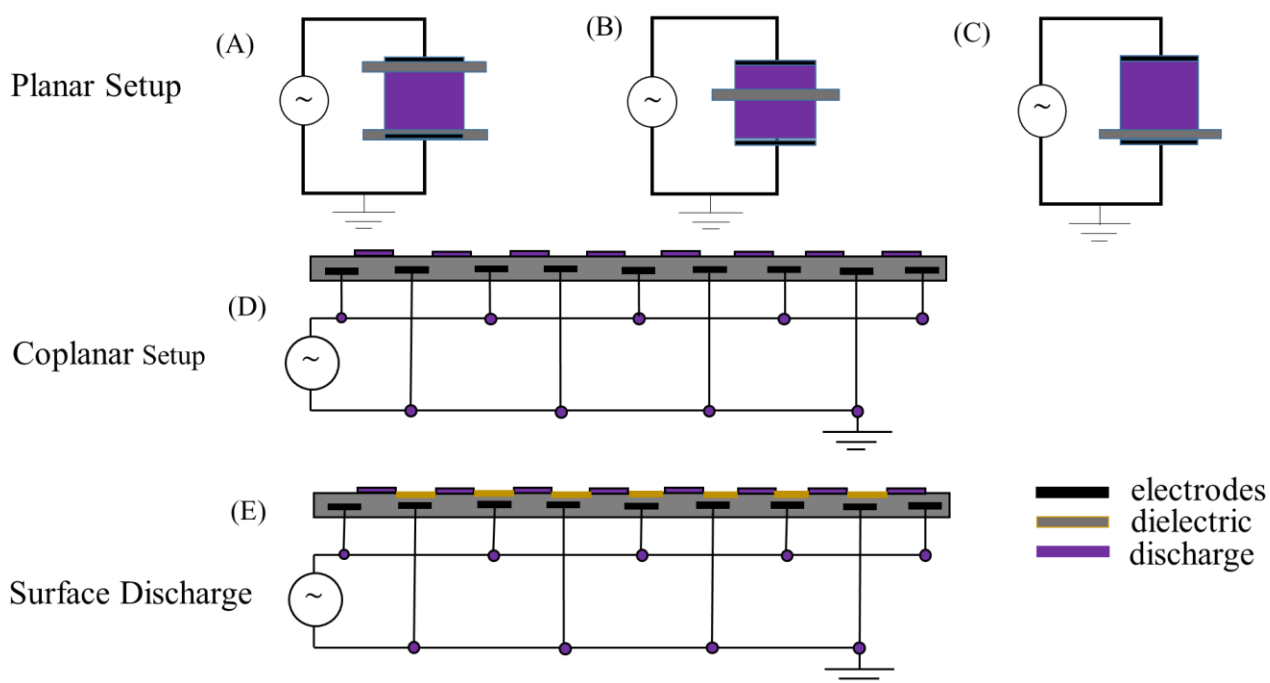
Figure 1.2 DBD setups with various configurations. Planar setup: (a) dielectric layer on both electrode, (b) dielectric in discharge, and (c) dielectric layer on one electrode, (d) Coplanar setup: the electrodes are embedded in the dielectric. (e) Surface discharge: one electrode is embedded in the dielectric discharge [7, 30, 31].

All these aforementioned gas discharges are adaptable to be applied for surface treatment with direct or indirect exposure model [7]. The advantages of DBD includes that it is able to utilize various combination of gases, with a low gas flow (down to 100 standard cubic centimeters or less) [3, 32]. Another advantage of DBDs is that no current flows through the treated target which may

better preserve the surface features. Combining this advantages with the flexible adaptability and various gas options, DBDs are widely used for treating the thermal sensitive surface, (e.g. fruits, vegetables, eggs, and skins) [30].

Atmospheric cold plasma jet (ACPJ). An ACPJ setup typically produces small 'plasma flames' that are generated in the radiofrequency range [22, 33]. Generally, there are two electrodes in the plasma jets setup (needle electrode and ring electrode). There is usually a few millimeters gap in between the electrodes, and the process gas is ignited at voltages of hundred-volts up to kilo-volts [33]. ACPJs can generate plasma with various gases, such as noble gases (e.g. helium, argon), or an admixture of several gases (e.g. nitrogen or oxygen) [7, 22]. The plasma generated by ACPJs with various configurations might have different characteristics for numerous applications. Figure 1.3 shows a schematic of the ACPJ applied for surface modifications. This ACPJ, kINPen ® was invented by the Leibniz Institute for Plasma Science and Technology (INP Greifswald e.V.) [7, 34].
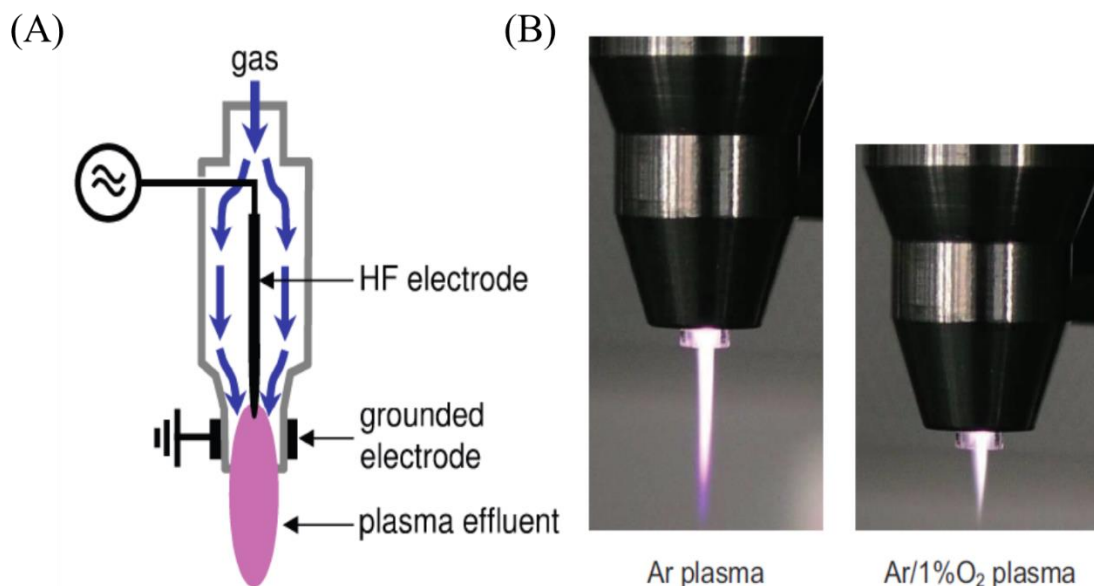
Figure 1.3 (a) Setups for atmospheric cold plasma jet. (b) Photo of an Ar plasma jet and Ar/1% O2 plasma jet [7, 34].

The inner electrode is connected to a high-frequency power (1.1-1.8 MHz) and the operating gas flows between the outer grounded and the inner electrode [7]. When applying the high-frequency power supply, the gas discharge is ignited from the top of the central electrode and

produces electrons, which interact with the surrounding gas molecules through inelastic collisions [7, 33]. Consequently, a high-velocity plasma effluent can be generated and expand to the surrounding position (outside the jet nozzle). With adjusting the operation gas, the jet effluent can reach a length of up to 12 mm [7]. The limitation of ACPJ is the restricted treatment area, which is typically adaptable for localized applications. However, the main advantage of plasma jets is that they can reach the narrow gaps or cavities that large discharge has difficulty accessing [35, 36]. Therefore, the predominant advantage of the ACPJ is its ability to penetrate into a small space or microstructure to achieve an accurate modification or treatment, such as for equipment gaps or root canals [36]. Another distinct advantage is that ACPJ generates a stable discharge in a region of inert gas and transports the plasma to a surrounding region of treating target. This spatial separation of plasma generation and surface processing provides flexibility in jet configuration to control plasma generation and maximize the treatment efficiency [35].

High Voltage Atmospheric Cold Plasma (HVACP). This is a novel HVACP technology, which is developed through research at Purdue University (U.S. Patent 8961894) [37]. In this HVACP system, ACP is generated, inside a package between dielectric barriers, with a gap of 3-5 cm between the two electrodes. A high voltage (up to 120 kV) is applied to generate reactive gas species (RGS) between two parallel electrodes [20]. The operating gas can be air, O_2, CO_2, N_2, He, Air, or a combination of various gases. The cold plasma was generated by applying a high voltage with low average current (0.2–1.0 mA) through the gas inside the package. This high voltage creates a strong electric field that generates free electrons that interact with nearby gas molecules (e.g. O_2, N_2, and CO_2) to form a quasi-stable charged gas species or plasma. This study uses air and modified air (MA65: 65% O_2 + 30% N_2 + 5% CO_2, <5% relative humidity). The resulting RGS, such as NO, NO_2, O, O_3, and hydroxyl radicals (OH), have bactericidal, fungicidal, and sporicidal characteristics [38-40]. The HVACP process generates much higher concentrations of RGS than other plasma devices due to its higher voltages, while the containment of RGS in the package enhances its effectiveness [41, 42]. The generated RGS would convert back into the original packaging gas within 24 h, leaving no chemical residuals [13, 43, 44]. This HVACP system can achieve more than 5 log reduction in treated food samples, such as strawberry, tomatoes, eggs within seconds to minutes [13, 41, 45]. Compared with conventional methods to achieve the inactivation of *Salmonella enterica (S. enterica)* and *E. coli* O157:H7 on fruits or vegetable seeds,

HVACP treatment can effectively reduce microorganism load by 4 log CFU/g without affecting their germination rates [1, 41, 46].

1.1.3   Plasma Diagnostics

The typical plasma diagnostic methods ar primarily based on mass spectrometry, spectroscopy using various electromagnetic regions and electrical probes [9, 47-50]. A schematic overview of plasma diagnostic techniques is shown in Figure 1.4. Electrical characterization is a fundamental technique to control the dissipated power and to characterize the plasmas. Optical imaging diagnostics can image the plasma morphology and its spatially and temporally resolved development [9]. The major challenge in plasma diagnostics is to detect, identify and quantify the predominant plasma species in the processing, interpreting the data of their energy contents, concentrations, reaction coefficient rates, lifetimes, and geometrical distributions [9, 50]. A whole diagnostic analysis allows an understanding of the main processes responsible for the plasma generation and properties [50]. However, there are numerous plasma species generated during the process and there concentrations/energies spanning several orders of magnitude. Some of the unstable species have short lifetimes. Although several techniques are adaptable to investigate various species, the sensitivity is poor to detect the minor ones; whereas many specific and powerful procedures are restricted to particular species. Therefore, several complementary techniques are combined to diagnostic plasma species. Moreover, unlike the experimental plasma reactors are normally designed to facilitate their characterization with the most appropriate setups, there is restricted access for the generated plasma in industrial reactors [50].
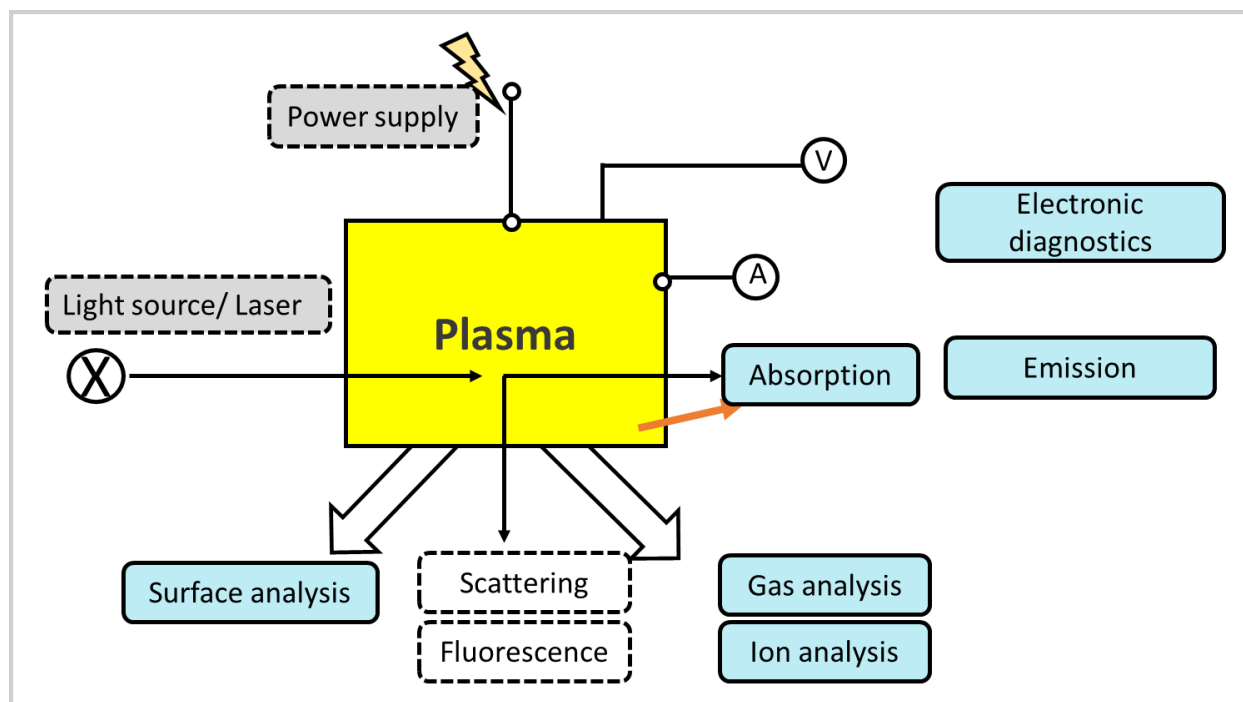
Figure 1.4 Schematic of the different plasma diagnostic techniques [9].

Optical Spectroscopy is a quantitative method for plasma diagnostic, one of the most prevalent diagnostic tool for plasma [51]. Optical emission spectroscopy (OES) is categorized as a passive method to record the light emitted from the species [51]. In OES, excited particles (atoms, molecules, ions) generate emission due to the decay process. The intensity of the emitted light is associated with the corresponding excited species and their densities. Numerous researchers have used OES to assess the ACP and its generated species during plasma treatment [52-55]. The complex reactions and its derived species, as well as the short living-time of RGS, restrict the accuracy of optical spectroscopy method to record the all the excited species [52]. Sarani *et al.* [56] used OES characterized ACP generated by plasma jet and investigated the effect of water content on plasma properties. A higher intensity of OH radicals in emission spectra was found in plasma generated in Ar/water (0.05%) mixture than pure argon [56].

Another optical method is optical absorption spectroscopy (OAS), known as an active method. The mechanisms of OAS is that a beam of collimated light from a visible, ultraviolet (UV), or infrared external source is directed through the plasma and the fraction of light absorbed by specific species is recorded [20, 57]. The absorption signal is associated with the particle density

in the lower/ground state [51]. The system typically includes a light source and a detector. The focal length of the spectrometer will affect the spectral resolution. Moiseev *et al.* applied UV–Vis (200–800 nm) OAS to assess plasma composition generated by a large-gap DBD using humid air [44]. The recorded absorbance spectra was de-convoluted by direct deconvolution and iterative methods to calculate the concentration of ozone and nitrogen oxides (O_3, NO_2, NO_3, N_2O_4). In addition to OES and OAS, laser-induced fluorescence is also employed as an optical method to diagnostic plasma. This method is a non-intrusive optical technique that can record the ground state groups of the reactive species [20, 58]. Laser-induced fluorescence is commonly used in semiconductor processing [59].

Mass spectrometry (MS) is a method to provide information about ions (positive and negative), as well as their energy distributions of during plasma operation. Recent studies used MS to investigated plasma-surface interactions through recording the fluxes of species at the surface [60]. Bolikov *et al.* [61] investigated the composition of glow discharge plasma in methanol vapor and acetone-nitrogen mixture. MS is feasible to detect the concentration of atoms, radicals and other fragments with fewer cross sections and more accuracy [61]. Skalny *et al.* [62] used MS to study the negative ions extracted from point to plane negative corona discharge in ambient air at atmospheric pressure [62]. The author reported that owing to the high sensitivity and excellent mass resolution of MS, more anions were detected in ACP which was not observable in previous studies [62]. The major technical restriction is that the mass and energy analyzers is require to maintain in a high vacuum condition [63]. Beyond this concern, MS is reported to be applicable for investigating long-living species and transient species during ACP treatment [60, 63, 64].

1.1.4   Treatment Parameters Control

The generation of HVACP is influenced by various operating parameters. Understanding of these complex relations between operating parameters and plasma generation is required in order to control and optimize the main processes which will be utilized in the various applications [3, 9]. The versatility of ACP can be accessed by the array of modes for its generation and process variables. The following section will discuss the various processing parameters for plasma generation and processing.

Operation parameters for plasma penetration and processing. In general, electric voltage, feed gas, gas flow, geometry (direct and indirect exposure), and materials are critical in generating various plasma, with numerous RGS, corresponding to distinct application properties (Figure 1.5).
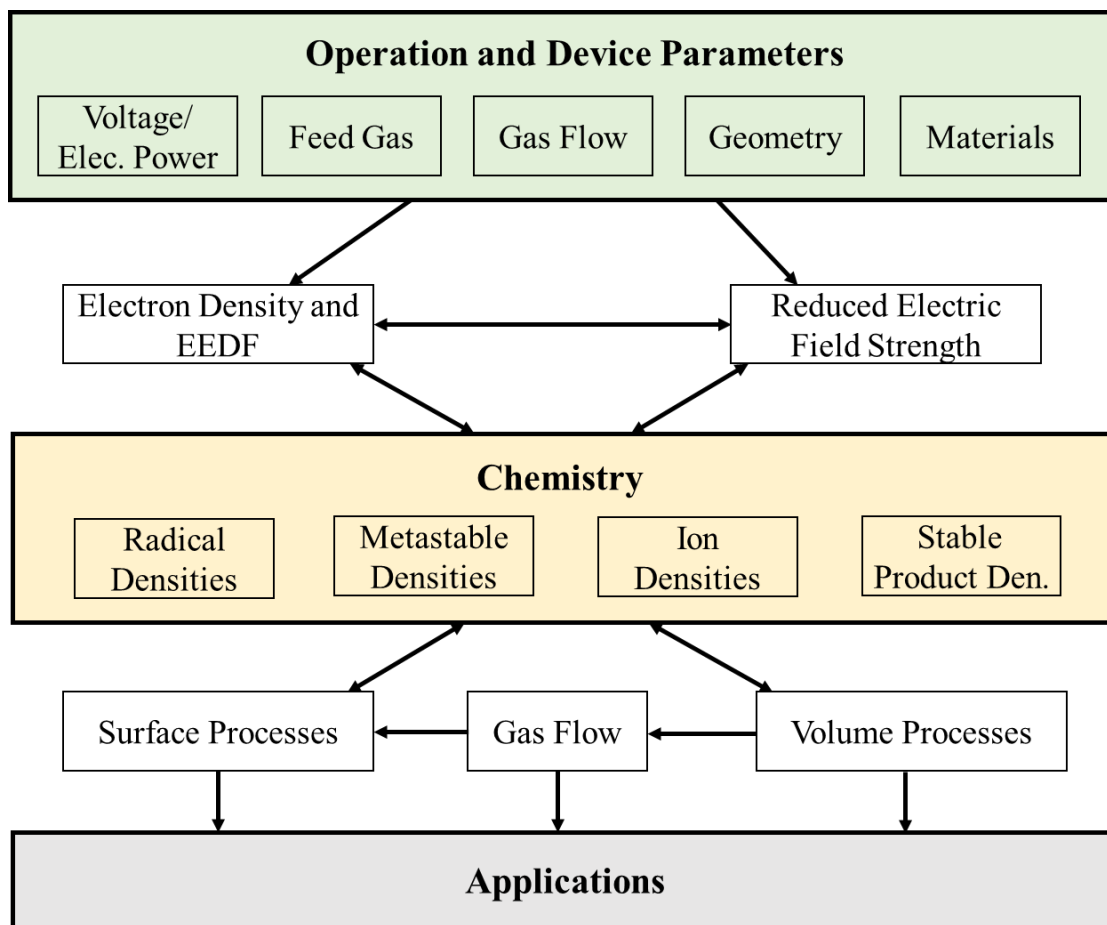
Figure 1.5 The relation between device and operation parameters, plasma physics, chemistry and application of plasma [3].

Voltage. The breakdown voltage for plasma generation is as a function of gas pressure and electrodes' gap, based on Paschen's law [65]. If gas components and electrode setup are assured, the breakdown voltage is a function of pressure and electrodes' gap (p.d) instead of the two variables: electrode distance d (mm) and pressure p (Pa). Under the cold electrode condition, there is always an optimal value of the product of pressure and distance (p.d) at which the breakdown voltage has its minimum value [66]. Ziuzina *et al.* reported that the breakdown voltage for air at atmospheric pressure with 1 cm distance between electrodes require a voltage of about 30 kV [67]. Increasing the voltage corresponds to a higher energy transferred into the plasma. This triggers

the generation of reactive species of higher density and reactivity in the plasma complex [68]. A previous study reported that ozone generation rate in the air at atmospheric pressure by DBD plasma at 13.5 kV was 1200 ppm/min which increased to 3750 ppm/min at 80 kV [69]. Numerous studies have shown that increasing the applied voltage also increases the overall efficacy of the desired results, such as microbial decontamination [18, 70], surface modification [65, 71, 72], and chemical degradation [73, 74].

Treatment Time. Treatment time is an important parameter for ACP processing. A number of studies reported that increasing the treatment time will increase the microbial reduction efficacy of plasma processing [15, 75]. Noriega *et al.* investigated disinfection effect of ACP on chicken meat and chicken skin contaminated with *Listeria innocua* [70]. The ACP treatment time varied from 10 s, 30 s to 8 min. Using He/ O_2 as plasma generation gas, the ACP pen was able to achieve 1.25 log (20 s), 1.61 (1 min), and 3.3 log (8 min) reduction, respectively [70]. Generally, the mechanisms related to that increasing the treatment time increases the concentration of the plasma RGS and also increases the sample exposure time, resulting in an increase in overall effects. Moreover, post-treatment processing, when stored the in-packaging products for some extended time will further increase the process efficiency [46, 72].

Type of Gas. The working gas used for plasma generation is responsible for most of the functional effects demonstrated by ACP processing. Plasma chemistry is highly complex. Previous reports indicated that air plasma consists of over 75 gas species involving almost 500 reactions [3, 39]. Various gases have been applied to generate plasma, such as O_2, N_2, Ar, He, or mixture those gases [76, 77], which have various efficacies on the treatment targets. The types of operation gas in the ACP process predominantly determine the quantity, category, and reactivity of RGS, in which affecting its treatment efficiency. Previous studies reported that high-oxygen gas was found to be more efficient in microbial inactivation than the air [1, 45].

Mode of exposure is critical in determining the plasma treatment mechanism and efficiency. Compared with indirect/remoted exposure model, direct exposure (treatment target is exposing directly, contacting within the plasma RGS) is preferable for high efficiency in microbial decontamination [20]. In the indirect exposure mode, the majority plasma RGS cannot reach the sample due to its short exiting time and self-quenching nature [39, 78].

Other factors affecting ACP treatment. Nature of samples and its surrounding factor (e.g. humidity) can also affect the effectiveness of ACP treatment [78]. A high humidity in the corn samples was found to be less efficient in removing aflatoxin in corn, reported by Shi *et al.* [46]. During HVACP treatment, higher concentrations of reactive oxygen species (ROS) and reactive nitrogen species (RNS) were generated in corn samples with low relative humidity [46]. In general, reaction efficiency and mechanisms in the plasma-solid and plasma-liquid interface are very distinct. Besides, the high humidity generated by vaporized water will also affect the plasma generation. Meanwhile, the characteristics of treated samples, such as pH, surface morphology, porosity, composition, and other factors may also affect the treatment efficacy [13, 78].

1.2   Agricultural and Biological Application of ACP

Generally, ACP is valuable for a wide range of applications. The current applications are summarized in Figure 1.6.

Atmospheric Cold Plasma Technology

Food Science — Property Modification, Enzyme Inactivation, Decontamination, Edible Packaging

Biomedicine — Wound Healing, Cancer Treatment, Dentistry, Gene Transfection

Further Applications — Air purification, Waste treatment, Exhaust Depollution, Analytical Chemistry
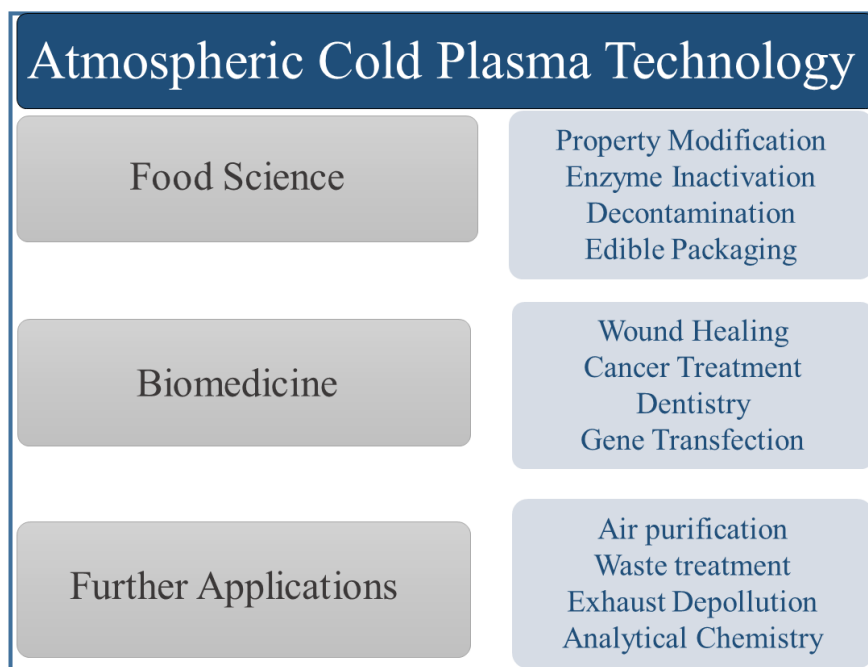
Figure 1.6 Overview of ACP applications in various areas [79].

Among the applications, the major focus of this section is to review the application of ACP in agricultural and biological aspects. ACP has shown promising results for shelf life extension by microbial decontamination and sterilization of food products including fruits, food packaging

materials, equipment cleaning, and biofilm control [80-82]. ACP is also applied into the degradation of pesticides, dyes, and other chemical toxicants in waste products generated through agricultural processing or food production plants [46, 74, 83]. Biological application of ACP includes medical device and package sterilization, cancer treatment and wound healing [34, 84-86].

1.2.1   Agricultural Applications

Plasma technologies have recently been explored for their possible contributions to the agricultural production and operations. Applications of cold plasma are explored at different stages of agricultural food production, such as decontamination of seeds, the germination enhancement in seeds, an enhancement of plant growth, insect and fungal control, and reclamation of contaminated soil [87]. In this section, microbial inactivation, food modification, and waste treatment will be reviewed.

1.2.1.1   Microbial Inactivation

Microbial contamination can occur in the process of harvesting, human handling, transportation or food processing [78]. One of the predominant advantages using ACP discharge is in-package treatment, providing decontamination process against cross-contamination or recontamination during food processing [16, 65, 88]. Cold plasma is feasible to generate RGS, of reactive microbiocidal effect, to decontaminate bacterial, yeast, spores effectively within the package, invested by numerous studies in vegetables, fruits, meats, and food ingredients [1, 15, 22, 89, 90].

The in-package decontamination process is particularly important for ready-to-eat foods (RTD) [1, 68]; these foods must be fresh and minimally processed, necessititing technologies that provide non-thermal treatment with minimal impact on product qualities. Hertrich *et al.* [91] employed cold plasma generated by a volume DBD system with an input voltage of 35 kV, in tomato-and-lettuce mixed salads packed with air in a commercial polyethylene terephthalate plastic package. The microbial load of inoculated *Salmonella*, originally from cherry tomatoes or lettuce, reduced by 0.75 log and 0.34 log CFU/g, respectively, indicating the effectiveness of cold plasma treatment in *Salmonella* decontamination in mixed salads [91]. A similar study was reported by Min *et al.* [92] that treating romaine lettuce by a volume DBD system at 42.6 kV for

10 min, achieved 1.1 log CFU/g reduction of *E. coli* O157:H7 in the lettuce leaf samples [92]. The microbial decontamination efficiency will be affected by the configuration of the plasma discharge, nature of the contamination, plasma transfer direction, as well as by the sample characters, such as the topography and compositions [91].

ACP could be an alternative approach for conventional techniques, such as chemical reagents (organic acids) or radiation to decontaminate fruits (strawberry, apple) and vegetables (lettuce, tomato) [42, 92-95]. *E. coli* (ATCC 25922), and *Salmonella enterica* were effectively inactivated by ACP on cherry tomatoes and apples [68, 96]. Due to the uneven surface of the strawberries, ACP treatment was less effective for decontaminating bacteria but still reduced their concentrations by 3 log CFU/g [97]. Similarly, a different effectiveness of cold plasma hydrogen peroxide (H_2O_2) solution in inactivation of the *E. coli* strain O157:H7, *Salmonella Typhimurium*, and *Listeria innocua* were found on tomatoes, baby spinach leaves, tomato stem scars, and cantaloupe rinds. Hydrogen peroxide itself, without plasma activation, is utilized as an antimicrobial agent but its effectiveness is not consistent [98]. Compared with treatment on tomatoes and spinach leaves, *Salmonella Typhimurium* and *Listeria innocua* were inactivated much more effectively than on tomato stem scars and cantaloupe rinds. However, *E. coli* O157:H7 was only effectively inactivated by cold plasma on tomatoes [94]. These results suggest that ACP can treat uneven surfaces. ACP can also be applied to treat meat products. Jayasenna *et al.* [99] investigated the microbial decontamination effect of cold plasma treatment on fresh pork and beef in a flexible thin-layer DBD plasma system. The populations of *Listeria monocytogenes*, *Escherichia coli* O157:H7, and *Salmonella* Typhimurium were reduced by 2.04, 2.54, and 2.68 logs CFU/g, respectively, with 10 min DBD direct treatment. No significant loss *(P< 0.05)* of texture was detected. The alteration of the physicochemical and sensory profile can be minimized with further operation optimization [99].

Besides fruits, vegetable and meat products, ACP has been applied to decontaminate dried foods, such as species, starch powders, almonds, and peanut [88, 100], as well as liquid foods, such as juice and milk [88]. Kim *et al.* [101] reported that treating milk in an air pack sample bag by cold plasma generated by DBD at 250 W, 15 kHz, achieved 0.98 log CFU/mL reduction for aerobic bacterial and 2.40 log CFU/mL reduction in *E. coli*, *Listeria* monocytogenes, and

Salmonella Typhimurium within 10 min [101]. More recent reports about microbial decontamination using ACP, is summarized in Table 1. 2.

Table 1.2 Summary of recent studies of ACP in microbial decontamination and detoxing of food [78].

Food Matrix	Microorganisms	Plasma Source	Treatment Conditions	Gas	Direct Indirect	Main Findings	Ref.
Apple juice	*Zygosaccharomyces rouxii*	DBD	P = 90 W, ET = 140 s, d = 4 mm	Air	Direct	5-log reduction CFU/mL, no effect on the contents of total soluble solids, reducing sugar, and total phenolics	[102]
Chicken eggs	*Salmonella enteritidis*	HVACP	V = 85 kV, f = 60 Hz, ET = 15 min	Air MA	Direct/ Indirect	Up to 5.53 log cfu/egg reduction	[45]
Corn	Aflatoxins	HVACP	V = 90 kV, f = 50 Hz, RH = 40%, ET = 10 min	Air MA	Direct/ Indirect	Degradation of aflatoxin reached 82%	[46]
Lamb meat	*Brochothrix thermosphacta*	DBD	V = 80 kV, f = 50 Hz, ET = 5 min	30% CO_2 /70% O_2	Direct	2 log reduction	[103]
Egg shells	*Salmonella Enteritidis*	ACPJ	V = 2–3 kV, f = 1 MHz, ET = 5 min, d = 12 mm	Ar	Direct/ Indirect	Reduction factor ranging between 0.22 and 2.27 log CFU/egg	[104]
Romaine lettuce	*Escherichia coli*O157:H7	DBD	V = 42.6 kV, RH = 22%, d = 5.0 cm, ET = 10 min	Air	Direct	0.4–0.8 log CFU/g decrease in the number of *E.coli*	[92]
Egg shell	*Salmonella enterica*	DBD	V = 25–30 kV, RH = 80%, f = 10–12 kHz, ET = 10, 25 min	He/O_2	Direct/ Indirect	Population reduction to below the detection limit (10^2 cells per egg)	[105]
Vacuum packaged beef loin	*Staphylococcus aureus, Listeria monocytogenes, Escherichia coli*	DBD	P = 20.7-29.9 W f = 9 kHz, d = 2 cm, P = 29.9 W	Air	Direct	≥2 log reduction	[106]
Blueberries	*Pesticides*	DBD	f = 50 Hz, V = 80 kV, d = 35 mm, ET = 5 min	Air	Direct	80.18% reduction for boscalid and 75.62% for Imidacloprid	[107]
Mackerel	*Total aerobic psychrotrophic, Pseudomonas*	DBD	f = 50 Hz, V = 80 kV, d = 35 mm, ET = 5 min	Air	Direct	1.3 log reduction	[108]
Grain	*Total mesofilic*	DBD	f = 50 Hz, V = 70 kV, d = 46 mm, ET = 6 min	O_2/CO_2/N_2	Direct	2.23 log reduction	[109]

Note: P = Power, V = Voltage, RH = Relative humidity, d = distance, f = frequency, ET = exposure time, MA = modified air.

Several mechanisms for the interaction between microorganisms with ACP have been proposed [110]. Due to the complexity of plasma generation, plasma transfer, and plasma-surface interactions, the mechanisms of plasma on microorganism decontamination is not completely understood. Based on the current study, charged species generated by ACP are identified as playing the predominant biological efficacy on the cells [111]. Various reactive species have been generated: ROS and RNS, such as NO_2, NO, OH, O_3, O_2, O, may interact with the cell surface and interior components [111]. The plasma may interact with the cell surface, such as a fatty acid (mostly polyunsaturated fatty acids) on the cell membrane, thereby destroying the structure and/or integrity of the cells [112]. The complex plasma etching and deposition reactions may lead to disruption of cell walls, by breaking of the chemical bond, erosion due to bombardment by radicals, and increases in surface roughness. Hydroxyl radicals generated from ACP will react with proteins and lipids on the cell membrane, causing cell lesions and perforations on the membrane. The loss of cell integrity will facilitate the diffusion of reactive species into the cell and cause the subsequent damage interior the cell. Consequently, electrons, radicals, and other derived reactive species can react with interior components of microorganism, damaging its DNA or RNA. In addition, other studies reported that the accumulation of intracellular charged particles may induce apoptosis, electrostatic disruption [113] and electroporation [110] of the cell [78]. However, the specific mechanism and cellular targets are still obscure and inconsistent due to the complexities of plasma transport and plasma-cell interactions [78].
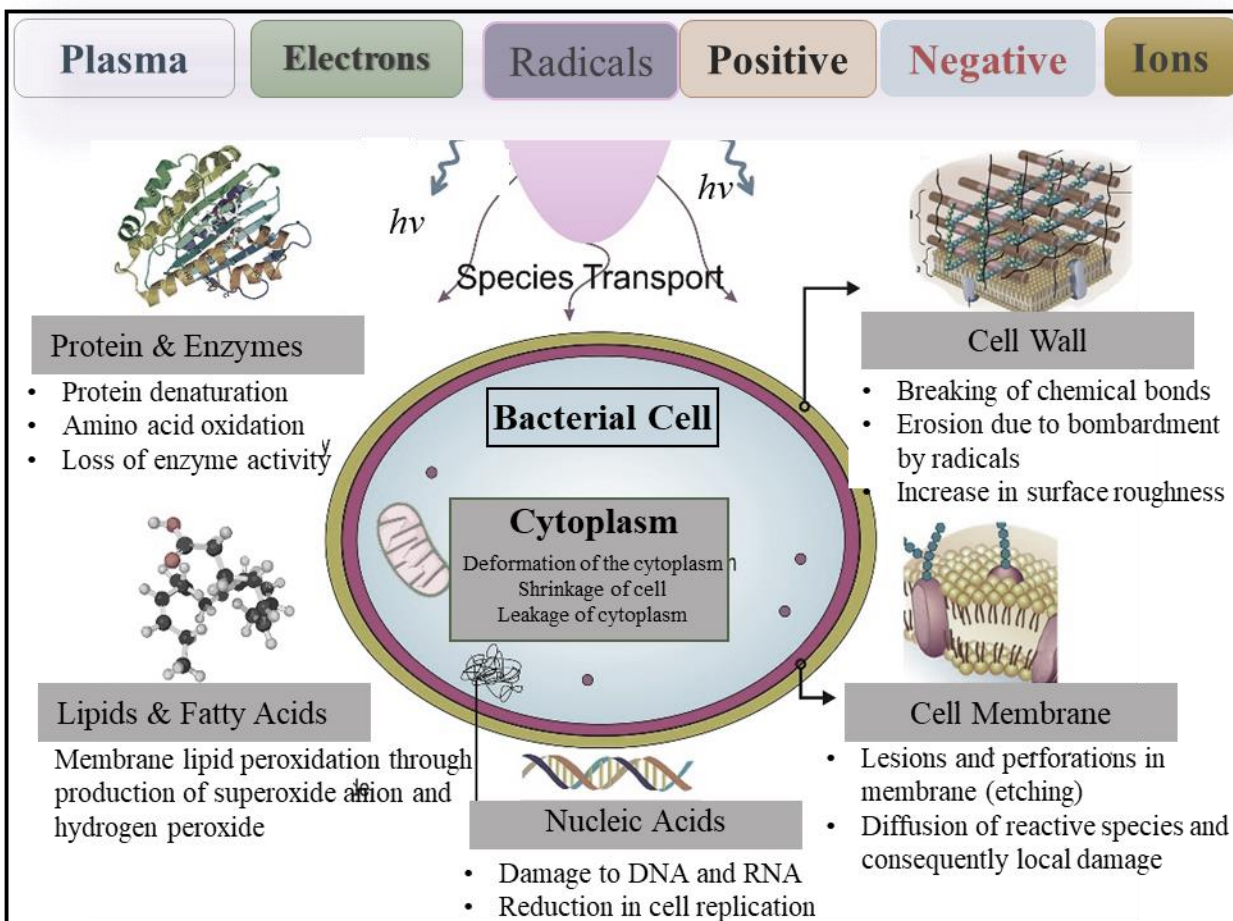
Figure 1.7   A proposed mechanism for applying ACP to microorganism inactivation (direct) [111].

1.2.1.2   Food Modifications

Altering food functionalities. ACP has also been employed for food processing to modify the functionality of food/ingredients, improve physiochemical properties of grains and the degradate agrochemical residues [78]. Protein, lipid, and carbohydrate are the major macromolecules in food that determine the quality, tech-functionality, and nutritional value of the food products or ingredients. Observations of these interactions have been previously reported in various studies. Applying ACP into protein-rich isolate from grain pea (Pisum *sativum*), solubility and water uptake ability increased by 191% and 113%, respectively [114]. Bahrami *et al.* [115] reported that ACP treatment may alter the functionality of wheat flour. The gluten inside the ACP treated wheat flour had a reduced molecular weight which consequently affected the network and water binding capacity of the dough [116]. Thirumdas *et al.* [117] reported that ACP may affect

the functional and rheological properties of rice starch by modifying its gelatinization temperature, retrogradation tendency, amylose content, and pasting temperature [13, 117]. With regards to various applications, ACP is employed to induce modifications of the raw ingredients to increase its desirable functionalities [118-120]. Conformational alteration of proteins in ACP treated samples, leads to an improved foaming ability, foam stability, fat binding capacity and solubility [116]. Plasma treated protein-based film (zein film) had improved film-forming properties and tensile strength [73, 121, 122]. A desirable improvement in the solubility, emulsion stability, and water holding capacity was reported in ACP treated peanut protein [123]. The plasma treatment was reported to be adaptable for modifying functionalities of starch ingredients, altering its pasting characteristics, water absorption, enzyme susceptibility, solubility and thermal properties [78]. Cooking time of black gram subject ACP treatment reduced dramatically from 30.25 to 20.45 min. And the water absorption capacity increased. Plasma etching and surface depolymerization can also aggrandize α-amylase activity (up to 1.21 folds) and water absorption in brown rice [124]. Table 1.3 summarizes recent studies applying ACP into functionality modification in food ingredients. The complexed physicochemical reactions between plasma and these macromolecules will be discussed in section 1.4.

Table 1.3 Summary of recent studies on functionalities modification of food ingredients using ACP [78].

Matrix	Power source	Gas	Treatment Parameters	Main Findings	Ref.
Banana starch	Corona electrical discharge	Air	P = 30-50 kV/cm, ET = 3 min	A significant ($p < 0.05$) increase in pasting temperatures and decrease in peak viscosity	[120]
Rice starch	DBD	Air	P = 60 W, ET = 10 min	Decrease in retrogradation tendency of starch gels and increase in pasting and final viscosities	[125]
Zein	DBD	Air	P = 75 V, ET = 10 min RH = 45 % d = 8 mm	Significant improvement in solubility and reinforcement of the tensile strength and surface hydrophilicity	[122]
Pea protein isolate	DBD	Air	P = 8.8 kV, f = 3.0 kHz, ET = 10 min d = 12 mm	Increased water and fat binding capacities and solubility to 113, 116 and 119%, respectively	[114]
Parboiled rice flour	Radiofrequency	Air	V = 80 kV, P = 50 W, d = 2 mm ET = 15 min	Decrease in hardness and stickiness, likewise endothermic enthalpy and crystallinity	[17]
Basmati rice flour	Radiofrequency	Air	P = 40 W, f = 13.56 MHz ET = 10 min	Increase in gel and flour hydration properties	[126]
Brown rice	DBD	Air	P = 250 W, f = 15 kHz, d = 20 mm ET = 20 min	Significant increase in α-amylase activity ($p < 0.05$), while significant decline in hardness ($p < 0.05$)	[124]
Brown rice	Radiofrequency	Air	P = 30-50 W, f = 13.56 MHz, ET = 10 min	Reduction of cooking time from 29.1 to 21.1 min and increase in water uptake	[127]
Parboiled rice	Radiofrequency	Air	P = 30-50 W, f = 13.56 MHz, ET = 5 min	Amplification in water absorption capacity and reduction in cooking time and hardness	[128]
Soybean oil	DBD	Air	P = 90 kV, f = 60 Hz, ET =1~12 h	Decline in iodine value from 133 to 92, viscosity changed; Saturated fatty acids increased 12%, monounsaturated increased 4.6%	[129]

Note DBD = Dielectric barrier discharge, f = frequency, P = Power, ET = exposure time, RH = Relative humidity, d = distance.

   Cleaning of allergens and toxins in food. Food allergy is a worldwide concern that brings an increasing attention to food industry [130]. The 'top 8' food allergens correspond to the predominant allergy incidence.   Protein allergens include liner epitopes and conformational epitopes that will bind with IgE, therefore, trigger a serious abnormal immunological response.

Recent studies have employed ACP as an alternative food processing technique to inactive or remove food allergens in foods [116]. Meinlschmidt *et al.* [131] used ACP to treat soy protein isolate. Through sodium dodecyl sulfate-polyacrylamide gel electrophoresis (SDS-PAGE) analysis, the investigator observed a reduced intensity of protein bands corresponding to the allergen protein (β-conglycinin (Gly m5) and glycinin (Gly m6), which indicates a potentially reduced allergenicity in ACP treated proteins. Shriver *et al.* reported that ACP treatment (in a DBD system) for shrimp tropomyosin, reduced it allergenicity by up to 76%   [132]. Though various reactions may be responsible for the loss of allergenicity, the major mechanisms are proposed to be the alteration of epitopes of the protein allergen. Protein allergens include liner epitopes and conformational epitopes that will bind with IgE, therefore triggering a serious abnormal immunological response. Structural alteration and protein fragmentation introduced by ACP treatment, consequently destroy its conformational epitope and linear epitopes [78]. The complex reaction between plasma and proteins will be discussed in section 1.4.1. Shi *et al.* [46] reported that using HVACP treatment for corn samples, achieved a degradation of aflatoxin in corn by 82% by in 10 min [46]. The aforementioned researchers illustrate the potential applications of ACP into removing allergens and toxins in food or food plant in the near future.

1.2.1.3   Waste Management

There have been extensive studies on waste management using ACP, such as controlling air-pollution, sterilization, and wastewater treatment [133].

Wastewater management. A large quantity of wastewater is generated in the process of harvesting, equipment cleaning, and food processing [134]. Some process may generate wastewater with organic chemicals, cleaning reagents or even toxins that may pollute the natural environment.   Purifing and reusing these wastewater meet the requirement of sustainable processing in life cycle assessment as well as reduce the operation cost [135]. Recent studies applied plasma into wastewater treatment to purify the water by the reactive species generated by plasma [134]. The synthesized ozone, H_2O_2, $OH^{\bullet}$, O^- and other species have strong oxidative stress and can eliminate the pollutants [134]. An efficient decontamination of wastewater was achieved within 120 s by ACP generated in a plasma jet system, operating at 25 kV [78].   Also ACP treatment reduced the microbial load of wastewater from blackberries by 0.41 log CFU/g with 180 s ACP treatment. In addition to decontamination of microorganisms, plasma is also applied to

destain the water by removing methylene blue [136]. Plasma can effectively purify, degrade, or destain the wastewater from contamination of microorganisms, industrial chemical residuals, or other pollutants by UV, radical, photons or other generated reactive species with various physiochemical reactions [78, 137, 138].

Other environmental applications of ACP include generating ozone and removing dust. Electrostatic precipitators use the physical properties of electrical discharge (such as ionization, charging, migration) to eliminate air-pollution through a (DC or AC) corona discharge [139]. Plasma gasifiers employ plasma torches in the bottom of the gasifier, firing into a bed of carbon to melt inorganics, forming glass aggregate and metal nodules that emerge from the bottom of the unit [140]. Plasma gasification facilities require a large amount of electricity to operate the plasma torch. These electrical consumptions are on the order of 15–20% of the gross power output of the plant [140, 141].

1.2.2 Biological Applications

One of the advantages of cold plasma is that it can be employed to interact with the biological surface with no thermal or electric damage to the cell [142]. This non-thermal character facilitates its broad biomedical applications, including cancer treatment, wound healing, blood coagulation, or tissue modification by electrosurgery [14, 85, 143].

1.2.2.1 Cancer Treatment

ACP could inactivate adhesion proteins of cancer cells, therefore, offering an innovative approach to plasma-assisted cancer therapy [85, 144]. Plasma was found to be able to initiated complex biochemical responses in cancer cells. Plasma killed melanoma skin cancer cell [14, 144]. ACP treatment induced the melanoma skin cancer cells to lose their shape and slowly cell activity, which indicated a cell suicide mechanism termed apoptosis [14]. Floating-Electrode DBD and kINPen jet were used to treat colon cancer cells under standardized conditions [145]. Hydrogen peroxide and reactive species generated by plasma served as a cell toxicity for colon cancer cells and inactive the cancer cells [146]. All these results strongly support the capability of ACP employing as a medical or therapeutic treatment in expanding its biomedical applications [14]. Although there are limited in vivo and clinical studies of plasma medicine, the growing findings

and applications of plasma-cell and plasma-therapeutic control will lead to innovative implications towards plasma medicine [146].

1.2.2.2   Wound Healing

ACP has been investigated for wound disinfection, as an alternative to antibiotic therapy, especially when antibiotic resistant bacteria are encountered [147]. Previous reports suggest that ACP on wound application is achieved by simultaneously disinfecting bacteria and promoting wound healing [148]. Plasma treatment can sterilize the wound, reducing microorganism infections without causing side effects for the patients [149, 150]. A previous study, exposing HaCaT keratinocytes directly to ACP generated by a DBD system, observed that ROS generated by plasma would case interact with the cell and affect its integrin expression [149, 150]. However, the precise mechanism of wound healing is still poorly understood. Therefore, it is important to explore the diffusivity and diffusion mechanism of RGS when applying ACP in skin treatment. With further investigations on the mechanisms of interactions between plasma and microorganisms, tissue/skin cells, and blood components, plasmas can be better applied to various clinical treatments [150].

1.2.2.3   Blood Coagulation

ACP can be introduced into stimulating coagulation of blood as a non-thermal approach, with low risk of bacterial cross-contamination and no negative effect on the treated tissues [146, 148, 151]. The previous study reported that ACP stimulated platelet activation and aggregation, as well as fibrin formation [152]. In addition, plasma treatment may affect the blood clotting conditions, pH and ionic strength of the blood [148]. Based on the current study, the reported blood coagulation rate in ACP treated blood samples increased fifteen times than that of control samples [146]. Moreover, the blood sample characters will also affect the coagulation rate during ACP treatment. A study reported that the coagulation rates of the blood control, blood with sodium citrate anticoagulant and blood from a patient with Hemophilia A, subject to DBD treatment, were distinct from each other [152]. The proposed mechanism for stimulating blood coagulation by ACP is that plasma treatment may be able to bypass the normal blood coagulation cascade and interfere directly with the later stages of the process [153].

1.3   Plasma Transport and Interactions during ACP Treatment

There are various research fields of ACP transfer and interactions with the solid and liquid matrix, such as electrodynamics, fluid dynamics, thermodynamics, atomic and molecular physics, interface science, which require a better understanding of the mechanisms and kinetics of physiochemical interactions between plasma with the matrix. This section reviews how plasma transfer into the treatment target and the physiochemical interactions at the interface: plasma-solid, and plasma-liquid interactions. With regards to the application of ACP on liquid and semi-solid food in this study, plasma-liquid interaction is of practical interest in this section.

1.3.1   Plasma-solid Interactions

In general, the plasma generation process is initialized with producing primary plasma, including electrons and ions, followed by the formation of chemically active radicals and ions [33]. The subsequent transfer of these electrons, ions, free radicals and electromagnetic radiation in the UV/VIS spectrum to the plasma-solid interface will trigger a series physicochemical reactions, including etching, deposition, recombination, de-excitation, and secondary emission from solids [33], as summarized in Figure 1.8.

Once the reactive species transport from the volume to the interface, plasma etching will be triggered by atomic oxygen species and generate derived volatile compounds [32]. These process will introduce the ablation of the first (atomic) layer of the surface, triggering a series of chemical modifications to the surface, such as removing bacteria, chemical residuals, as well as altering its affinity or hydrophobicity [154]. Modification of the surface polar groups by ACP can be employed to alter the surface with higher surface tension, adhesiveness, and wettability, which is beneficial for material manufacturing [32, 33]. Besides etching effect, active species are able to decompose or be absorbed into the surface and initialize reactions with the target. Some of the large nuclei of material and dust particle may be formed on the surface; desorbed species and activated species in the plasma derived from recombination can deposit on the surface [33].

The distance between plasma and surface is critical, regarding the treatment efficiency. When ACP is close to the treatment target, short-living reactive species (such as photons, electrons, and radicals) play the predominant role in treatment efficacy. The analysis should focus on diagnostic and interpret short-living reactive species. In the case of long-distance or indirect ACP

treatment, reactive species that have long-living time (such as nitric oxide or ozone) is critical, where short-living species are unable to reach to the surface and no local current exists [33].
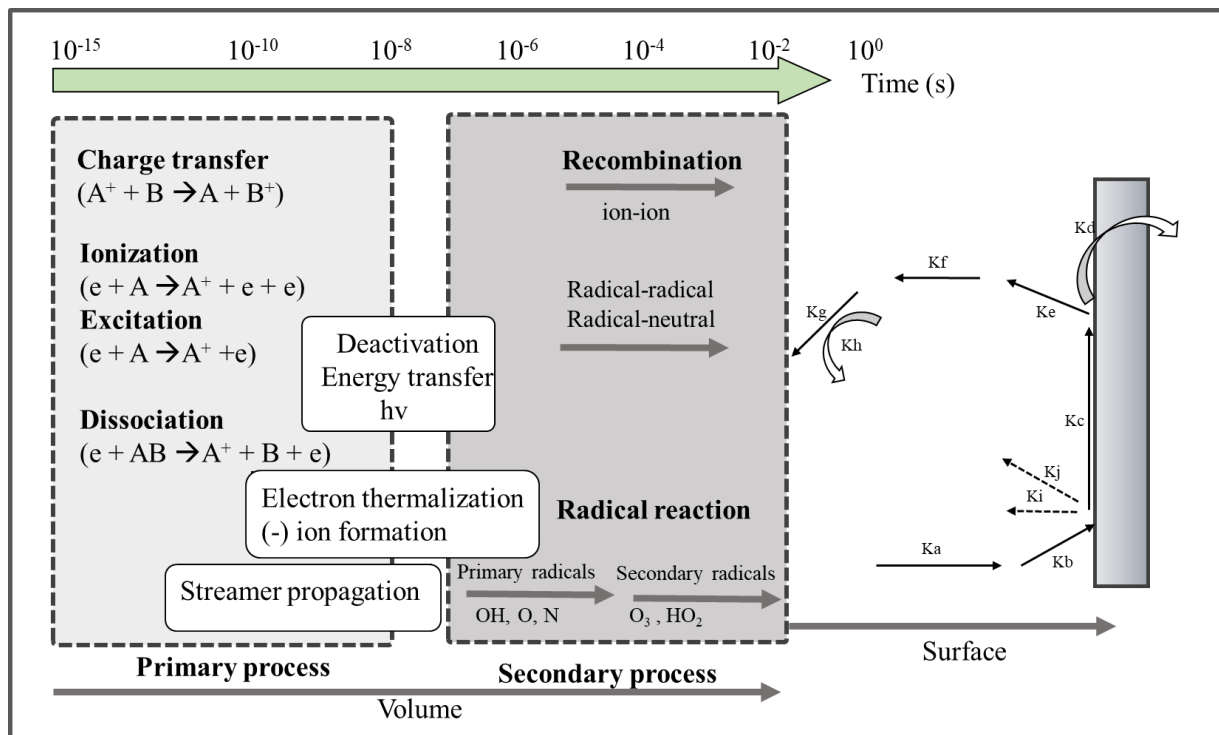
Figure 1.8 Schematic of proposed plasma-solid interface reactions. Active species with a kinetic rate constant Ka arrive at the surface and can be either absorbed (Kb), then initiate the consequent chemical reactions with the surface (Kc), or they can migrate into the surface (Kd). Reversibly, the surface species may also be removed by desorption (Ke) and migrate back into the gas phase (Kf). They may form larger nuclei of material and dust particles (Kg). Finally, the product resulting from the recombination between desorbed species and activated species in the plasma can fall back to the surface (Kh) [33].

1.3.2 Plasma-liquid Interactions

1.3.2.1 Interfacial Reactions

The dynamical reactions between plasma-liquid interfaces are highly complex and challenging to investigate. The understanding of plasma-liquid interactions and, especially, the transfer process from the gas to the liquid phase is critical for the control of ACP applications. Numerous studies have reported the state of the art and major challenges of plasma-liquid interactions [155]. However, most of these studies focus on aqueous solutions with limited distance (<1 cm) [3]. The previous report used 0D, 1D and 2D method modeling plasma species penetration into liquid and proposed a series of physiochemical interactions [156], demonstrated in Figure 1.9.

In the direct exposure model, diffusion, advection, local heating, surface tension, charge deposition and secondary emission are involved in the physical process. The chemical process includes surface electrolysis, charge transfer, hydrolysis, recombination, ionization, collisional relaxation and redox reactions. In the case of indirect exposure, there are limited physicochemical reactions at the plasma-liquid interface (Figure 1.9). Comparing with Figure 1.8, more physical and chemical processes are involved in the bulk plasma, the liquid, and the plasma-liquid interface. Once absorbed into the liquid interface, free electrons, the ions, radicals and derived species will trigger numerous physical and chemical reactions within the liquid [39].
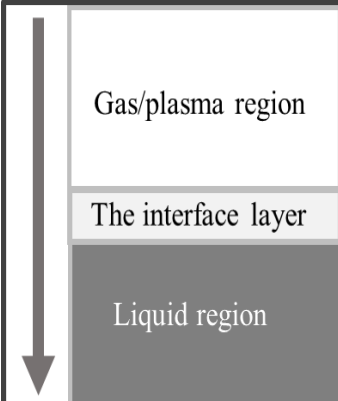
	Direct plasma-liquid interaction		Indirect plasma-liquid interaction
Gas/plasma region	**Physical processes:** • Diffusion • Advection • Local heating • Surface tension • Charge deposition • Secondary emission	**Chemical processes:** • Surface electrolysis • Charge transfer • Hydrolysis • Electron-ion recombination • Ion-ion recombination • Penning ionization • Collisional relaxation • Redox reaction	**Physical processes:** • Diffusion **Chemical processes:** • Charge transfer • Hydrolysis • Ion-ion recombination • Redox reaction
The interface layer			
Liquid region			

Figure 1.9   Schematic of proposed plasma-liquid interface reactions, with a comparison of direct and indirect exposure model [156].

These physical and chemical reactions may vary based on the discharge types and configurations of the plasma setup. Generally, they can be simply classified as plasma over the liquid and plasma inside the liquid. Once the excited and ionized species are generated within the discharge, they will travel towards the cathode or to the treating target [157]. This transfer process of plasma from the volume to the liquid interface is determined by the characteristics of the species and the relevant transport limitations. Based on the diffusivity, stability, and solubility, reactive species are able to penetrate into the liquid-phase boundary layer at the solution surface. As it transferring and accumulating in the liquid, some of them may interact with the interior components and trigger additional reactions [157]. In the complex systems, additional factors and processes may occur, such as evaporation, sputtering of the liquid surface, or electrolysis [157].

Properties of plasma (species population, density) are essential in plasma-surface interactions as it can predetermine the plasma processes and subsequent chemical reactions [39]. RGS generated by ACP is summarized in Table 1.4. However, previous reports indicated that the plasma-liquid interactions are very complex, including 53 species and 624 chemical reactions in the plasma region and more than 109 chemical reactions in the plasma-liquid boundary layer, as a function of treatment time and energy scale [158]. When generated in the liquid, RGS are able to interact on short time-scales with the medium that supports the discharge. Compared with reactions in the gas phase discharge, the reaction rates and reaction efficiencies are very different due to the complex synergetic effects (RGS dissolving, dissociation, reaction with the media or aqueous solutions) [156]. For instance, some of the reactive species, such as hydroxyl radicals and O_3, are diffusion controlled, (the treatment efficiency is limited due to its diffusivity), which can only be detected in the region of a few micrometers beyond the interface boundary [156]. There are numerous reactive species generated in plasma regions, air gap region and liquid region, proposed in the list in Table 1.4. A model was developed based on the assumption of these species category, with a consideration of their stability (lifetimes ($T_{1/2}$, s) is shown in Table 1.5) [157], solubility, and diffusivity (shown in Table 1.6), to predicts the plasma penetration mechanisms at the plasma-liquid interface [39]. The key challenge for studying plasma diagnostic and model development is to understand the formation pathway of reactive species and their derived chemical compounds as the treatment proceeding [39].

Table 1.4 . Reactive gas species generated by air plasma [39, 156].

Region		Species
Plasma/gas region	Cations	N^+, N_2^+, N_3^+, N_4^+, NO^+, N_2O^+, NO_2^+, H^+, H_2^+, H_3^+, O^+, O_2^+, O_4^+, OH^+, H_2O^+, H_3O^+
	Anions	e, O^-, O_2^-, O_3^-, O_4^-, NO^-, NO_3^-, H^-, OH^-, N_2O^-, NO_2^-
	Neutrals	$N(^2D)$, $N_2(A^3\Sigma)$, $N_2(B^3\Pi)$, H, N, H_2, N_2, H_2O, $O(^1D)$, O, $O_2(a^1\Delta)$, O_3, OH, HO_2, H_2O_2, O_2, NO, NO_2, NO_3, N_2O_3, N_2O_4, N_2O_5, HNO_2, HNO_3, N_2O, HNO
		NO, N_2O, NO_2, NO_3, N_2O_3, N_2O_4, N_2O_5, HNO, HNO_2, HNO_3, N, N_2, O_2, O, $O_2(a^1\Delta)$, O_3, OH,
		HO_2, H_2O_2, H_2, H_2O
Liquid region		O_{aq}, $O_2(a^1\Delta)_{aq}$, O_{3aq}, OH_{aq}, HO_{2aq}, HO_{3aq}, H_2O_{2aq}, N_{2aq}, O_{2aq}, H_{aq}, H_{2aq}, N_2O_{3aq}, NO_{aq}, NO_{2aq}, NO_{3aq}, N_2O_{4aq}, N_2O_{5aq}, HNO_{2aq}, H^+_{aq}, $HO_2^-_{aq}$, OH^-_{aq}, O^-_{aq}, $O_2^-_{aq}$, $O_3^-_{aq}$, $NO_2^-_{aq}$, $NO_3^-_{aq}$, O_2NOOH_{aq}, $O_2NOO^-_{aq}$, $ONOO^-_{aq}$, $ONOOH_{aq}$, HNO_{3aq}, N_2O_{aq}, H_2O_{aq}

Table 1.5 Typical lifetimes of selected reactive species that may be generated by ACP in the plasma-liquid interface (*this is based on a model of half-lives in a 1 M linoleic acid solution at pH 7.4*) [157].

Active species	Lifetimes ($T_{1/2}$, s)
$OH^\bullet$	$<10^{-9}$
$O_2^{\bullet-}$	$<10^{-6}$
$RO^\bullet$	$\sim10^{-6}$
$CO_3^{\bullet-}$	$\sim10^{-6}$
$NO_2^\bullet$	$\sim10^{-6}$
$ONOO^{\bullet-}$	10^{-2}
$NO^\bullet$	$1-10$
$^1O_2$	10
$RO_2^\bullet$	$5-20$
NO_3^-, NO_2^-	stable
H_2O_2, $HOCl$	stable

Table 1.6 Estimated effective diffusion distance (EDL) of ionic species [156].

Species	EDL[m]	Species	EDL[m]
N^+	1.1×10^{-7}	OH^+	2.8×10^{-7}
N_2^+	2.2×10^{-7}	H_2O^+	3.1×10^{-7}
N_3^+	7.4×10^{-7}	H_3O^+	3.3×10^{-5}
N_4^+	7.0×10^{-8}	O^-	5.4×10^{-7}
NO^+	3.0×10^{-5}	O_2^-	1.4×10^{-6}
NO_2^+	7.1×10^{-5}	O_3^-	1.3×10^{-6}
N_2O^+	4.5×10^{-7}	O_4^-	2.0×10^{-6}
O^+	1.0×10^{-7}	NO^-	3.6×10^{-7}
O_2^+	2.1×10^{-6}	NO_2^-	9.4×10^{-6}
O_4^+	1.6×10^{-5}	NO_3^-	6.2×10^{-5}
H^+	2.0×10^{-7}	N_2O^-	6.7×10^{-5}
H_2^+	2.1×10^{-7}	H^-	2.7×10^{-7}
H_4^+	4.7×10^{-7}	OH^-	1.8×10^{-6}

1.3.2.2   Fluid Dynamics, Heat Transport, and Mass Transport

Mechanisms of "fluid dynamics", "heat transport", and "mass transport" play an important role in in the process of plasma generation, plasma-liquid interface interactions [39].

Fluid dynamics. The previous report indicated that the general process followed conventional transport theory, adaptable in a system with laminar flows or turbulent flows of gas

or liquid system [39]. This indicates any mixing, physical agitation, surrounding factors, or the internal natures of the interface may affect the mass/energy transport process. The situations can be generally dived into:

(i) "two phases separated by a mostly stable interface with a well-defined area";

(ii) "a continuous gas phase and discontinuous liquid phase", such as the droplets of liquid is immersed in a gas flow;

(iii) "a continuous liquid phase with the discontinuous gas phase", where the bubbles of gas are immersed in liquid);

(iv) "a completely turbulent phase".

Heat and Mass Transport. Besides the aforementioned factors, chemical reactions, phase change, and electric field operation, as this transfer process proceeding may affect the transport properties and introduce enthalpy alteration. Liquid evaporating, vapor condensing and dissolving are associated with the Joule heating of electric discharges in contact with liquids, which may affect the heat and mass transfer during ACP treatment. Therefore, the interfacial stability predetermined the interface reactions and mass transfer. Ions, photons, and radicals arrive and react with the interface through physical and chemical reactions, which is associated with the surface charging, electric fields and currents at the surface. In the HVACP system, a high electric fields ($> 90\,\mathrm{kV}$) driving current facilitates the transfer of ions and charged species from gas phase through the plasma-liquid interface. The following reaction rates, stabilities, diffusivities and solubilities of these species determine the concentration of transfer process. A long living-life and good solubility is preferable to facilitate the species penetrating into the interface and react with the bulk liquid. Monitoring the mass and heat transfer is challenging due to its dynamic and complex nature. It is important to resolve its mass conservation (such as reaction rate and boundary flux) and energy conservation (powder density) in the plasma-liquid interface model. Other aspects of plasma transfer, such as movement of neural species, periodic steady state of species, and setup configuration should also be included in the model assumptions when studying the plasma-liquid interface interactions [39, 156].

1.4   Interactions between Plasma and Macromolecules in Food System

1.4.1   Plasma-proteins Interactions

There are multiple proposed mechanisms for plasma-protein interactions. The predominant reason may be the alteration in protein conformation induced by plasma reactive species, including the cleaved peptide bonds, oxidized amino acid side residuals, and form the protein-protein cross-linkages. The following section summarized the physicochemical reactions between plasma and proteins in the previous report and proposed the reaction mechanisms. The detailed mechanism is investigated in **CHAPTER 4**.

Modification of amino acids by plasma. Oxidation of sulfhydryl groups was found by investigating cysteine under plasma discharge, reported by Ke *et al.* [159]. Plasma was generated by argon arc-discharge operating at 1–2 kV. Cysteine can be readily transformed to cystine, due to the direct and indirect interaction with oxygen radicals and hydroxyl radicals [159]. These radicals generated by argon arc-discharge caused the conversion of cysteine to cystine, confirmed by FTIR analysis. Misra *et al.* also reported that oxidation of protein sulfhydryl groups and subsequent disulphide bond formation between cysteine moieties was found in wheat flour treated by ACP under 60 and 70 kV for 10 min [160]. Oxidation of sulfhydryl groups contributed to an improvement in mixing time and dough strength after plasma treatment [160]. A direct plasma treatment using a DBD system lead to a permanent inactivation of RNase A within a few minutes. The mechanism of this efficient inactivation was proposed to the configuration change, investigated through circular dichroism spectroscopy. Moreover, the modification of methionine to the methionine sulfoxide was detected through mass spectrometry analysis, which corresponds to the enzyme inactivation [161]. In another study, radiolysis of a simple α-amino acid, such as glycine, was also found in plasma treated protein samples, which reported that deamination was a major chemical consequence in plasma treatment [162]. In plasma treated whey protein (DBD system under 70 kV using air for 60 min), an increase of carbonyl groups and the surface hydrophobicity that revealed the oxidation effect of plasma treatment on amino acid residues of the whey protein [163].

The reactions between plasma species and amino acid have been investigated by exposing 20 amino acid in solution by low-frequency cold plasma jet using helium gas at 5 kV with a

frequency of 13.9 kHz, at room temperature and humidity [164]. The side groups of 14 amino acids were modified, and sulfur-containing and aromatic amino acids were preferentially oxidized among the 20 amino acids. Analysis through high-resolution mass spectrometry revealed that chemical modifications of the amino acids included:

(i) "hydroxylation and nitration of aromatic rings in tyrosine, phenylalanine, and tryptophan";

(ii) "sulfonation and disulfide linkage formation of thiol groups in cysteine;"

(iii) "sulfoxidation of methionine";

(iv) "deamidation and ring-opening of five-membered rings in histidine and proline" [164].

Zhou *et al.* [165] similarly reported that the oxidation of amino acids side groups by plasma-generated species may be divided into four categories, including "hydroxylation, nitration, dehydrogenation, and dimerization". Among these reactions, the relative reactivates of amino acids interact with plasma were also prosed, in descending order: "sulfur-containing carbon-chain amino acids > aromatic amino acids > five-membered ring amino acids > basic carbon-chain amino acids" [161, 164].

Structural alteration. Cold plasma treatment may alter three-dimensional structure of proteins. Ji *et al.* [123] investigated the secondary structure and techno-functionalities of peanut protein isolate subjected DBD plasma treatment (using air at 35 V with 45% relative humidity for 4 min). A reduced α-helix and β-turn content and an increased β-sheet and random coil content were observed in plasma treated protein samples, indicating the protein unfolding. Moreover, improved functionalities, including protein solubility, emulsion stability, and water holding capacity of protein gel, were achieved in peanut protein isolate subjected 8 min plasma treatment. The author proposed that this may be associated with the exposure of buried groups and active sites in the unfolded proteins [123]. Zein film was also investigated under ACP treatment (using air at 75 V with 45% relative humidity for 10 min), the secondary structures of zein changed as treat time proceeding. The content of β-sheets increased significantly for all treated samples, random coil and β-turn decreased with the increase of treatment time [122]. Whey protein isolate subject cold plasma treatment had structure modifications with a certain degree of protein unfolding, as confirmed by dynamic light scattering and HPLC, with improved foaming and

emulsifying capacity [163]. In plasma-treated sodium caseinate film, treated by DBD system at 60 and 70 kV, 50 Hz with 53% relative humidity up for 5 min, a disruption in the inter-helical structure without losing its helical configuration of the protein molecules, confirmed by X-ray diffraction and fourier-transform infrared spectroscopy (FTIR) spectra [166]. A DBD system was also used to inactivate alkaline phosphatase (at 60 kV, 50 Hz with 53% relative humidity up for 5 min). A more than 90% enzyme activity reduction was observed after 300 s treatment. Circular dichroism and chemometric results indicated a loss of secondary structures (α-helix and β-sheet) of the plasma-treated alkaline phosphatase, which corresponded to the enzyme inactivation. These alterations of protein structure attribute to the modification of techno-functionalities in the food system [116].

Cleavage of protein. Cleavage of peptides bound was found by exposing protein under electron beam plasma treatment [167]. Vasilieva reported that a partial degradation of the peptide –CO-NH-bonds in protein primary structure was observed in protein samples treated by electric beam plasma using O_2 and N_2 at <50 °C, confirmed by IR spectroscopy [167]. The formation of low molecular weight peptides further confirmed the partial degradation of the peptide bonds. Previous studies show that ROS such as ozone and OH can lead to significant changes in protein structure finally cause the cleavage of proteins into peptides. The main pathway in sulfur-sulfur bond cleavage could be the addition of an oxygen and hydrogen atom (originated hydroxyl radical or other active species) to the sulfur-containing atoms to form R-SH and R-SO, leading to split-off protein parts [116]. Segat *et al.* [163] reported an increase in the carbonyl content and an increase in the number of amino acid side chain groups which may be caused by peptide bond cleavages, in plasma treated whey protein isolate. However, Cleavage of peptide bound is not widely reported in plasma treated protein. This may due to the high energy of the covalent band, compared with hydrogen bound, electrostatic interactions, which stabilize the primary structure of proteins.

Protein-protein interaction and aggregation. The major protein-protein crosslinking efficacy introduced by ACP treatment was the formation of disulfide bonds (S-S). Ji *et al.* [123] reported plasma treatment (using air at 35 V with 45% relative humidity for 4 min) of peanut protein isolate lead to a decrease in the total free sulfhydryl group content. This was caused by the oxidation of free -SH groups to form disulfide bonds (both intra- or inter-molecular). These protein

crosslinking, as well as protein-protein aggregation, lead to an increase in particle size from 996 nm to 1208 nm. Dong *et al.* [121, 122]investigated the DBD plasma treatment efficacy on zein powers (using air at 75 V with 45% relative humidity for 10 min) and reported that ozone, generated by plasma, act a strong oxidizing agent, changed the thiol groups (SH) to disulfide bonds.

The protein-protein interaction may be enhanced due to the protein unfolding and pH decrease. The hydrophobicity of whey protein increased subject plasma treatment [163]. Plasma leads to a decrease of secondary structure, which may result in the exposure of buried hydrophobic groups, which enhanced hydrophobic interactions. Xu *et al.* [1] reported the formation of nitric acid induced by RNS such as NO_2, NO_3 and N_2O_4, which leads to the acidification of aqueous solutions. The pH decrease may alter the electrostatic interaction between proteins, which increased protein-protein aggregation.

Enzyme inactivation by cold plasma. Lackmann *et al.* [161] reported that RGS were generated through synergistic effects of emitted particles and photons owing to photochemical reactions in the gas phase during plasma jet treatment. Among the RGS, ROS, predominantly atomic oxygen, ozone, and singlet delta O_2 have a relatively high reactivity. ROS could trigger the observed bacterial reaction by oxidizing macromolecules either directly or indirectly. Enzyme GAPDH was used as a model protein to explore the inactivation mechanism of protein by plasma. The study reported that reactive photons and high concentrated ozone generated by plasma interacted with GAPDH and other cellular components that triggered the cell inactivation. Enzyme inactivation was observed in various studies [38, 93, 161, 168-170]. However, when applied atmospheric-pressure glow discharge plasma jet into the manipulation of lipase [168], the enzyme reactivity increased after exposing lipase to plasma.

1.4.2   Plasma-lipid Interactions

Lipids are an important component of food, it is crucial to protect them from deterioration when they are exposed to extreme food processing conditions. Reactions such as oxidation, polymerization or hydrolysis change physical and sensory properties by the formation of volatiles or other reaction products that change the quality of food products. The second scenario is an area that is rapidly growing, modifying chemical structures by exposing them to plasma RGS. ACP generates RGS that interact with food nutrients, changing the chemical structure by attaching

moieties, breaking bonds, or crosslinking molecules. Therefore, cold plasma has a potential as a food processing approach. This section will be focused on the analysis of the effect of RGS in lipids. First, ACP has been investigated as a tool to accelerate lipid oxidation. Besides, lipids are treated with cold plasma to manipulate its composition and obtain products with modified properties.

Lipid oxidation. The mechanism of lipid oxidation has 3 stages: initiation, propagation, and termination [171]. ROS, formed by cold plasma, are superoxide anion (O^-_2), hydroperoxyl radical (HO_2), hydroxyl radical (OH), nitric oxide (NO), hydrogen peroxide (H_2O_2), most of them linked to lipid oxidation [172]. Linolenic acid (C18:3) get oxidized 2.4 times faster than linoleic acid (C18:2), and the latter 40 times faster than oleic acid (C18:1) [173, 174]. Atomic oxygen can have two orders of magnitude higher in oxidation rates than molecular oxygen, it reaches the double bonds of unsaturated fatty acids, which is the target to initiate lipid oxidation [175]. ACP treatment of beef and dairy products determine that the presence of oxygen increase oxidation rate [176]. Oxidation of food products is a parameter often used as a marker of shelf life. ACP has been studied as an accelerated method of analysis for lipid oxidation, using a plasma jet at 6-15 kV for 60 min [177-180]. The authors identified specific aldehydes and ketones that can be used as markers of lipid oxidation. Another study using ACP treating fish oil revealed that nonanal content (a secondary oxidation product of unsaturated fatty acids with 18 carbons) in an 11-week natural ageing oxidation of fish oil is 16.8%, with an accelerated test (6 h/100°C) it reaches 381.9 µg/g. A 60 min cold plasma treatment with air/O_2, generate 28.1ug/g of nonanal [180]. Therefore, this correlation between natural ageing oxidation and cold plasma accelerated oxidation (by the formation of volatiles) can be used as markers to determine the shelf life of fish products.

Hydrogenation. Cold plasma has been investigated as an approach to reduce the number of double bonds in lipid by a hydrogenation reaction [129]. Hydrogenation is an "oleochemical process", intending to a conversion the state of lipid from a liquid into solid [78]. The conventional method to generate partially hydrogenated oil, commonly employs catalyst (nickel powder) at high temperature and pressure, with an incorporation of hydrogen into the hot liquid oil [78]. HVACP has been reported to be an alternative approach for producing partially hydrogenated oil without generation of trans fat [129]. A direct exposing of soybean oil to DBD system for 12 h, was able to decrease the iodine value from 131 to 92 with a 32.3% increase in saturated fatty acids content.

The treated samples had a decrease in polyunsaturated fatty acids and no generation of trans-fats, which is feasible with regards to the food quality [78]. Plasma was demonstrated to be adaptable to alter the chemical structure of substrates by deposition, cross-linking, etching, and the energy levels of hydrogen species increased over time [129]. Therefore, HVACP provides an alternative method with expediency treatment over conventional hydrogenation process at ambient temperature, atmospheric pressure, and absence of catalyst [78].

Polymerization. ACP has been studied as an alternative process to polymerize vegetable oil to obtain bio-lubricants from renewable sources. Nitrogen gas and air were used to treat soybean oil, in a DBD equipment with the oil flowing through the electrodes, for 0-9 h at 90 °C [129, 181, 182]. Treatment conditions allow opening the double bond of unsaturated fatty acids, capture plasma species, forming nitrogen cyclic structures and polymers. After a 9 h treatment, the percentage of carbon/hydrogen reduced, and nitrogen/oxygen increased. The polymerized oil has a high viscosity and improved tribological characteristics.

1.4.3   Plasma-carbohydrate Interactions

According to recent scientific reports, starch can also be modified using the ACP processing. The plasma species will interact with starch can modify in three different possible mechanisms, including cross-linking, depolymerization and plasma etching [125].

Cross-Linking or Grafting. The cross-linking or grafting occurs between the polymeric chains of starch molecules, induced by free radicals and energetic electrons formed during plasma generation [183]. The hydroxyl radicals (OH) generated by ACP, could cleave the glycosidic bonds. Deeyai *et al.* [119] reported that after the plasma treatment of starch, they have observed an increase in the relative area of the peak at 924 cm^{-1} designated to the C-O-C linkage. The grafting degrees of the cellulose/chitin mixture which was estimated using X-ray photoelectron spectroscopy, varied from 31.1% to 58.7% after the ACP treatment. The RGS generated by the gas discharge plasma and the polymeric molecules interact with each other, leading to cross-linking reaction [184].

Depolymerization. The bombardment of high energetic ions of plasma may cause depolymerization of amylose and amylopectin side chains of starch molecules, resulting in smaller fragments [125]. Bhat and Karim [185] reported that the major compounds after the radiolysis of

carbohydrates are formic acid, acetaldehyde, and formaldehyde. The formic acids formed to indicate a destruction of amylopectin chains of starch molecules. Lii *et al.* [186] have reported that plasma operation gas can be dived into two groups based on the capability of depolymerizing starches: 1) less active gas (hydrogen and air plasma) and 2) more active gas (ammonia and oxygen plasma). Misra *et al.* [187] reported that oxygen present during the plasma generation undergoes serious of reactions leads to the formation of hydroxyl radicals (OH) and ozone. Ozone cleaves the bond between the C_2- C_3 and also glycosidic bond can lead to depolymerization. Therefore, plasma operation gas category is critical in plasma-carbohydrate reactions.

Plasma Etching. Thirumdas *et al.* [188] observed that due to plasma etching of rice, there is an increase in leach out of amylose molecules during cooking operations and a decrease in cooking time of rice. A similar effect of plasma etching was also reported by Chen *et al.* [189] in low-pressure cold plasma treated brown rice. The etched surface eases water into starch granules along with temperature due to this it may alter thermal, functional and rheological properties.

1.5   Research Hypothesis and Objectives

To studying HVACP treatment on food processing, especially with focused applications in microbial inactivation and protein modification, we divide the study into parts:

CHAPTER 2 and CHAPTER 3 evaluate the interactions between HVACP and microorganisms in liquid and semi-solid food; identify whether/how plasma transfer into semi-solid food and what is the relationship between microbial inactivation and plasma transfer. The **hypothesis** is that 1) HVACP can inactivate microorganism in both liquid and semi-solid food. 2) The synergetic effects of between the plasma reactive species that penetrate into the sample and the products derived from interactions will inactive the microbes as this penetration proceeding.

CHAPTER 4 explores the interactions between plasma and proteins in the food system. We **hypothesize** that HVACP can be applied to enzyme inactivation and protein modification, with a mechanism of introducing protein structural alteration, protein-protein aggregation, peptide-bond cleavage and amino acid modifications.

CHAPTER 2.   HIGH VOLTAGE ATMOSPHERIC COLD PLASMA INDUCED MICROBIAL INACTIVATION AND QUALITY CHANGE IN ORANGE JUICE

2.1   Abstract

Although atmospheric cold plasma is well known for nonthermal microorganism inactivation on food surface surfaces, few studies examine its application to liquid food within a package. This chapter studies microbial (*Salmonella enterica* serovar Typhimurium, *S. enterica*) inactivation efficacy of HVACP and the physicochemical interactions between HVACP (up to 90 kV) and biomolecules including an enzyme (pectin methylesterase-PME) and vitamin C in orange juice (OJ) under various processing conditions. Both direct and indirect HVACP treatment of 25 mL OJ induced greater than a 5 log reduction in *S. enterica* following 30 s of treatment with air and MA65 gas with no storage. For 50 mL OJ, 120 s of direct HVACP treatment followed by 24 hours storage induced a 2.9 log reduction of *S. enterica* in air and a 4.7 log reduction in MA65 gas; 120 s of indirect HVACP treatment followed by 24 hours storage resulted in a 2.2 log reduction in air and a 3.8 log reduction in MA65. No significant ($P < 0.05$) Brix or pH change occurred following 120 s HVACP treatment. Applying 120 s HVACP direct treatment reduced vitamin C by 56% and pectin methylesterase activity by 74% in air and 82% in MA65. These results demonstrate that HVACP can effectively inactivate *Salmonella* in OJ. Plasma is also able to react with biomolecus in OJ which might affect its quality.

2.2   Introduction

Foodborne pathogens are an increasing concern worldwide. The Center for Disease Control and Prevention (CDC) reports that 1.2 million illnesses and 450 deaths (31% of food-related deaths) occur in the United States annually due to *Salmonella* infections [190]. The 2013 *Salmonella* annual summary stated that *Salmonella enterica* serovar Typhimurium (*S. enterica*) was one of the most commonly isolated serotypes, causing 12.8% of all human salmonellosis illnesses [191], mostly in ready-to-drink (RTD) food.

The risk of contamination by spoilage and pathogenic microorganisms in RTD food is of concern because these products are consumed raw without further preparation or cooking. Orange

juice (OJ), one of the most prevalent sources for bioactive compounds, is an RTD beverage that is usually pasteurized for safety. The current standard for OJ processing and preservation requires reducing microorganism concentration by 5-log cycles (USFDA, 2001). Thermal treatment of OJ at 90 °C for 1 min is currently used to prevent microbial spoilage and inactivate the pectin methylesterase (PME) more than 90-98% [192]. However, thermal pasteurization can adversely affect texture, destroy heat-sensitive nutritional components (such as vitamins), degrade bioactive compounds, and cause unfavorable flavor [193-195]. Vitamin C concentration has reduced by 50 % after pasteurization at 90 C° for 2 min [194]. Therefore, non-thermal techniques are attractive to industry because they can potentially maintain food safety with minimal quality loss [15, 25, 196].

Increasing consumer demand for safe, minimally processed foods has motivated the food industry to investigate new non-thermal processing techniques. Current commercial techniques, including high pressure processing (HPP) and pulsed electric fields (PEF), are expensive due to capital investment, increased labor, and product type [197]. High voltage atmospheric cold plasma (HVACP) treatment offers distinct advantages for food decontamination, including reduced capital and operational costs [2]. Plasma consists of highly energetic species, including photons, electrons, positive and negative ions, free radicals and excited or non-excited molecules and atoms [198]. In atmospheric cold plasma (ACP), the electron temperature is much higher than the ion and neutral temperatures. Therefore, ACP treatment is particularly attractive for food treatment since it does not require extreme process conditions compared to classical preservation methods, such as heat treatments, which adversely impact food texture and bioactive nutrients. While ACP has been commonly used in industrial processes, such as electronics cleaning, bonding plastics, or binding dye to textile fibers, its potential remains untapped in the food industry [149, 199, 200]. HVACP treatment can significantly reduce foodborne pathogens and spoilage microorganisms [16, 22, 95, 97, 201].

The novel, in-package HVACP technology used in this study applies a high voltage (up to 90 kV) to either dry air or modified atmospheric gas (65% oxygen and 30% nitrogen) with the packaging material as a dielectric barrier [46]. We generated the cold plasma by applying a high voltage with low average current (0.2-1.0 mA) through the gas inside the package. This high voltage creates a strong electric field that generates free electrons that interact with nearby gas molecules (O_2, N_2, CO_2, etc.) to form a quasi-stable charged gas species or plasma. The resulting

reactive gas species (RGS), such as NO, NO$_2$, O, ozone (O$_3$), and hydroxyl radicals (OH), have bactericidal, fungicidal, and sporicidal characteristics [202-204]. The HVACP process generates much higher concentrations of RGS than other plasma devices because of its higher voltages while the containment of RGS in the package enhances its effectiveness [41]. Many groups have studied the mechanism of bacterial inactivation by ACP [205-210]. The bactericidal effect arises due to breaking down or causing surface lesions on the bacterial cell wall, loss of membrane integrity or membrane permeabilization, or damaging membrane or intracellular proteins and nucleic acids [68, 97, 211, 212]. In the HVACP process, the RGS convert back to the original package gas (e.g., air) within a few hours, leaving no chemical residuals while significantly reducing microorganisms when present [2]. So far, few studies report ACP induced microbial decontamination in OJ for larger volumes (up to 50 mL compared to past studies at 50 µl [46] using high voltage (up to 90 kV, rather than <50 kV [81] using dielectric barrier discharges (DBDs) to generate ACP, nor for exploring HVACP induced physical and chemical effects in OJ. Therefore, this study provides one of the first feasibility analyses of using HVACP for microorganism inactivation in a relatively large scale (up to 50 mL) of OJ.

The present study assesses the physicochemical interactions between high voltage atmospheric cold plasma (HVACP) and *Salmonella enterica* serovar Typhimurium (*S. enterica*), as well as biomolecules including enzyme, vitamin C and other components in orange juice (OJ) under different conditions, which result in changing OJ's physical and chemical properties. HVACP was generated in a sealed bag, packed with air or modified air (MA65). The effects of plasma exposure model (direct or indirect), treatment time, and post-storage of HVACP were explored on *S. enterica,* pectin methylesterase, vitamin C and other components in orange juice.

2.3   Materials and Methods

Sample Preparation and Bacterial Inoculation

Salmonella enterica serovar Typhimurium ATCC 14028 (*S. enterica*) was obtained from Department of Food Science, Purdue University. *S. enterica*. strains were grown overnight in Tryptic Soy Broth (TSB, Difco^{TM}, MD, USA) at 37 °C for 24 h, in a shaking bath. Samples of OJ was inoculated at 0.1% with the overnight culture to achieve an initial population of approximately 5 log CFU/mL. The initial cell concentration effect on *S. enterica* inactivation

was investigated and optimized to maximize *S. enterica* reduction and exclude cell concentration effects. The optimization procedure included inoculating OJ with an initial concentration of 5-8 log CFU/mL of *S. enterica*, and comparing the inactivation rate after HVACP treatment at 90 kV for 2 min. Correlation between the D-value and initial cell concentration (log) is linear [213].

The Xylose lysine deoxycholate (XLD, Difco^{TM}, MD, USA) selective media was used to enumerate organisms in pre- and post-processed samples. We used peptone water (Bacto, MD, USA) to prepare ten-fold dilution series of samples and plated out 0.1 mL aliquots of relevant dilutions on solid media. Plates were incubated at 37 °C for 24 h and survivors (CFU/mL) were enumerated. We analyzed the duplicate plates for each dilution to determine the number of colony forming units (CFU) and report the counts as the average of three independent HVACP treatments. Treated and untreated samples were enumerated immediately and the following storage at 4 °C for 24 h and 48 h to assess the impact of post-treatment storage.

Sample Packages

Pasteurized orange juice (Tropicana, FL) free of any preservatives and fresh squeezed orange juice (Sunkist, CA) were purchased from a local grocery store. We only use fresh squeezed orange juice to study the enzyme inactivation; all other experiments were performed with pasteurized orange juice. We placed 25 mL and 50 mL OJ samples (control and inoculated with *S. enterica*) onto a Petri dish (diameter: 85 mm) in a storage box, flushed with filling gas for 3 min and sealed it with dry air (<5% relative humidity) or MA65 (65%O_2 + 30%N_2 + 5%CO_2, <5% relative humidity) using a Cryovac® B2630T (Sealed Air, North Carolina, USA) high barrier film to retain the plasma and reactive gas species (RGS). The gas composition in the box has been tested using detector tubes (Dräger-Tubes®, Houston, TX) to confirm its purity of filling gas (air or MA65).
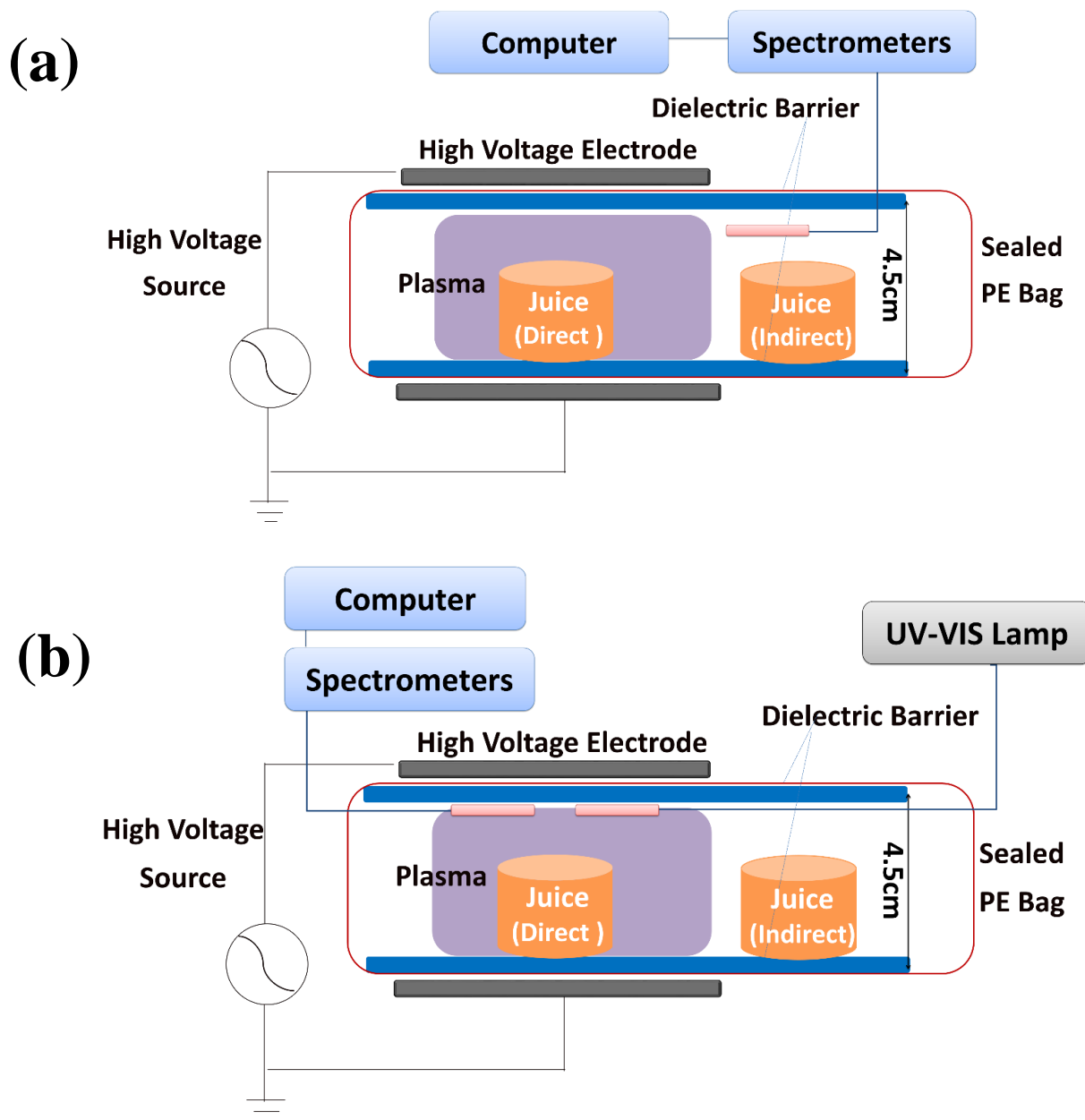
Figure 2.1 Schematic of the experimental setup employed for high voltage atmospheric cold plasma (HVACP) treatment of orange juice (OJ) (direct and indirect). (a) Optical emission spectroscopy (OES). (b) Optical absorption spectroscopy (OAS)

The HVACP device (Figure 2.1) is an atmospheric low temperature plasma generator employed for in-package plasma treatment [129]. We applied up to 90 kV [41]. The HVACP system included a transformer (Phenix Technologies, MD, USA) with an electrical energy input voltage of 120 V (AC) at 60 Hz. A combination of dielectric barriers were assembled to achieve

maximum RGS generation for each gas-package combination. We placed the package between two 15.24 cm diameter aluminum electrodes with a gap of 4.44 cm, and the two Cuisinart® (Cuisinart, New Jersey, USA) polypropylene layers ($355 \times 272 \times 2.20$ mm) above and below the package as additional dielectric barriers. We, directly and indirectly, exposed 25 and 50 mL of OJ to 90 kV for 30, 60, and 120 s. The treated samples were stored in a refrigerator at 4°C for 24 h to study the dependence of microorganism population on post-treatment storage. XLD agar (Difco) was used to enumerate *S. enterica*.

Optical Emission Spectroscopy (OES) and Optical Absorption Spectroscopy (OAS)

We used optical emission spectroscopy (OES) to characterize the reactive gas species generated in the plasma during the treatment and optical absorption spectroscopy (OAS) to investigate the gas composition post-discharge [44, 214]. OES and OAS were measured using an HR2000+ Spectrometer and 400 mm optical fibers produced by Ocean Optics (FL, USA). The fibers had a numerical aperture of 0.22 and were optimized for use in the ultraviolet and visible portion of the spectrum with a wavelength range 190 nm to 1100 nm. The distance between the optical fiber and the plasma chamber was 140 mm. The OES spectra were corrected for background noise and recorded every 30 s during the HVACP treatment at 90 kV. The data was recorded and analyzed using OceanView Optics Software (Dunedin, FL). We identified the peaks by comparing them with the NIST Atomic Spectra Database [129].

We investigated the post-discharge gas composition using OAS. Using a UV-visible (UV-Vis) deuterium-hydrogen lamp as light source, we measured the transmitted light with an Ocean Optics (HR2000+) spectrometer. The optical probes (insulated UV-Vis collimators) were aligned inside the sealed package for all experiments, with an optical path length of 2.4 cm between the probes. Based on Moiseev's method, we used the Beer-Lambert law to calculate the concentrations of ozone (O_3) and nitrogen oxides (NO_2, NO_3, N_2O_4) by averaging concentration along a wavelength interval where each species has an absorption cross-section maximum or values much higher than other absorbent species [44].

Color, pH and Brix measurement

Juice color was measured using a HunterLab colorimeter (ColorFlex modelA60-1010-615, Hunter Associates Inc., Reston, VA) at 20 ± 1 °C. The instrument (65°/0°geometry, D25 optical

sensor, 10°observer) was calibrated using white (L = 92.8; a = -0.8, b = 0.1) and black reference tiles. Expressing color values as L^* (whiteness/darkness), a^* (redness/greenness), and b^* (yellowness/ blueness) allows us to calculate the color difference (ΔE) in OJ after treatment by

$$\Delta E = \sqrt{(L^* - L_0)^2 + (a^* - a_0)^2 + (b^* - b_0)^2}, \tag{1}$$

where L_0, a_0, and b_0 are the color values of control juice samples. Depending on the magnitude of ΔE, one can characterize the development in color difference during storage time as not noticeable (0–0.5), slightly noticeable (0.5–1.5), noticeable (1.5–3.0), well visible (3.0–6.0) and great (6.0– 12.0) [215]. We performed the color measurement in triplicate.

The pH of treated and untreated orange juice samples was measured using a digital pH-meter (Orion model 420A, Allometrics Inc., Seabrook, TX). Continually stirred samples (10 mL) were measured at 20 °C.

We measured Brix using an ATAGO™ refractometer (Digital Hand-Held Pocket Refractometer PAL-1) at 20 °C. The refractometer of the prism was cleaned with distilled water after each analysis.

Vitamin C Determination

We used a high-performance liquid chromatography (HPLC) system to measure the total vitamin C content, including ascorbic acid (AA) and dehydroascorbic acid (DHAA), based on Ayhan's method [216]. A Hewlett-Packard liquid chromatograph (Wilmington, DE) equipped with an auto-sampler and a detector at 254 nm was used. We calculated the HPLC chromatograph peak area using a Hewlett-Packard integrator (HP3396 Series II). A reversed-phase C-18 column (5 µm particle size, 4.6 mm diameter, 250 mm length, Hewlett-Packard) and a Hewlett-Packard C-18 guard column separated the AA using methanol and acidified water (10:90, v/v) as a mobile phase. The water was acidified (0.01%, v/v) with phosphoric acid (90%). The mobile phase was filtered using a 0.45 µm membrane filter (Micron Separations Inc., Westboro, MA) and degassed using ultrasound before passing through the column at a flow rate of 0.5±0.01 mL/min. We observed a standard calibration curve by using L-ascorbic acid (Sigma Chemical Co., St. Louis, MO) in concentrations ranging from 5 to 80 mg/100 mL. The OJ was derivatized with dithiothreitol before analysis to reduce the DHAA to the AA. We centrifuged the OJ at 8000g for 10 min in a

Beckman Microfuge E (Beckman Instruments Inc., Palo Alto, CA) to remove pulp and coarse cloud particles. We injected 10 µL of the supernatant into the column using the HPLC auto-sampler. We determined the reproducibility of six-time analyses per each orange juice sample based on a relative standard deviation ± 5%.

Pectin Methyl esterase (PME)

PME activity was determined by titrating the liberated carboxyl group at pH 7.5 (30 °C) based on the methods reported by Rouse and Atkins [217]. After mixing the OJ sample (from freshly squeezed juice) well, we transferred 5 mL into 50 mL of a 1% pectin substrate solution in 0.2 M sodium chloride. The sample was titrated to pH 7.5 with 0.2 N NaOH, which was maintained for 30 min by titrating 0.05 N NaOH to the sample. The volume of 0.05 N NaOH consumed during this time was recorded. We determined the PME activity, P_a in PME units (PMEu) per gram by

$$P_a = \frac{V_N N_N}{m \times (30 \text{ min})},\qquad(2)$$

where V_N is the volume of NaOH in mL, N_N is the normality of NaOH, and m is the mass of the sample in grams.

Statistical Methods

We used SAS Version 10.1 (Statistical Analysis Software, Cary, NC) to analyze all resultant gas concentrations and microbial populations. Statistical analysis of results utilized a general linear model (GLM) for unbalanced datasets and Analysis of Variance (ANOVA) procedure for balanced data. We determined the mean differences by using Duncan's LSD Test for separations of means showing significant differences ($P < 0.05$). The mean and standard deviation were calculated for the log reduction of microorganisms for each set of experiments. A 95% confidence interval was used for all procedures.

2.4 Results

2.4.1 Effect of HVACP on the Microbes in OJ

2.4.1.1 Effect of Gas Composition
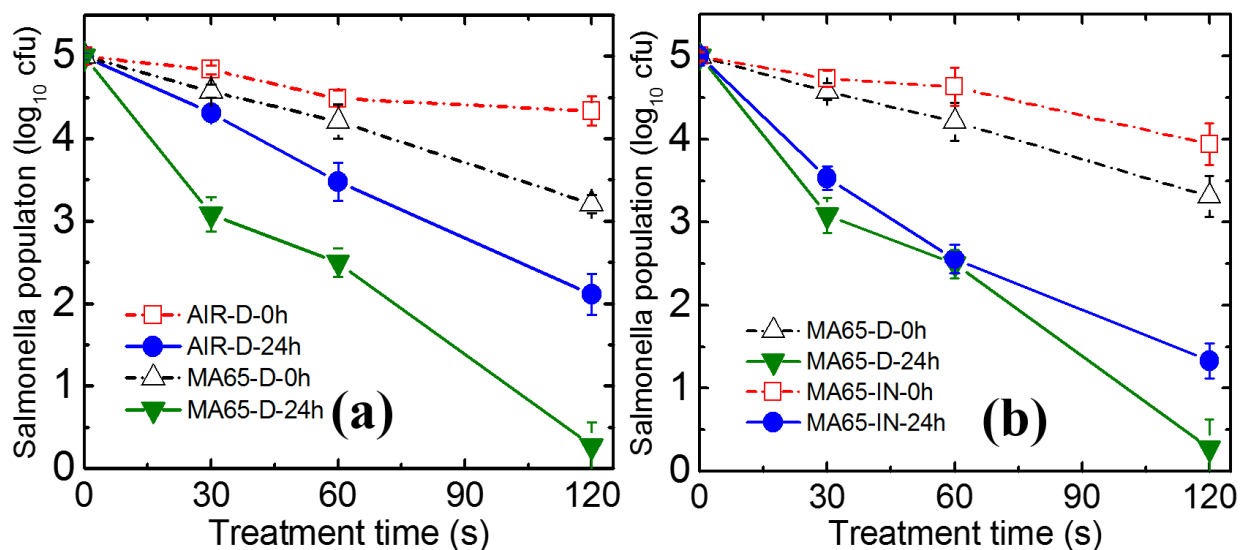
Figure 2.2 The survival of Salmonella enterica serovar Typhimurium (S. enterica) population (log10 CFU) is as a function of treatment time. (a) 50 mL OJ packed with air or MA65 are treated with HVACP at 90 kV. OJ subject direct HVACP treatment: (□) air packed; (△) MA65 packed. HVACP treated OJ after 24 h post-storage: (●) air packed; (▼) MA65 packed. (b) 50 mL OJ packed with MA65 are treated with HVACP at 90 kV directly or indirectly. OJ subject HVACP treatment: (△) direct treatment; (□) indirect treatment. HVACP treated OJ after 24 h post-storage: (▼) direct treatment; (●) indirect treatment. Values represent the mean and standard deviations of three replicates.

Figure 2.2 shows the effect of the gas composition on the *S. enterica* inactivation. A 2 min HVACP treatment with air or MA65 as the fill gas followed by 24 h of post-treatment storage resulted in *S. enterica* inactivation with only a 2 min HVACP treatment. In this study, we determine the inactivation of *S. enterica* by using XLD to enumerate the population difference before and after treatment. The sublethally injured cells, which can reproduce and form colonies on Tryptic Soy Agar (TSA) but not in XLD, were not counted as surviving/viable bacteria after HVACP treatment because they lost metabolic activity [218].

The population of *S. enterica* in OJ decreases with treatment time. Immediately after subjecting OJ to 2 min of HVACP direct treatment, decreased *S. enterica* population by 0.65 and

1.75 log in air and MA65, respectively. The population of *S. enterica* continued to decrease after 24 h of post-treatment storage (incubation OJ without opening the package at 5°C). Following 24 h of post-treatment storage, the population of *S. enterica* in 50 mL of OJ subjected to 2 min HVACP treatment decreased by 2.81 log (air) and approximately 5 log (MA65) without recovery. This indicates that HVACP generated RGS remain in the package and can inactivate *S. enterica* after removing the electricity. MA65 is more effective in inactivating *S. enterica* in OJ compared with air, which may correlate to the different RGS generated during HVACP treatment.

2.4.1.2   Direct vs. Indirect

Figure 2.2 shows that both direct and indirect HVACP treatment can achieve microbial decontamination. Other studies [68, 212] demonstrated direct plasma treatment more efficiently inactivated *S. enterica* than indirect treatment. There is no significant difference ($P < 0.05$) between direct and indirect treatment for short (< 1 min) HVACP treatment time. A 2 min direct HVACP treatment of 50 mL OJ resulted in a 1.75 log (MA65) reduction immediately (0 h) after treatment while indirect treatment induced a 0.85 log (MA65) reduction (Figure 2.2 a). Applying a 24 h post-treatment storage after 2 min HVACP with MA65 reduced *S. enterica* population by 3.78 log with indirect exposure and by greater than 5 log (under the population threshold for detection) with direct exposure (Figure 2.2 a). In Figure 2.2 b, the high microbial inactivation in direct (MA65-D-24h) compared with indirect (MA65-IN-24h) exposure at 120s may arise due to undetectable RGS, UV light, electroporation [219] or other short-lived species (many of which are not available for OJ during indirect treatment) that may also have microbiocidal effect. This high inactivation effect in direct treatment has been reported previously [63, 212]. Stoffels *et al.* [63] reported that during direct treatment, the most reactive short-living species (such as charged species and certain radicals) have the highest probability of reaching the surface [63]. Also, the bombardment of charged RGS in direct treatment [146] may facilitate RGS diffusion into the liquid to generate microbiocidal compounds [220, 221]. An electric field will enhance the mass transfer by electroporation [219], which facilitates RGS diffusion. Dobrynin *et al.* [146] reported that the microbiocidal effect of plasma treatment in the liquid may be enhanced due to energetic ion bombardment [146]. In the 50 mL OJ sample, there is no significant difference between direct and indirect treatment for short treatment times. Differences detected following 24 h of post-storage incubation (Figure 2b) indicate that the long-living RGS, including hydrogen peroxide,

and ozone, contribute to the microbiocidal effect of HVACP. Therefore, both direct and indirect treatment can achieve a 3.5-5 log *S. enterica* reduction in 50 mL OJ with 2 min HVACP treatment and 24 h post-storage.

2.4.1.3 Effect of Sample Height and Exposure Surface Area
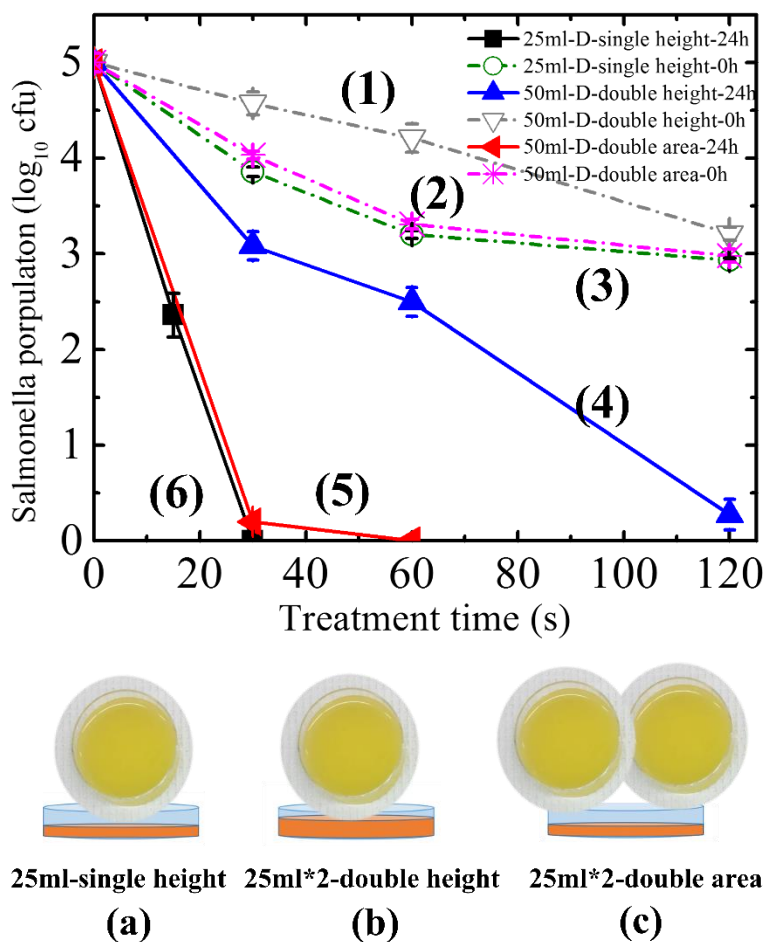
Figure 2.3 The survival of S. enterica population (log10 CFU) is influenced by exposure surface and sample height. 25 mL or 50 mL of OJ packed with MA65 treated directly with HVACP at 90 kV. The survival of S. enterica population (log10 CFU) is as a function of treatment time. OJ subject HVACP treatment: (1) 50 mL OJ with double height (9 mm); (2) 50 mL OJ with double area (56 cm2×2); (3) 25 mL OJ with single height (4.5 mm). HVACP treated OJ after 24 h post-storage: (4) 50 mL OJ with double height; (5) 50 mL OJ with double area; (6) 25 mL OJ with single area (56 cm2). Values represent the mean and standard deviations of three replicates test.

We next investigated the effect of sample height and exposure surface area on the *S. enterica* inactivation efficiency of HVACP treatment. With the same exposure surface area, the inactivation

of *S. enterica* in 25 mL OJ (sample a, Figure 2.3 a) is higher than 50 mL OJ (sample b, Figure 2.3 b). Within 30 s, HVACP direct treatment achieved greater than 5 log reduction (detection limit) of *S. enterica* in sample (a); however, it required 120 s to achieve 5 log reduction in sample (b) with double height (10mm). With the same sample volume (50 mL), the inactivation of *S. enterica* with the double exposure surface (Figure 2.3 c) in OJ is higher than the single exposure surface of OJ (Figure 2.3 b). Within 60 s, HVACP achieved greater than 5 log reduction of *S. enterica* in sample (c). This indicates that for a certain volume of OJ, increased exposure surface and minimized sample thickness will achieve a high *S. enterica* inactivation efficiency, which may accelerate RGS diffusion into OJ. This agrees with other reports [222, 223]. Microbial inactivation efficiency of plasma is influenced by the sample depth, sample volume, and food composition [223]. Therefore, increasing the exposure surface and minimizing OJ sample thickness is critical for maximizing *S. enterica* decontamination using HVACP.

2.4.1.4   Optical Emission Spectroscopy
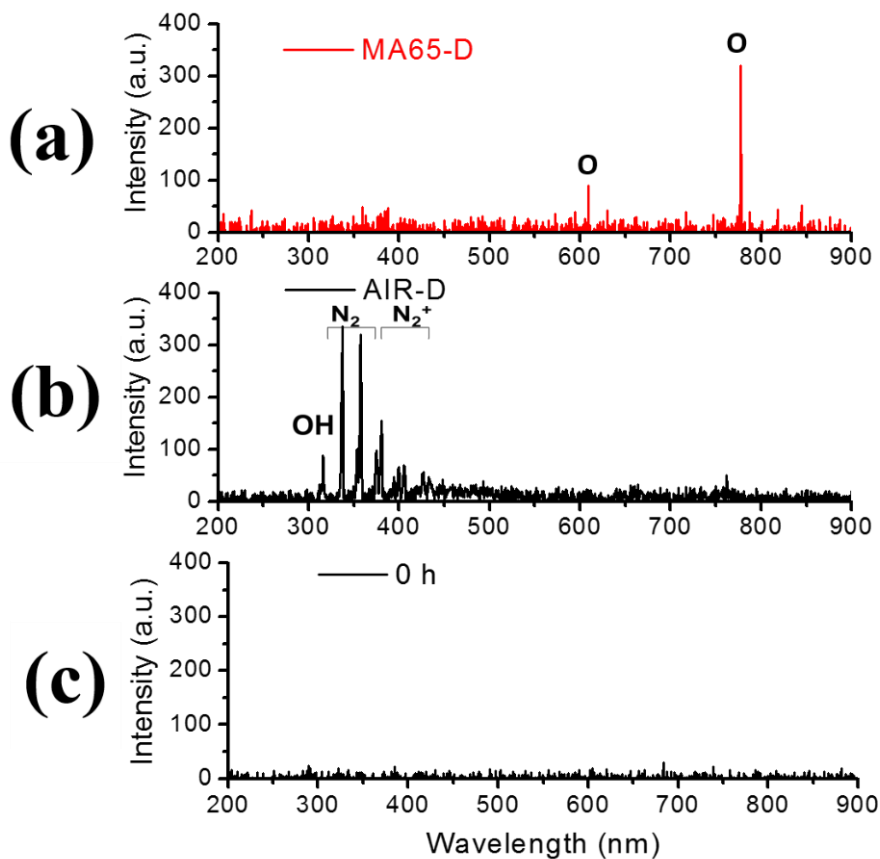
Figure 2.4 Optical emission spectroscopy results of MA65 (a) and air (b) packed OJ during HVACP treatment (direct) at 90 kV for 2 min. (c) Optical emission spectroscopy of control.

Table 2.1 The major peaks in the spectra correspond to the emissions of excited species.

Wavelength (nm)	309	336	357	380	390	405	426	616	673	686	777
Species	OH	N_2	N_2	N_2	N_2^+	N_2^+	N_2^+	O_2^+	O_2^+	O_2^+	O

We used OES to characterize the different main emissions of the RGS generated by air and MA65 during direct and indirect treatment. Figure 2.4 and Table 2.1 show that the recorded spectrum consists of various molecular and atomic nitrogen and/or oxygen species. During treatment, both direct and indirect treatment can generate RGS, which have microbiocidal effects.

The major peaks in the spectra correspond to the emissions of excited species of atomic nitrogen and atomic oxygen, including the nitrogen second positive system N2(C-B) [224], the first negative system N2+ (B-X) (at 336, 357, 380, 390, 405, 426 nm) and optical transitions of the O atom, including 616 nm and 777 nm [225, 226]. The OH peak around 309 nm was also identified. Figure 2. 4 indicates that using MA65 as the fill gas generates primarily reactive oxygen species (ROS) while air generates reactive nitrogen species (RNS), which may contribute to the different microbial decontamination efficiency. At the same time, the different active ions and free radicals reach the liquid phase and produce various biologically active reactive species (PRS) in the liquid phase [146, 209], including long-lived PRS, such as hydrogen peroxide (H_2O_2), ozone (O_3), and nitrate ion (NO_3^-), and short-lived PRS, such as hydroxyl radical (OH^-), superoxide (O_2^-), and singlet oxygen [227]. The signal will disappear after removing the field from the sample due to the short-living life of the atomic species and will either generate long-living species through complicated reactions or react with the liquid phase. There are more than 75 species generated among 500 reactions as a function of treatment time and energy scale [158], which have microbiocidal effects and are undetected by OES.

2.4.1.5   Optical Absorption Spectroscopy
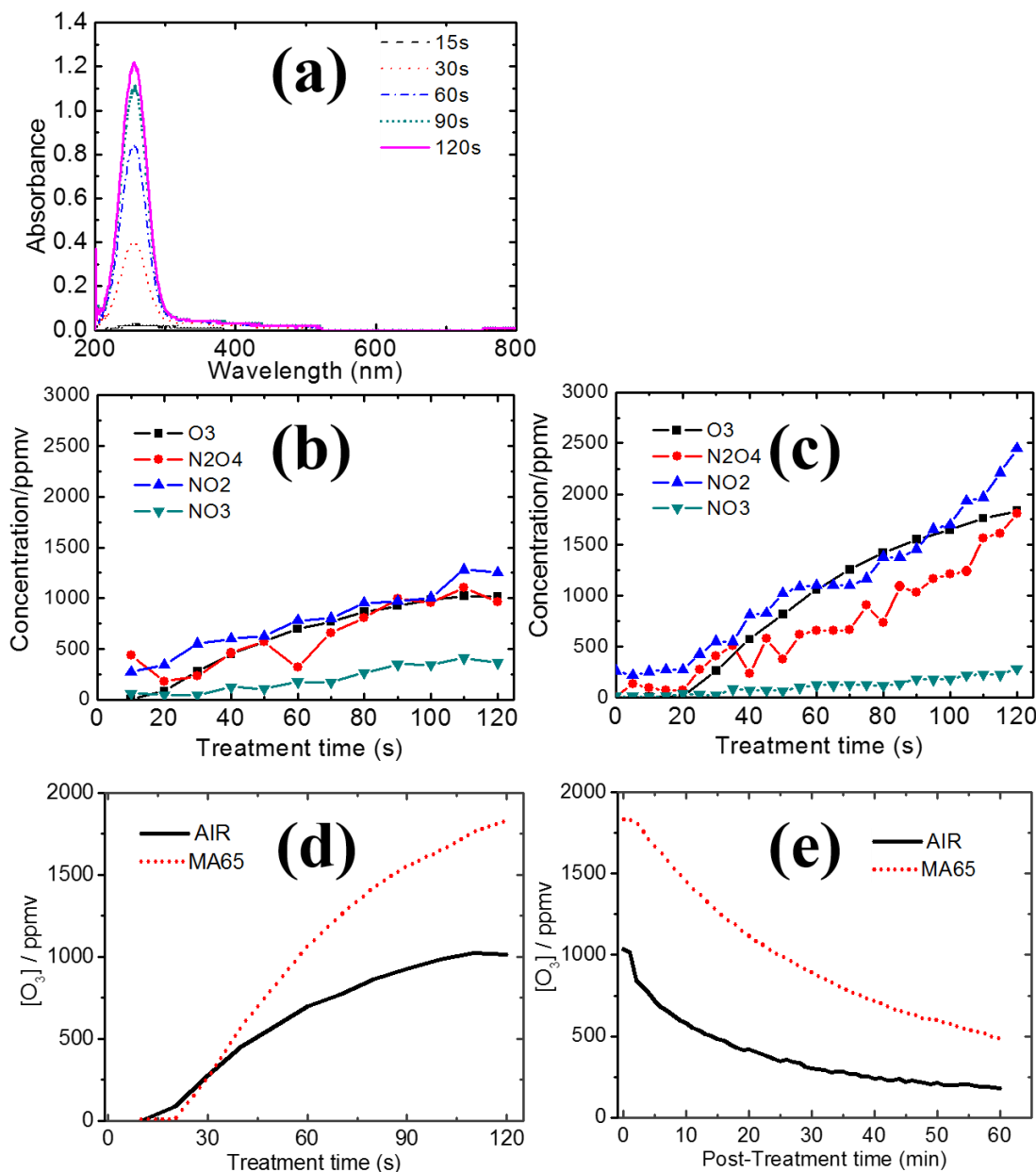
Figure 2.5 (a) Optical absorption spectroscopy (OAS) signals of MA65 packed OJ during HVACP treatment (direct) at 90 kV for 2 min. (b) (air) and (c) (MA65), Concentration of reactive gas species (O3-black, NO2-blue, NO3-green, N2O4-red) of MA65 packed OJ during HVACP treatment (direct) were calculated from OAS signals of Figure 2.5 a, based on the Beer–Lambert law by averaging concentration along a wavelength interval. (d) O3 concentrations in air (straight line) and MA65 (●) packed OJ (50 mL) during HVACP treatment (direct) at 90 kV for 2 min, (d) O3 concentrations during post-treatment storage.

Figure 2. 5a shows the typical absorbance during HVACP treatment with the intensity increased with increasing treatment time. The concentration of O_3 and nitrogen oxides (NO_2, NO_3, N_2O_4) was calculated based on their optical absorbance [44, 228], as shown in Figure 2. 5b. Within 2 min of HVACP direct treatment, O_3 concentrations were 1660 ppmv in MA65 and 990 ppmv in dry air (5% humidity) packed samples. These high concentrations of O_3, as well as NO_2, NO_3, and N_2O_4 generated by MA65 may contribute to its higher microbial inactivation rate than air. Therefore, using MA65 which has a higher concentration of O_2, as the plasma generation gas enhances its microbial inactivation effectiveness, as observed in other studies [45, 204, 229]. Upon turning off the HVACP, the OAS signal slowly decreased (fitting second order polynomial model- MA65: $y = 0.3315x^2 - 42.692x + 1891.9$, $R^2 = 0.9977$; air: $y = 0.2821x^2 - 28.278x + 902.32$, $R^2 = 0.9627$) indicating the correlated RGS do not disappear immediately and can continue inactivating bacteria during post-treatment. This is consistent with the extra reduction during the post-treatment (Figure 2.2 and 2.3). However, HVACP generates numerous additional species that could contribute to the observed mechanisms and should be considered, such as HONO, HO_2NO_2, and HNO_3 [214], which currently are not measurable with OAS.
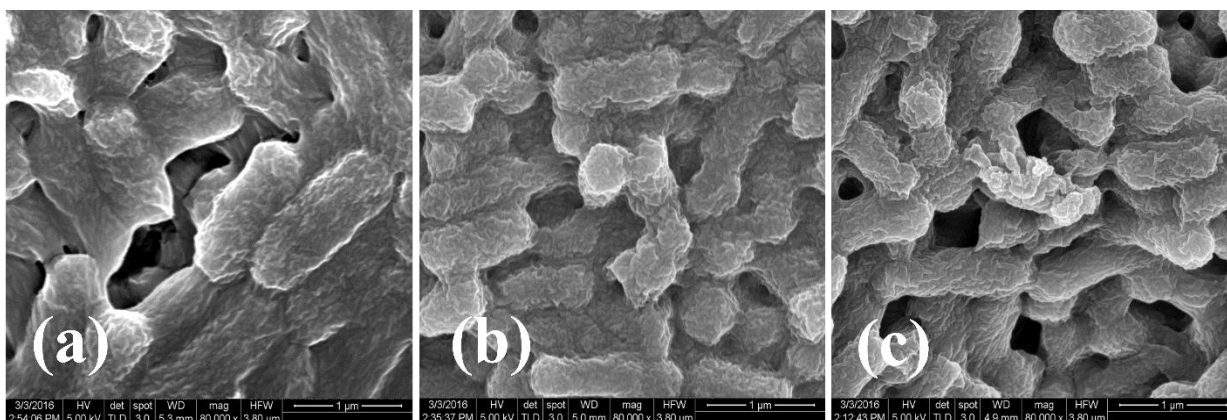
Figure 2.6 Scanning electron microscope image of S. enterica cells in the control and OJ subjected HVACP treatment (direct) at 90 kV for 120 s. S. enterica were isolated from OJ by centrifugation and washed with phosphate buffer saline. (a) Control, (b) air packed, (c) MA65 packed OJ.

2.4.1.6   Structure Analysis Using Scanning Electron Microscope

Figure 2.6 shows an SEM image of *S. enterica* cells in the control and in OJ subjected to HVACP treatment for 120s. *S. enterica* in the control have relatively smooth bacterial cell walls

(Figure 2.6 a), while the cell surface wrinkles and the cell lyses for HVACP treated *S. enterica* in both air and MA65 packed OJ samples (Figure 2.6 b, c). This is consistent with other reports [97, 212, 230]. Cell morphology has changed compared to the control. In Figure 2.6c and its replications, SEM showed cell alterations in HVACP-treated bacteria surface morphology and loss of integrity. Severe physical damage, including etching and irregular surfaces on the *S. enterica* cells, also occurred. Han *et al.* [165] reported that HVACP induced microorganism inactivation occurred due to RGS either reacting with the cell membrane or damaging intracellular components (e.g., nucleic acids, proteins/enzymes) [165]. The mechanism of various RGS on the bacteria could be investigated by checking the effect on cell membrane integrity: absorbance of intracellular components is at 260 nm for nucleic acid, at 280 nm for protein.

2.4.2 Effect of HVACP on the Enzyme, Vitamin C and other components of OJ

2.4.2.1 Pectin Methylesterase
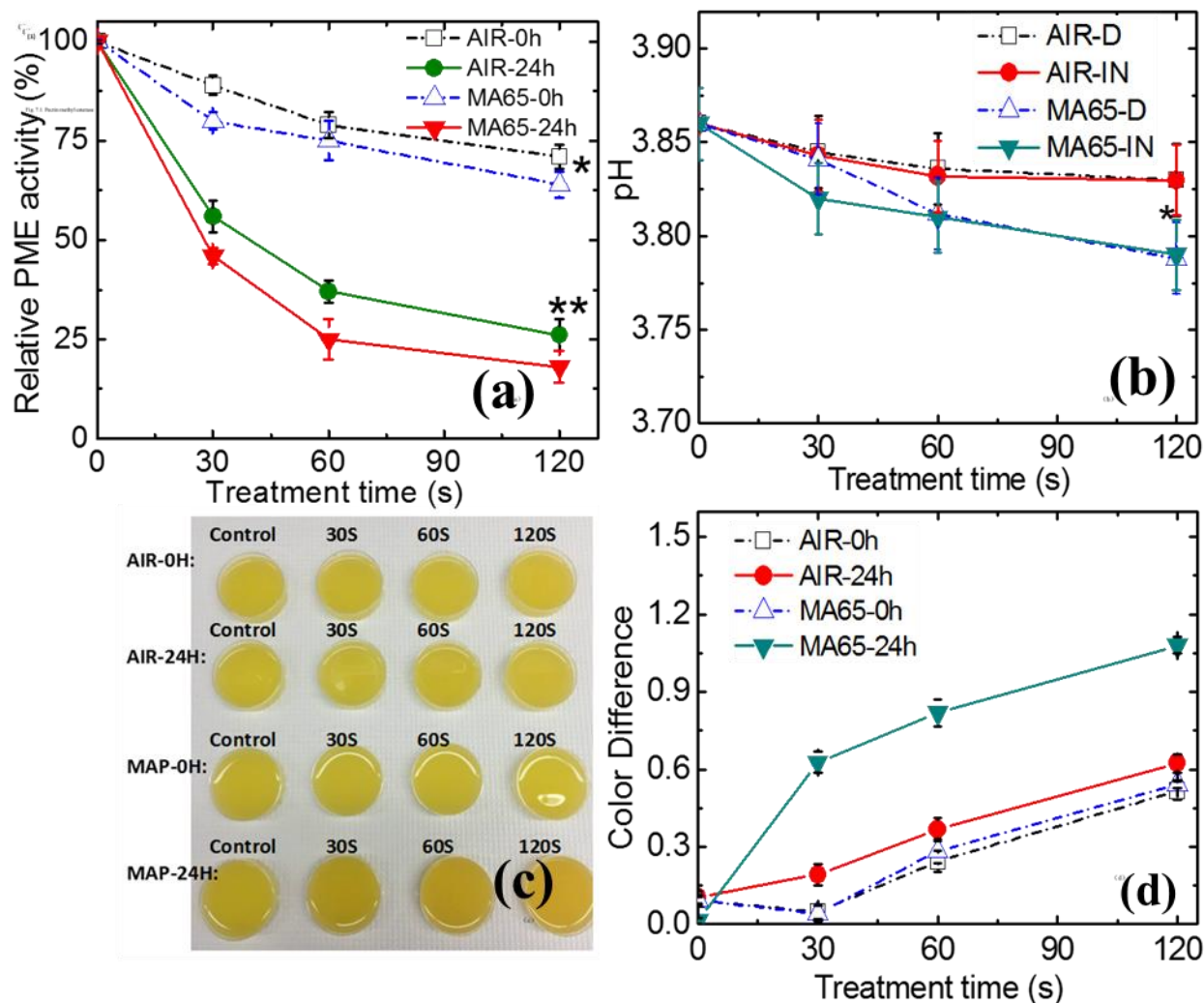
Figure 2.7 (a) Pectin methylesterase (PME) activity. (b) pH of OJ packed with air and MA65 subjected HVACP treatment (direct) at 90 kV for 120 s. (c) Color observation and (d) The color difference (ΔE) of OJ packed with air and MA65 subjected HVACP treatment (direct) at 90 kV up to 120 s. Color OJ subjected HVACP treated at 0 h and after 24 h post-storage were compared.

Figure 2.7a shows the residual activity of the PME as a function of treatment time. The activity of PME decreased with increasing HVACP treatment time using either air or MA65 as the fill gas. 24 h post-treatment storage further inactivates PME by 73-76% compared to its activity in fresh

OJ. A 16% residual PME activity was observed after OJ pasteurization at 66°C for 60 s and 99% PME was inactivated at 90°C for 60 s [231]. Therefore, a higher PME inactivation may be achieved by increasing HVACP treatment intensity. The inactivation of PME may relate to its structural modification, which was caused by RGS, and the PRS generated in the liquid phase. The mechanism of PME inactivation by HVACP treatment has not been reported before. It is estimated that ROS initiated structure modification of PME by oxidative attack leads to loss of enzyme functionality, which is consistent with other reports [93, 232-234] confirmed that hydroxyl radicals (OH), superoxide anion radicals (O_2^-), hydroperoxy radicals (HOO) and nitric oxide (NO) generated from plasma sources may modify reactive side-chains of the amino acids, such as cysteine, and aromatic rings of phenylalanine, tyrosine, and tryptophan, leading to loss of enzyme activity. Figure 2.7a also indicates that using MA65 as the fill gas more efficiently inactivate PME, for which may relate to its higher ROS species concentration. For instance, the concentration of O_3 in MA65 (1810 ppm) is higher than air (930 ppm) at 120 s, indicating a higher oxidative capacity. However, the generation of hydroxyl radicals and nitrous/nitric acid in the liquid phase [208, 220, 235] may also accelerate the PME inactivation. The PRS transported from the gas phase into the liquid transform via successive reactions into products that inactivate enzymes [236]. Therefore, RGS and PRS generated in the liquid inactivate PME in OJ during HVACP treatment.

2.4.2.2 Vitamin C Content

Vitamin C content is an important parameter to evaluate the nutritional quality of OJ [196, 237]. Vitamin C is heat-labile and easily destabilized during thermal processing or post-storage [238, 239]. In this study, vitamin C content is the total concentration of AA and DHAA, which is consistent with industry requirements and other studies [238, 240]. Figure 2.8 shows the vitamin C content after HVACP treatment compared with untreated OJ. The vitamin C concentration decreases as a function of increasing treatment time: from 53 mg/100mg (control) to 41 mg/100mg (in air) and 24 mg/100mg (in MA65), after 2 min HVACP treatment subject 24 h post-storage. A minimum of 30 mg of vitamin C per 100 mL of juice is required to meet the commercial standard (US Food and Drug Administration, 2016). This loss of vitamin C may arise due to the high concentration of ROS and RNS in the RGS generated by HVACP. AA is sensitive to O_3 and easily degraded by other free radicals [241, 242]. Traditional thermal processing frequently uses a higher temperature to establish more excessive PME inactivation but inevitably induces vitamin C

breakdown. The previous report indicated that OJ subject conventional thermal treatment at 90 C°
for 2 min [194], the retention of vitamin C was less than 50 %. Since HVACP is a non-thermal
processing technology, it may better preserve vitamin C by using a different fill gas to generate
RGS and may inactivate PME while preserving vitamin C concentration.

2.4.2.3 pH, Brix, and Color

HVACP treatment reduced pH from 3.86 to 3.80 (Figure 2.7b); ºBrix did not change
significantly ($P < 0.05$) in OJ after HVACP treatment (data not are shown). The pH decrease
might be due to the formation of nitric acid (HNO_3) and nitrous acid (HNO_2) in the liquid phase
[220]. Helmke *et al.* (2011) reported that pH following plasma treatment depended strongly on
treatment time [243] which is consistent with the results in Figure 2.7b. Further analysis of the
acid profile may better explain the mechanism of the pH shift since OJ has its own buffering
capacity, consisting of citric acid, malic acid, and ascorbic acid.

Figure 2.7c shows pictures of OJ with air/MA65 before and after post-storage, demonstrating
the color of OJ subject to HVACP treatment. The United States Department of Agriculture (USDA)
assigned 40 points out of a scale of 100 points for color for the commercial classification of OJ.
Grade A OJ must have a color number between 36 and 40 points, while grade B OJ has color
numbers ranging from 32 to 35 points [244, 245]. However, according to Cserhalmi *et al.*'s report
that it is more valuable to compare the color difference (ΔE) values of OJ [215]. Figure 2.7d shows
ΔE, which is the sum of the square of the changes in L^*, a^*, and b^*. We consider ΔE because the
consumer will more likely perceive the total change in color than the individual L^*, a^* or b^* values.
Treating OJ with HVACP for 120 s yielded ΔE of 0.51 (air) and 0.54 (MA65), which were
classified as slightly noticeable (0.5-1.5). The largest ΔE for HVACP treated OJ was 1.08, which
is still within the range of slightly noticeable (0.5-1.5), following 24 h of post treated-storage of
OJ packed with MA65 [215]. Although some color parameters presented statistical difference ($P
> 0.05$), the characteristic juice color remained in the expected ranges for OJ with a slight increase
in ΔE. Different plasma gas resources (e.g., helium) or reduced treatment time may mitigate the
slight color change.

2.4.3 Discussion

The effect of HVACP on *S. enterica* inactivation depends on the mode of plasma exposure, gas type, exposure surface area, and treatment time. It is hypothesized that HVACP primarily inactivate microorganisms in liquid food by creating RGS and subsequent PRS (generated by RGS in the liquid phase through chemical reactions), which induce DNA/protein alteration, integrity loss and cell lysis [208, 209, 246]. Charged species were identified as the major contributors to the microbiocidal effect. ROS, including hydroxyl radicals (OH), hydrogen peroxide (H_2O_2), and the superoxide anion (O_2^-), induce DNA breakdown inside the cells [146]. A combination of plasma induced membrane pore formation and peroxidation may lead to cell damage/apoptosis and loss of bioactivity and functionality [146, 207]. Various CAP-microorganism inactivation models have been proposed, including direct destruction of microbial genetic material by UV irradiation, cell surface etching induced by RGS, volatilization of compounds and intrinsic photodesorption of UV photons [22]; and that is followed by PRS formation in the liquid phase [46, 247, 248] reported that ROS and RNS played dominant roles in microbial inactivation by reacting with various macromolecules on the microorganisms' outer surfaces (such as membrane lipids), or inside the microorganisms (protein and nucleic acids) to induce microbial death or injury in OJ. Therefore, the higher concentrations of ROS and RNS generated by HVACP, characterized by OES and OAS (Figure 2.5), may enhance microbial inactivation. In this study, treatment factors, such as using MA65 with high O_2 concentration to generate effective RGS (Figure 2.4) or using direct treatment with a large surface exposure combined with sufficient treatment time, may facilitate interactions between RGS and *S. enterica* to optimize microbial inactivation (Figure 2.2 and Figure 2.3).

The quality of OJ, including PME activity, pH, color and vitamin C content, depends on HVACP treatment time, fill gas, exposure model, and post-storage time. This is primarily related to the specific RGS formed and their concentrations under various conditions. ROS and RNS initiate multiple chain reactions, resulting in numerous chemical reactions and species, including the following [33]:

$$OH + NO \rightarrow NO_2^- + H^+ \tag{1}$$

$$O + H_2O \rightarrow 2OH^- \tag{2}$$

$$2OH \rightarrow H_2O_2 \tag{3}$$

$$OH + H_2O_2 \rightarrow OOH + H_2 \qquad (4)$$

$$OH + NO_2^- \rightarrow OH^- + NO_2 \qquad (5)$$
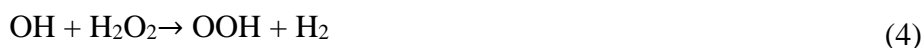
Surowsky *et al.* [33] reported the following chemical reactions occur at the gas-liquid interface: (1) acid-base reactions, (2) oxidation reactions, (3) reduction reactions caused by reductive species (e.g., H and HO radicals) and (4) photochemical reactions initiated by UV radiation from the plasma [33]. The pH decrease in Figure 7.2b occurred due to the formation of nitrous and nitric acids, excited nitrogen species, and their products (NO_2^-, NO_3^-), as well as singlet oxygen during plasma treatment, which is more predominant in non-buffered solutions [15]. Oxidation reactions initiated by ROS and RNS are the most important plasma-related reactions which may inactivate microorganisms and degrade organic compounds. This may be responsible for the vitamin C loss and color alteration [242]. In this study, using MA65 as process gas combined with a longer treatment time is preferred for inactivating PME and *S. enterica* in OJ. However, color retention was greatly reduced during subsequent storage using MA65 as a process gas, whereas the color was less affected by the use of ambient air, which was consistent with previous studies [249]. Therefore, adjusting the gas composition to control the gas RGS formation can minimize both color alteration and vitamin C loss. Therefore, elucidating the inactivation mechanism and reaction rate between HVACP to PME, vitamin C, and other chemical compounds will enable the development of an efficient HVACP system for decontaminating *S. enterica* in OJ without quality alteration.

2.5   Summary

This study examined the physicochemical interactions between high voltage atmospheric cold plasma (HVACP) and biomolecules including *Salmonella enterica* serovar Typhimurium (*S. enterica*), enzyme, vitamin C and other components in orange juice (OJ) under different conditions. Efficient *S. enterica* inactivation has been achieved by using either air or MA65 as the fill gas in HVACP treatment of OJ. We achieved more than 5 log reduction of *S. enterica* in 25 mL OJ within 30 s of direct or indirect HVACP treatment using either air or MA65 as fill gas. For 50 mL OJ, 120 s of direct HVACP treatment and 24 h storage induced a 2.9 log reduction of *S. enterica* in the air and a 4.7 log reduction in MA65 gas. Therefore, MA65 more effectively inactivates *S.*

enterica in OJ compared to air, likely due to the different RGS generated during HVACP treatment. Using MA65 as the fill gas, extending treatment time, and expanding exposure surface can maximize inactivation of *S. enterica* population and PME activity of HVACP treatment. The concentration of vitamin C decreased by 56% after 120 s HVACP direct treatment in 25 mL air packed OJ compared with untreated OJ. No significant color, brix, nor pH change occurred following 120 s HVACP treatment. Therefore, we conclude that HVACP treatment can be an effective non-thermal technology to control, or potentially eliminate *Salmonella* in OJ without quality alteration. The mechanisms of the physicochemical interactions between HVACP and bacteria will be examed in next Chapter.

CHAPTER 3. PENETRATION AND MICROBIAL INACTIVATION BY HIGH VOLTAGE ATMOSPHERIC COLD PLASMA IN SEMI-SOLID FOOD

3.1 Abstract

Multiple studies have demonstrated atmospheric cold plasma as an effective non-thermal technology for eliminating bacteria, spores and other microbial contaminants from food and non-food surfaces. However, few studies have applied this technique to semi-solid food within a package. This study evaluates the efficacy and the interaction mechanism of high voltage atmospheric cold plasma (HVACP) on *Salmonella enterica serovar Typhi* (*S. enterica*) decontamination in agar gel with different compositions. HVACP was generated by a dielectric barrier discharge in air and a modified atmosphere (MA65: 65% O_2) in sealed bags. Agar gels of various densities with a pH indicator were inoculated with *S. enterica* (10^7>CFU) and exposed directly (between the electrode) or indirectly (adjacent to the electrode) to 90 kV at 60 Hz for up to 1.5 hours. HVACP induced greater than 6 $\log_{10}$ (CFU) reduction (both with air and MA65) in the plasma penetrated zone with a pH change. Inactivation of bioluminescence cells in the plasma penetrated zone confirmed that the plasma, and its generated reactive species, inactivates microbes as it penetrates into the gel. A two-minute HVACP treatment induced greater than 5 $\log_{10}$ (CFU) *S. enterica* reduction in applesauce. In summary, these results demonstrate that HVACP can be an effective non-thermal technology to control or even eliminate bacteria populations in semi-solid food.

3.2 Introduction

Atmospheric cold plasma (ACP) has been applied as a novel non-thermal technology in multiple biological, medical, and agricultural fields, including waste treatment, surface modification, nanomaterial synthesis, food processing, cancer treatment, and wound healing [14, 84, 90, 96, 250, 251]. The advantages of ACP include reduced capital and operational costs [2] [197], flexible application to both liquid and solid matrices [78], and easier handling and maintenance [1]. A major limitation for applying ACP in these applications is its limited

penetration depth through liquids and solids [87, 252, 253]. Therefore, quantifying the penetration capacity of ACP species and the impact of this penetration on ACP efficacy will benefit future experimental design and broaden the application of this non-thermal technique.

Many previous studies assess ACP for treating the surface of solids or liquids for surface modification [254-258], sterilization [16, 22, 42, 86, 259, 260], and chemical catalysis [1, 83, 129, 163]. Industrial applications include food processing [16], waste treatment [138], biomedical applications [261, 262], material processing, and chemical engineering [263, 264]. However, the mechanism of the plasma and its reactive gas species (RGS) diffusion into the matrix, penetration capacity, or the relationship between this penetration and its modification/sterilization efficacy, is not fully understand. Previous reports indicated that the plasma-liquid interactions are very complex, including 53 species and 624 chemical reactions in the plasma region and more than 109 chemical reactions in the plasma-liquid boundary layer [156]. This increases the challenge of modeling and understanding the mass transfer across the gas-liquid boundary due to the complex and multi-disciplinary nature of the wide range of chemical species and physical effects, including radical and RGS, ions, electrons, (V)UV emission, electric fields, heat and neutral gas flows across the gas-liquid interface [265]. Yang [266] used a one-dimensional diffusion-drift model to simulate the transfer of plasma from the gas phase into liquid phase. The density of the plasma and its generated RGS and its diffusivity into tissue was highly related to the electric field. Another study investigated the mass transfer of the RGS in the gas-liquid layer by using a one dimensional drift-diffusion model [267]. Beyond the five main RGS (OH, H_2O_2, HO_2, O_2^-, and O_3), some of the RGS generated in high electric fields are short-lived, therefore losing their density as it penetrated [267].

While many studies have investigated the impact of ACP on the bulk solid/liquid matrix [16, 163], few studies have explored the penetration capacity of plasma-generated reactive species (PRS) into semi-solid materials, such as tomato sauce or toothpaste, or the relationship of PRS penetration on treatment efficacy. The semi-sold material is an important component in many biological, pharmaceutical, and environmental applications [270]. Penetration depth is also critical for wound healing and biofilm removal either applications require treating multiple layers with thicknesses of several μm to cm [271, 272]. Previous studies in plasma chemical or physiochemical mechanisms and its penetration capacity were usually performed using water and a limited timescale of 1ns ~ 100s, with a limited penetration depth from 10^{-4} cm ~ 10^{-1} cm [155, 156, 273].

Therefore, penetration capacity at an increased time scale, coupled with the physiochemical efficacy as the PRS penetrate during ACP treatment, is particularly interesting and will facilitate the expansion of the application of ACP to other matrixes.

This study investigates the penetration capacity of plasma/PRS generated by direct or indirect high voltage atmospheric cold plasma (HVACP) into a semi-solid material or food matrix and its impact on microbial inactivation. It specifically considers agar (agarose) gel as a model system to be treated by various durations of HVACP at 90 kV with air or modified gas (MA65: 65% O_2, 30% N_2, 5% CO_2) as the packing gas. Adding pH indicator into the gel enabled the tracking of the depth of pH change, which corresponds to the perpetration depth of PRS generated by HVACP. We propose a one-dimensional diffusion-drift-reaction model to analyze the distance and mechanism of PRS penetration. The penetration of PRS and its relationship with microbial reduction of *Salmonella*/bikyyoluminescent cell in the agar gel was investigated, followed by a validation in a food sample: *Salmonella enterica serovar* Typhi (*S. enterica*) inactivation in applesauce by HVACP treatment.

3.3   Materials and methods

Sample Preparation and Bacterial Inoculation

Salmonella enterica serovar Typhimurium ATCC 14028 (*S. enterica*) was obtained from ATCC. *S. enterica* was grown overnight in Tryptic Soy Broth (TSB, Difco^{TM}, MD, USA) at 37 °C for 24 h, in a shaking bath.

This study uses agar gels with various concentrations of agarose because they have stable physiochemical properties and have been broadly utilized as a standard model to mimic skin/brain tissue in biomedical studies and meats or sauces in food processing, Agar (Agarose) gel (Bacto, MD, USA) with concentrations of 0.25%, 0.5% 1%, 2% (w agarose/w distilled water) were dissolved into deionized water with pH adjusted to 6.5. The solution was heated to 80 °C in a boiling water bath under continuous mechanical agitation for 10 min, then cooled at room temperature to reach 30°C. Adding the pH indicator-methyl purple induced a color change from bright green to purple at a pH of 4 in the agar solution. *S. enterica* was added into the agar solution to achieve an initial population of approximately 7 log CFU/mL. The mixture was cooled in 4 °C

to achieve a gel state within 2 min (to avoid an uneven distribution of *S. enterica* caused by gravity) and stored at 4°C.

Sample Packages

The 25 mL agar gel samples (inoculated with *S. enterica*) in jars (diameter: 3.5 cm) were placed in a storage box and flushed with either dry air (<5% relative humidity) or MA65 (65% O_2 + 30% N_2 + 5% CO_2, <5% relative humidity) for 3 min using a Cryovac® B2630T (Sealed Air, North Carolina, USA) high barrier film to retain the plasma and reactive gas species (RGS). The gas composition in the box was analyzed using detector tubes (Dräger-Tubes®, Houston, TX) to confirm the purity of the fill gas (air or MA65).

High Voltage Atmospheric Cold Plasma (HVACP) Treatment

The HVACP device (Figure 3.1) is an atmospheric low temperature plasma generator employed for in-package plasma treatment [1, 129]. The HVACP system included a transformer (Phenix Technologies, MD, USA) to deliver a maximum output voltage of 120 kV (AC) at 60 Hz. We typically applied voltages up to 90 kV [41]. A combination of dielectric barriers were assembled to achieve maximum PRS generation for each gas-package combination. The package was placed between two 15.24 cm diameter aluminum electrodes with a gap of 6 cm, and the two Cuisinart® (Cuisinart, New Jersey, USA) polypropylene layers ($355 \times 272 \times 2.20$ mm) above and below the package as additional dielectric barriers. Agar gel with concentrations of 0.25%, 0.5% 1%, 2% were exposed directly and indirectly to 90 kV for 0.5, 1.0, and 1.5 hours.
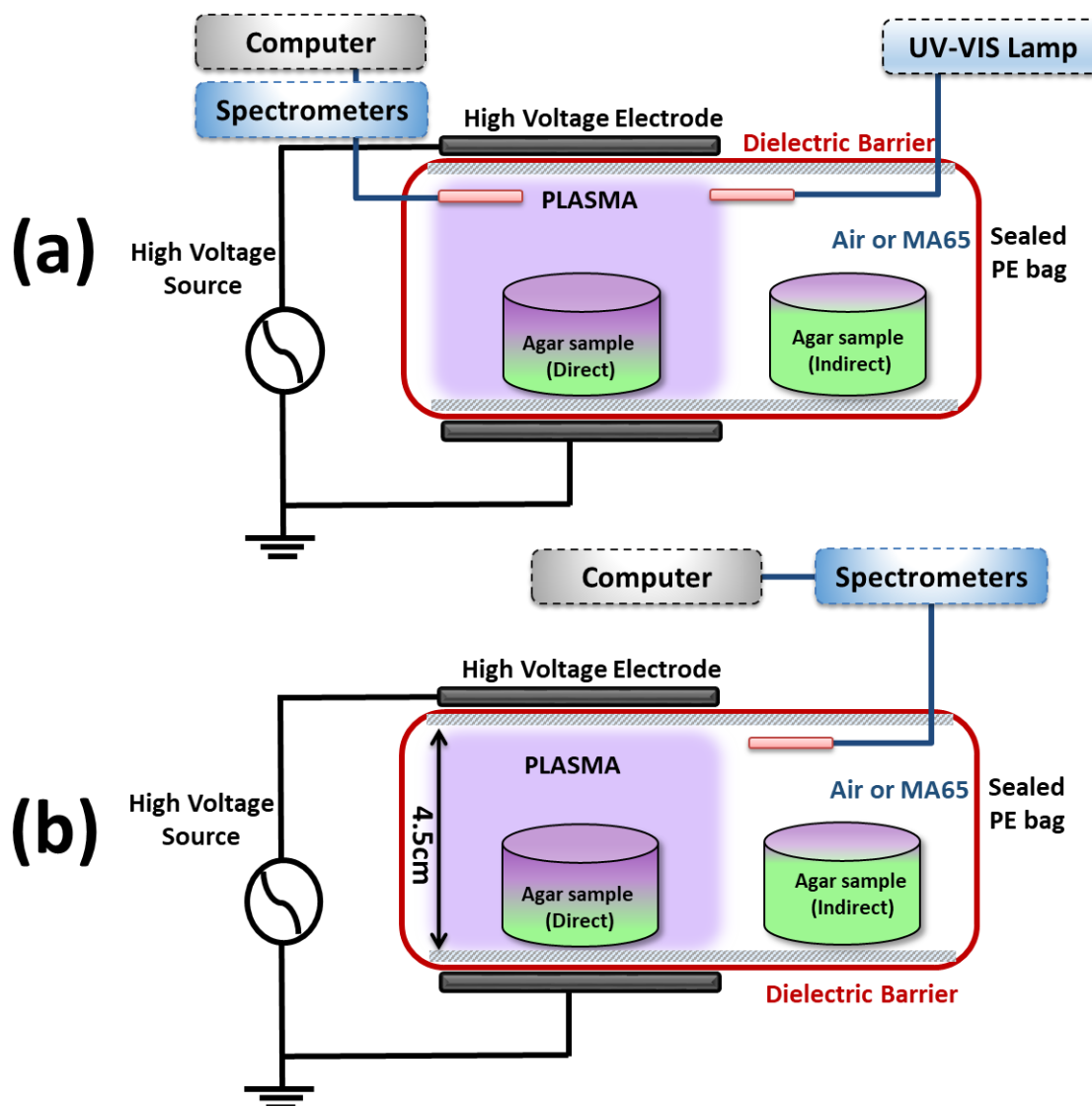
Figure 3.1 Schematic of the experimental setup employed for high voltage atmospheric cold plasma (HVACP) treatment of an agar sample (a glass bottle with top-side open) with both direct and indirect exposure: (a) Optical emission spectroscopy (OES); (b) Optical absorption spectroscopy (OAS).

Measurements of Penetration Depth and Microbial Inoculation

HVACP induced the gel color to change from bright green to purple (Figure 3.1.) due to the pH change [274]. The treated gel was sliced into five zones from the surface to the bottom: gel surface, color changed area, critical line, 0.25 cm beyond the critical line, and non-color-changed area (Figure 3.2a). The depth of the PRS penetration was measured as the distance between the gel

surface and the line where the color first changed to purple (shown in Figure 3.2a). The penetration depth for each sample was an average of three measurements.

In each zone, a 1g gel sample was recovered in sterilized 0.1% peptone water (Bacto, MD, USA), vortexed, serial diluted and 100 uL of each dilution was plated on Xylose lysine deoxycholate (XLD, Difco^{TM}, MD, USA) selective media. Plates were incubated at 37 °C for 24 h and survivors (CFU/mL) were enumerated. Analyzing duplicate plates for each dilution yielded the number of colony forming units (CFU) with the counts reported as the average of three independent HVACP treatments (detection limit is 10^1 CFU/mL).

Optical Emission Spectroscopy (OES) and Optical Absorption Spectroscopy (OAS)

Optical emission spectroscopy (OES) and optical absorption spectroscopy (OAS) was performed to characterize the RGS generated in the plasma during the treatment [44, 214]. OES and OAS were measured using an HR2000+ Spectrometer and 400 mm optical fibers produced by Ocean Optics (FL, USA). The fibers had a numerical aperture of 0.22 and were optimized for use in the ultraviolet and visible portion of the spectrum with a wavelength range between 190 nm and 1100 nm. The distance between the optical fiber and the plasma chamber was 140 mm. The OES spectra were corrected for background noise and recorded every 30 s during HVACP treatment at 90 kV. The data was recorded and analyzed using OceanView Optics Software (Dunedin, FL). The peaks were identified using the NIST Atomic Spectra Database [275].

The post-discharge gas composition was measured by OAS, using a UV-visible (UV-Vis) deuterium-hydrogen lamp as the light source. The transmitted light was measured with an Ocean Optics (HR2000+) spectrometer. The optical probes (insulated UV-Vis collimators) were aligned inside the sealed package for all experiments, with an optical path length of 2.4 cm between the probes. The Beer-Lambert law was used to calculate the concentrations of nitrogen oxides (NO_2, NO_3, N_2O_4) by averaging concentrations along a wavelength interval where each species has an absorption cross-section maximum or values much higher than other absorbent species [44].

Ozone and NO$_X$ Concentration

We measured the concentration of ozone and NO_X following HVACP treatment in accordance with RGS [46], which gave rapid and straightforward results. Detector tubes (Dräger-

Tubes®, Houston, TX) were used to characterize the concentration of ozone (Dragger, CH21001) and NO_X (Dragger, CH31001) immediately after HVACP treatment. We collected 5 or 20 mL gas samples by syringes and analyzed by detector tube using an Accuro Gas detect Pump (Draeger Safety AG & Co. KgaA, Germany). Each tube contained colorimetric indicators, so the length of the color changed area is proportional to the concentration of specific gas. All samples were recorded as an average three measurements.

Preparation of Agar Gel with Bioluminescent Cell and its Bioluminescent Imaging

Bioluminescent *E. coli K12-lux* was obtained from the Applegate culture collection (West Lafayette, IN USA). This luminescent strain contained the *luxCDABE* gene cassette from *Photorhabdus luminescens* cloned into pCRII (Invitrogen, Carlsbad, CA), resulting in constitutive luminescence at 490 nm [276]. Bioluminescence is an energy-dependent process requiring ATP and reducing power from NADPH and $FMNH_2$, which therefore physiologically stresses the cell and may reduce the amount of light that is produced [276].

A 2% agar (solution) was inoculated with *E. coli K12-lux* to achieve an initial population of approximately 7.5 log CFU/mL. A 7×4 cm gel cassette was prepared by pouring the agar between two glass plates that were sealed with rubber on the sides and one end. Once solidified, we placed the resulting gel cassette horizontally into a storage box (vertical to the electric field), flushed it with filling gas (dry air) for 3 min, and sealed it with a high barrier film, as shown in Figure 3.6a. It is 2.important to note the PRS can only penetrate from side I (4 cm^2) into the gel. The agar plate was treated directly using HVACP at 90 kV for 1 h.

Spatial and in situ determination of bioluminescence in the treated gel plate on surfaces was determined using an Andor iXon low light imaging CCD camera (Andor Technology Plc, Belfast, Northern Ireland). Image software (Caliper Life Sciences, Hopkinton, MA, USA) was used to detect and quantify total photon emission (number of photons/s/cm^2) from defined regions of interest within each image.

HVACP Treatment of Apple Sauce

After purchasing applesauce (organic, unsweetened) from a local grocery store, we placed 30 g samples (control and inoculated with *S. enterica*) onto a Petri dish (diameter: 85 mm) in a

storage box, flushed with filling gas for 3 min, and sealed it with dry air or MA65 using a high barrier film to retain the plasma and RGS. Applesauce samples were treated with HVACP at 90 kV for 2, 4, 6 and 8 min with direct exposure. The treated samples were stored in a refrigerator at 4 °C for 24 h to study the dependence of microorganism population on post-treatment storage. XLD agar (Difco) was used to enumerate *S. enterica*. The morphology of *S. enterica* in the control and HVACP treated applesauce, was characterized using scanning electron microscopy (SEM) based on Ref. [[277]].

3.4   Results

3.4.1   PRS Penetration and Physiochemical Reactions
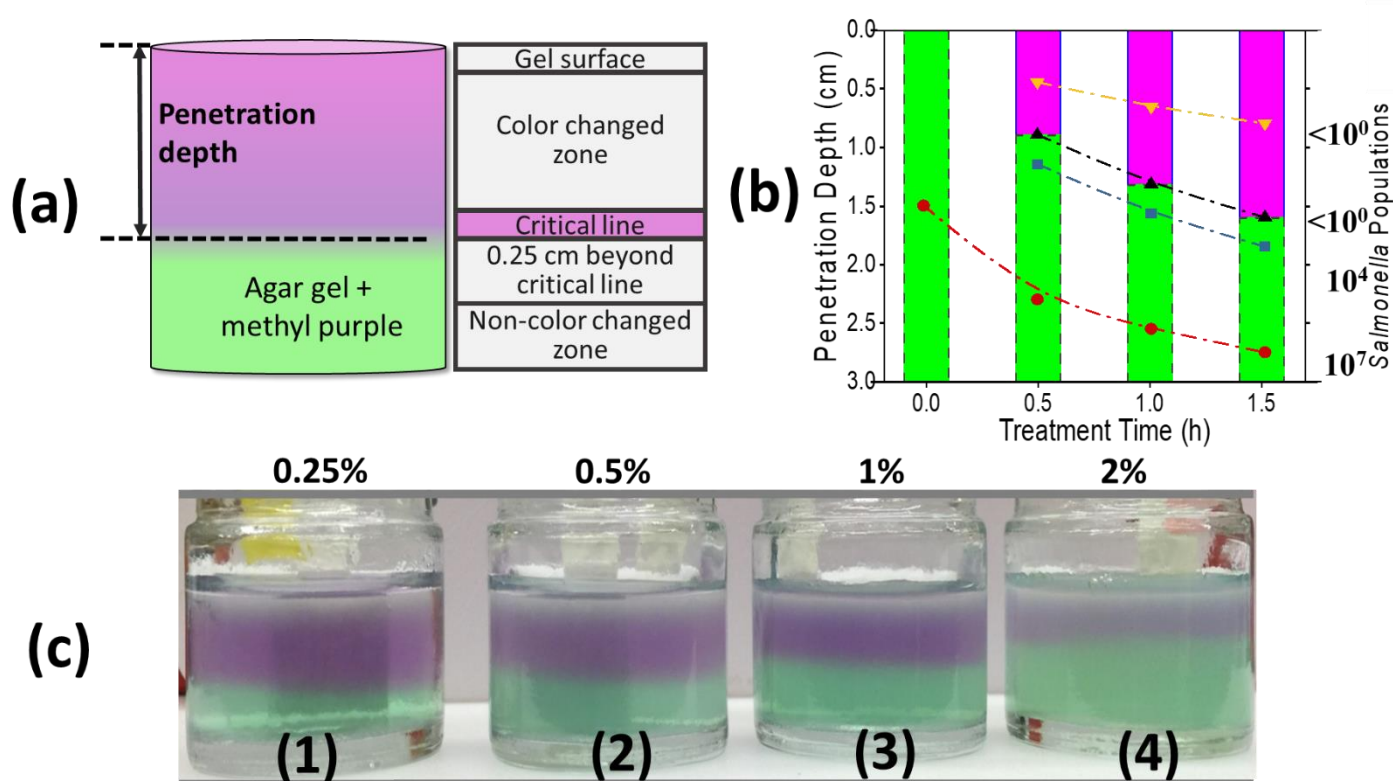
Figure 3.2 (a) Scheme of 5 divided penetration zone in HVACP treated agar gel before analysis; purple shows the PRS penetration as a consequence of a pH change from 7 to 3.2. (b) Penetration depth and its microbial population (CFU) as a function of treatment time. (c) Gel with various agar percent composition with pH indicator (methyl purple), packed with MA65 and treated with HVACP for 1 h. Agar: (1) 0.25%, (2) 0.5%, (3) 1%, (4) 2%.

HVACP treatment can generate plasma/PRS that will penetrate into the semi-solid material and generate a series of physiochemical reactions, including a pH decrease and microbial inactivation. Figure 3.2c shows that gels with various agar percent composition and pH indicator (methyl purple) with HVACP for 1 h caused the PRS penetrated zone to change color from green to purple. Color change corresponded to pH decreases from 7 (initial) to 3.2 (critical line (Figure 3.2a)), primarily due to the generation of nitrate and nitrite as confirmed by nitrate/nitrite acid test strips (data not shown). This mechanism was previously described [278, 279]: the nitrogen oxides (NO and NO_2) formed by gas-phase reactions of dissociated N_2 and O_2, can dissolve in water rapidly, forming nitrite NO_2^-, and nitrate NO_3^- by the reactions summarized as follows:

$$NO + O + M^* \rightarrow NO_2 + M^* \tag{3.1}$$

$$NO_2 + OH + M^* \rightarrow HNO_3 + M^* \tag{3.2}$$

$$NO + OH + M^* \rightarrow HNO_2 + M^* \tag{3.3}$$

$$NO_2\,(aq) + NO_2\,(aq) + H_2O_{(l)} \rightarrow NO_2^- + NO_3^- + 2H^+ \tag{3.4}$$

$$NO\,(aq) + NO_2\,(aq) + H_2O_{(l)} \rightarrow 2NO_2^- + 2H^+ \tag{3.5}$$

$$2NO_2\cdot + H_2O_{(l)} \rightarrow NO_2^- + NO_3^- + 2H^+ \tag{3.6}$$

$$4NO\cdot + O_2 + 2H_2O_{(l)} \rightarrow 4NO_2^- + 4H^+ \tag{3.7}$$

$$NO_2\,(aq) + OH \rightarrow \quad NO_3^- + H^+ \tag{3.8}$$

$$NO_2^- + H_2O_2 \rightarrow O{=}NOO^- + H_2O \tag{3.9}$$
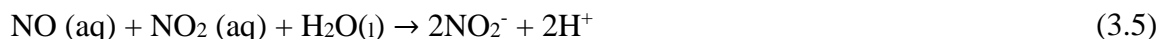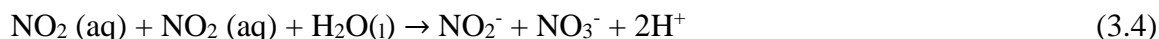
where M^* is a third body collision partner [280]. The reactions between NO_2 and OH radical may also generate peroxinitrous acid (ONOOH) or its conjugate base peroxynitrite ($O{=}NOO^-$) (subsequently decay into NO_3^-) in the aqueous phase. Peroxynitrite may also be generated by the reaction of nitrite anion with H_2O_2 [75, 279].

Previous studies detected these acid products and their penetration capacity [156, 208]. Formed nitrogen radicals NO. and NO_2. possess strong cell toxic properties and were the major cause of the cytotoxicity of nitrites under acidic conditions (known as *acidified nitrites*) [281]. Covering the gel with lids and applying HVACP treatment for one hour induced no color change in the gel, indicating the pH decrease (color change) was primarily caused by the PRS generated by HVACP and transported from the gas phase into the gel.

Enumerating the residual *S. enterica* population in each zone of the gel after HVACP treatment demonstrated the microbial inactivation by HVACP in the semi-solid material. Figure 3.2b showed more than 6 $\log_{10}$ microbial inactivations between the gel surface and the critical line. A 1-2 $\log_{10}$ reduction of *S. enterica* population occurred in the zone 0.25cm beyond the critical line, while the color did not change. No microbial reduction was detected in the bottom (opposite to the open side) non-color changed zone. This indicated the close relationship between microbial inactivation efficacy and PRS penetration into the gel.

When laying the gel perpendicular to the electric field (only one opening on the side of the gel accessible for PRS to transport horizontally into the gel and electric field applied vertically to the gel, shown in Figure 3.5), > 6 $\log_{10}$ microbial inactivation occurred in the zone where the color changed and no microbial inactivation occurred in the non-color changed zone (data not shown). This confirmed that the predominant reason for pH decrease and microbial inactivation was the penetration of PRS generated by HVACP.

The penetration rate of PRS in the semi-solid material was affected by properties of the semi-solid material, including concentration/density, porosity, temperature, chemical composition, and HVACP treatment parameters, such as electric field, exposure model, fill gas and treatment time. This study evaluates the effect of gel concentration, plasma treatment time, exposure model, fill gas.

3.4.2   Penetration Depth in Agar Gel with Air and MA65 as Packing Gas

The penetration capacity of PRS was evaluated by measuring the depth of color change in the gel with various agar concentrations after HVACP treatment. The agar was treated at 90 kV for 1 h. The penetration depth (a purple region in Figure 3.2b) increased with increasing treatment time. This penetration was induced by the molecular motion caused by a concentration gradient and electric field. The reactions between PRS and media may reduce the concentration of PRS and generate its derivatives (see discussion). The penetration depth of PRS in gels containing 0.25%, 0.5%, 1% and 2% agar, were 1.31cm, 1.06cm, 0.95cm, and 0.69cm, respectively (Figure 3.2c); therefore, the penetration depth was greater for a lower agar concentration for a given treatment time, which is consistent with previous report [282]. This is primarily because the concentration of agarose in the gel will highly affect the intrinsic three dimensional structure of the gel, which is

often described as a mesh. Within this homogenous structure, based on Fick's law and free volume theory [283], the void in the gel of lower concentration agarose is bigger, hence is easier for the solute molecule to transport, corresponding to a higher PRS penetration depth within the same treatment time.

Efficacy of filling gas (air and MA65) on PRS penetration into the gel was investigated by treating the gel at 90 kV and measuring the penetration depth at each time point. Using air or MA65 as packaging gas generated different RGS (ROS and RNS) in the plasma state, and this may lead to a variance in PRS penetration. However, the penetration depth of PRS was no the statistical difference ($P>0.51$) with air or MA65 (Figure 3.3a, 3b). This may be due to the concentrations of PRS generated by air and MA65 were both very high (>7500 ppm), which had reached the maximum solubility of the PRS, based on Henry's law [156]. It was reported that the H_2O_{2aq} and O_{3aq} concentrations follow very similar spatial profiles, both reaching their peak values at the gas-liquid surface and then following a very similar parabolic decay into the liquid bulk [156]. These two species have high chemical stability in the aqueous phase and their distributions were diffusion-limited [39]. Therefore, in this study, using air or MA65 as filling gas to generate plasma by HVACP will penetrate at a similar rate (depth/time) in agarose gel.
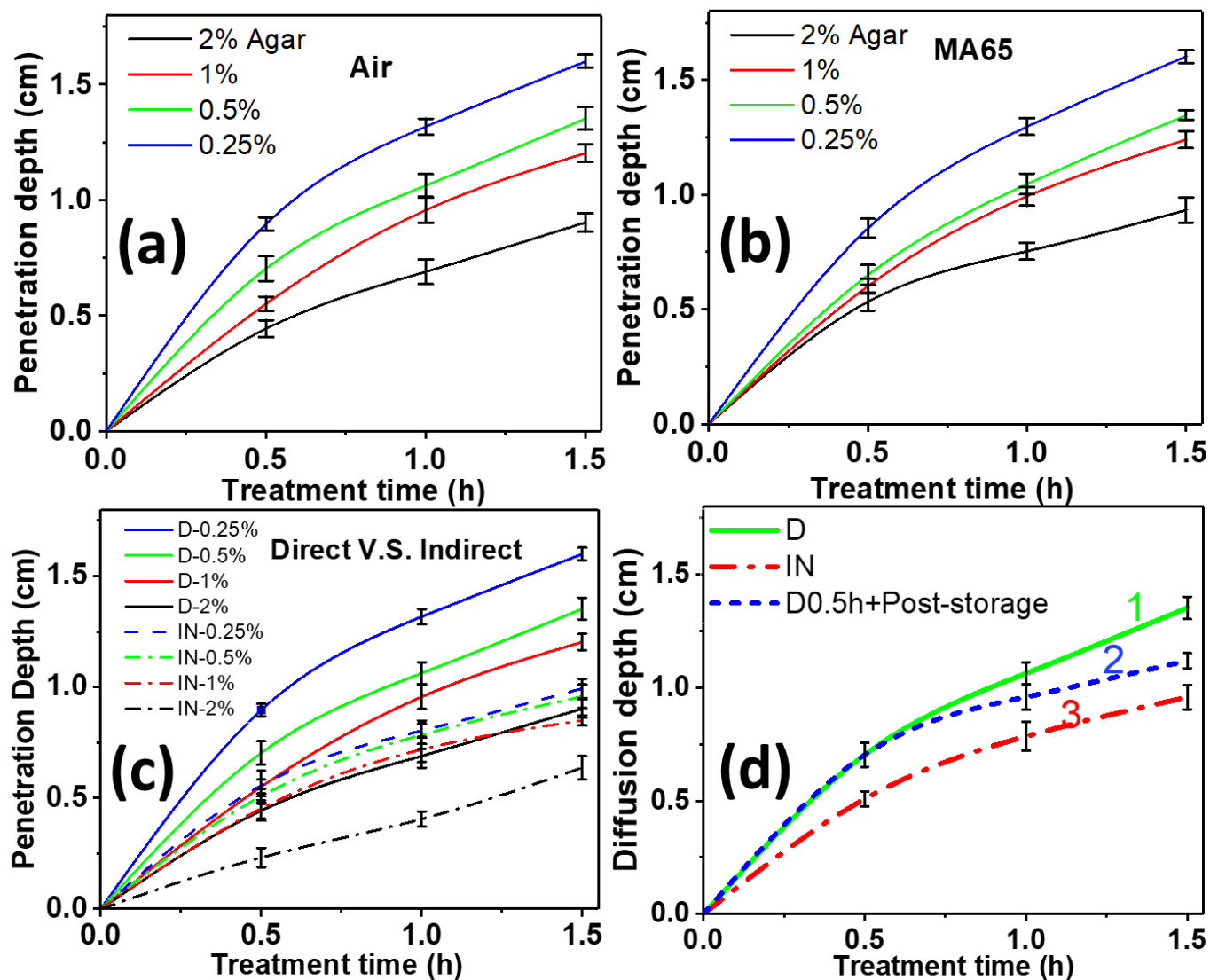
Figure 3.3 Gel with various agar percent composition (0.25%, 0.5%, 1%, and 2%) with pH indicator (methyl purple), packed with air (a) (c) (d), and MA65 (b). The gel was treated at 90 kV with HVACP up to 1.5 h directly for (a) and (b). (c) A comparison of penetration depth in the gel of various agar concentration at direct and indirect exposure model. (d) a comparison of penetration depth in 0.5% gel of direct, indirect, gel with 0.5 direct treatment followed by post-storage.

3.4.3 Direct/Indirect Exposure and Post-storage

PRS under direct exposure during HVACP treatment has a larger penetration depth than indirect exposure (Figure 3.3c). After 1.5 h HVACP treatment, the penetration depths for gel concentrations of 0.25%, 0.5%, 1.0%, 2.0% were 1.61, 1.35, 1.20, 0.90 cm under direct exposure, and 0.99, 0.95, 0.85, 0.64 cm under indirect exposure, respectively (Figure 3.3c). This high penetration depth under direct exposure may be related to the high concentrations of plasma/PRS within the electric field as well as the drift effect established by the electrostatic field. Plasma category and concentrations were characterized by OES and OAS (see below). Both direct and indirect exposure of HVACP treatment can generate PRS that can penetrate into agar gel, indicating HVACP treatment can be applied indirectly by transporting the PRS to the target media without exposing to the electric field. However, HVACP treatment under direct exposure had a larger penetration rate within the same treatment time, due to the combined efficacy of electrostatic field and high concentration of PRS. The drift motion in indirect treatment had been significantly reduced. During indirect treatment, only long-lived species reached the targeted surface, because recombination events took place inside the effluent in which most metastables and ions recombine to neutral species. The density of ions, electrons, and metastable species were much lower (close to zero) outside of the electric field. Therefore, direct exposure is preferred to achieve fast penetration into the gel.

A comparison between direct and indirect (continuous treatment), and post-storage (0.5 h direct + post-storage/no treatment) of HVACP treated gel (0.5%) was shown in Figure 3.3d. For the first 0.5 h, the penetration depths for direct exposure (samples 1 and 2) were higher than indirect (sample 3). Removing the electric field and leaving the box for post-storage (sample 2) resulting in a reduced penetration capacity compared to continuous treatment (sample 1, 3), which is consistent with our proposed model.

3.4.4   OES, OAS and RGS Concentration
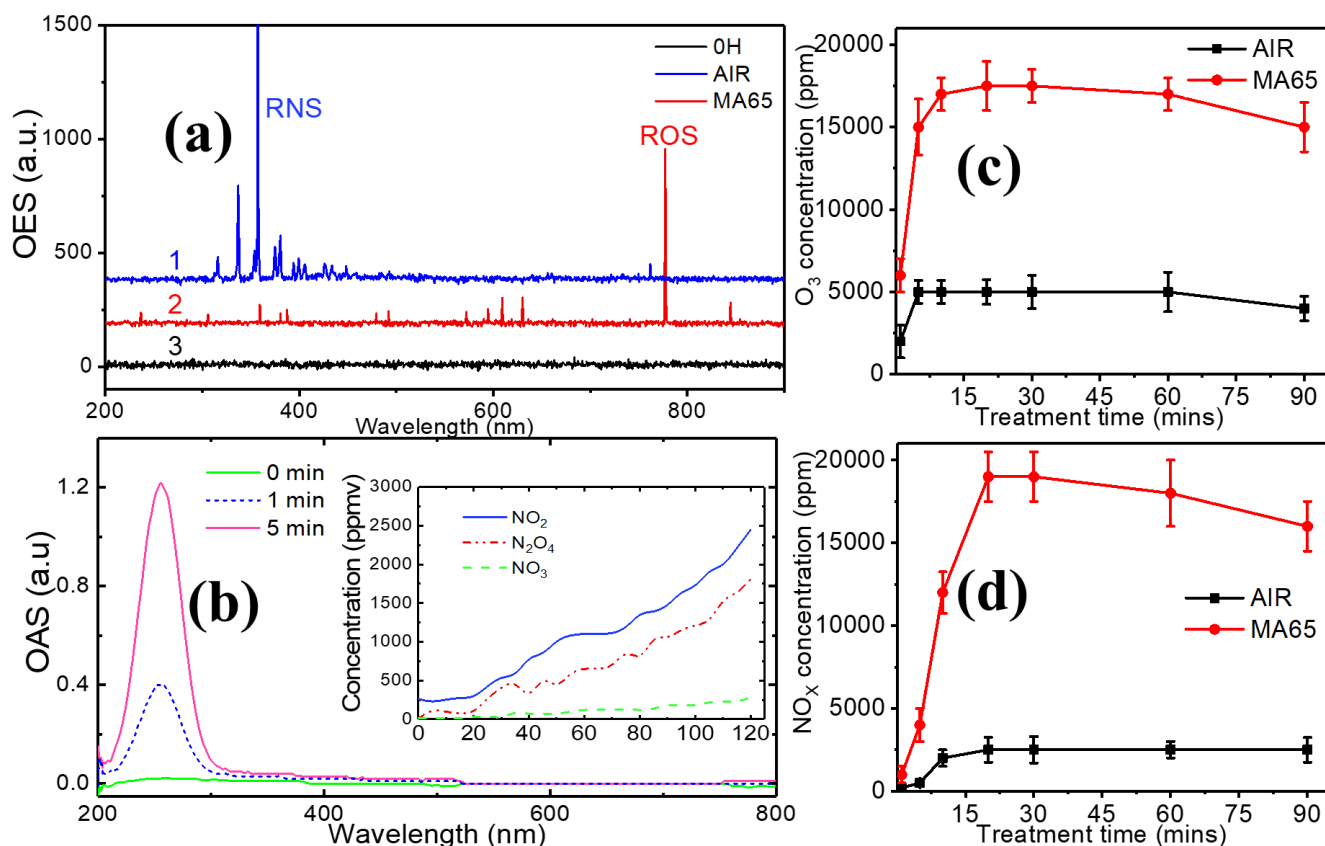
Figure 3.4 (a) Optical emission spectroscopy results of Air (a1) and MA65 (a2) packed agar gel during HVACP treatment (direct) at 90 kV for 10 min. (a3) Optical emission spectroscopy of control. (b) Optical absorption spectroscopy signal of MA65 packed agar gel and its calculated concentration of NO2, N2O4, NO3. (c) O3 concentration (d) NOX concentration results from text strip.

The different main emissions of the RGS generated by air and MA65 during HVACP treatment and its concentration were characterized by OES, OAS, and gas detector tubes. The recorded spectra consist of various molecular and atomic nitrogen and/or oxygen species during HVACP treatment (Figure 3.4). The major peaks in the spectra corresponded to the emissions of excited species of atomic nitrogen and atomic oxygen, including the nitrogen second positive system N_2(C-B) [224, 280], the first negative system N_2^+ (B-X) (at 336, 357, 380, 390, 405, 426 nm), and optical transitions of the O atom, including 616 nm, 777 nm and 844.6 nm [225, 226]. MA65 plasmas (line 2) contain primarily reactive oxygen species (ROS: such as OH, O, H_2O_2) while air plasmas (line 1) consist primarily reactive nitrogen species (RNS, such as NO˙, ONOO¯,

and NO_2^-) (Figure 3.4a), which corresponding to different RGS concentration during and after the treatment. The concentrations of each nitrogen oxide (NO_2, NO_3, N_2O_4) were calculated from the OAS signal (Figure 3.4b) [44].

MA65 generated more ROS species than air, as confirmed by strip test. Ozone concentrations increased up to 17 500 ppm in MA65 and 5000 ppm in the air with 10 min HVACP treatment and remained at saturation concentrations for up to 1 h (Figure 3.4c and 3.4d). The ozone concentrations decreased less than 12%, which may arise due to the transport into the gel phase, self-decomposition or reaction with the media afterward. Then the same trend arose for the concentration of NO_X, which reached saturation when the generation rate equaled the decomposition rate, then decreased approximately 15.8% after 1.5 h. The nitrogen oxides (NO and NO_2) formed by gas-phase reactions can dissolve in water rapidly, forming nitrous acid, nitric acid, or peroxynitrous acid. This induced the pH decrease and other physicochemical effects in the gel phase and the concentration decrease of NO_X in the gas phase. Both the concentrations of ozone and NO_X were higher in the MA65 packaged sample than in air. This may relate to the 3.1× higher concentration of oxygen in MA65 than air, which generates more ROS, confirmed by OES (Figure 3.4b).

3.4.5 Plasma Penetration on Microbial Inactivation
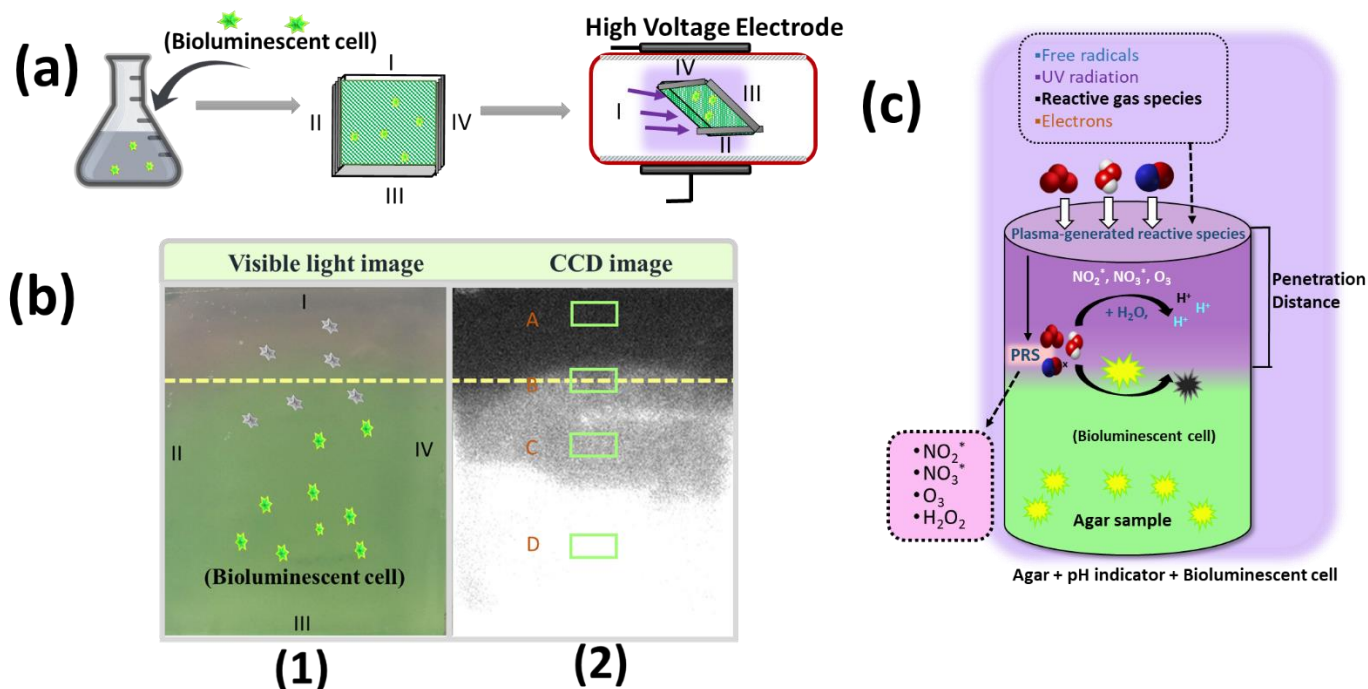
Figure 3.5 (a) Schematic of the agar gel preparation (with bioluminescent cell). The gel was sealed in a glass box, with only 'I' side open to PRS. The gel was laid down horizontally to make the PRS penetration perpendicular to the electric field. (b) Images of HVACP treated agar gel (at 90 kV for 2 h with air as filling gas): (1) visible light image, (2) Charge-coupled device (CCD) image, to view of the gel after exposing to HVACP treatment. (c) Proposed mechanism for PRS penetrating into a gel with the bioluminescent cell.

Tracking the residual microbial population as the PRS penetrated into the agar elucidates the impact of PRS penetration on microbiocidal efficacy. Figure 3.5b shows images of the gel with bioluminescent cells after HVACP treatment (prepared based on Figure 3.5a) with the brightness intensity proportional to the bioluminescent cell population. Comparing Figure 3.5b-1 with the luminescent image Figure 3.5b-2 (collected by luminometer) showed that the brightness intensity decreased significantly in the color/pH changed zone, indicating that the penetration of PRS into the gel inactivated the microbial population.

Figure 3.5c demonstrates the proposed mechanism of this process. As PRS penetrate into the semi-solid material, they and their physiochemical reaction products, including H_2O_2, O_3, nitrous acid, nitric acid, or peroxynitrous acid, will reduce pH and inactivate the bioluminescent cells.

The drift effect was weak in this situation since the only open side of the gel (the side I in Figure 3.5a) was perpendicular to the electric field. Therefore, the predominantly driven motion for PRS, in this case, was molecular diffusion, which corresponds to the major microbiocidal impact in the gel. Non-pH related PRS, predominantly H_2O_2 (confirmed by H_2O_2 strip, QUANTOFIX®), induced a 2-3 log_{10} microbial reduction in the zone 0.25 cm beyond the critical line. The penetration capacity of H_2O_2 was higher than nitrous/nitric acid and $O_3(aq)$, reported by Liu *et al.*, [156]. Although in the gas phase, O_3 is chemically stable with a much lower concentration than H_2O_2 due to its small Henry's coefficient of ~0.23 [284]. The concentration of $H_2O_2(aq)$ is always threefold to fivefold higher than those of $O_3(aq)$, and $NO^{-3}(aq)$, $NO^{-2}(aq)$, $HNO_2(aq)$ in the aqueous phase [156]. Acidic pH contributed partially to the microbiocidal effect, but acidification alone is not sufficient for bacterial inactivation in this case [1, 40, 208]. After recovering pH by soaking the HVACP treated gel (pH=3) in a phosphate buffer (pH=7), the photon intensity distribution was consistent with Figure 5b2 and the living bioluminescent cells cannot be recovered after adjusting the pH back to 7. This confirmed the proposed mechanism that PRS penetrate into the semi-solid material and induce a complicated set of physiochemical reactions/products that synergistically decrease pH and inactivate microorganisms. Hence, pH/color alteration in the semi-solid material may be used to track the concurrent microbial inactivation during HVACP treatment.

3.4.6   Inactivation of *S. enterica* in Applesauce
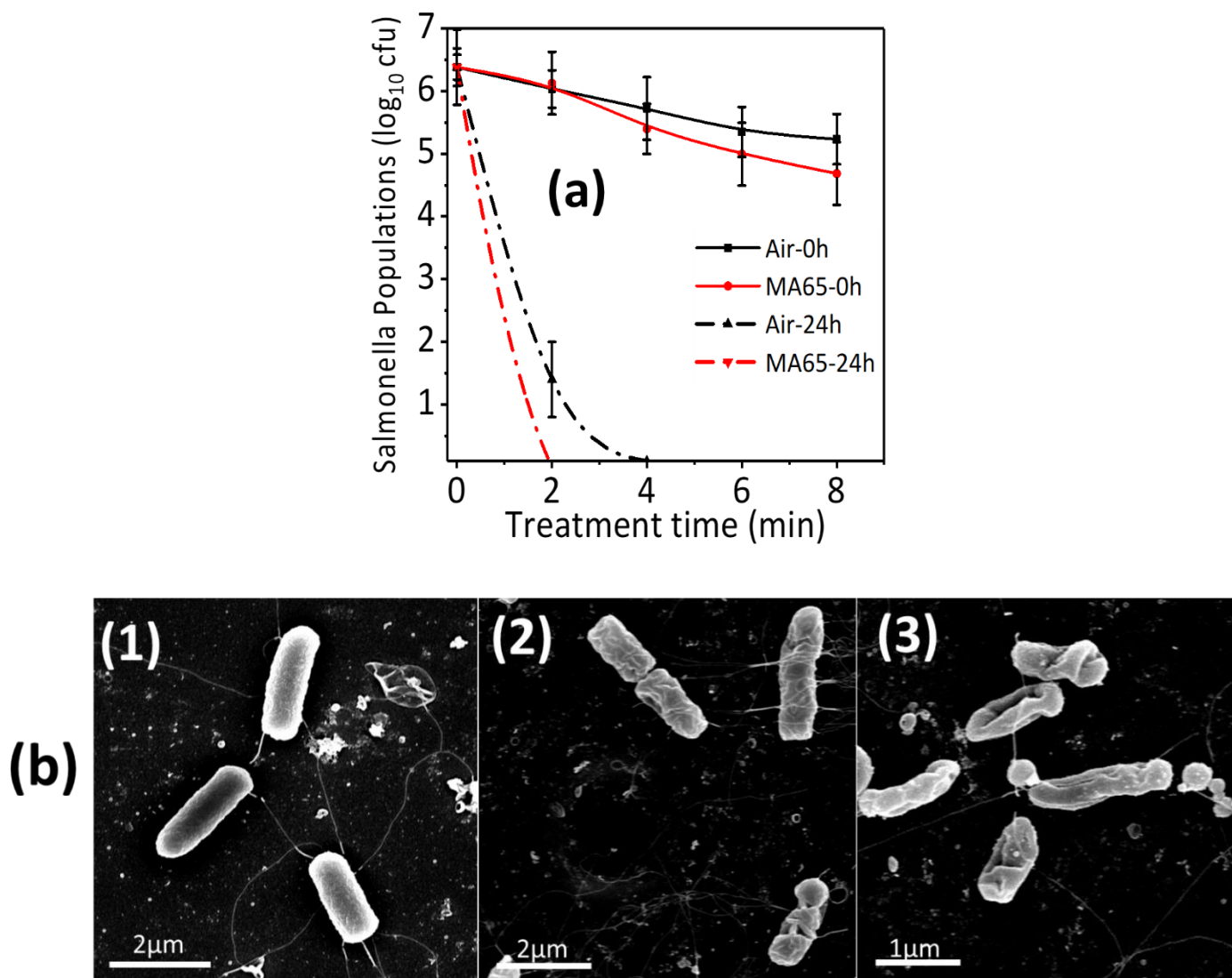
Figure 3.6 (a) The survival of Salmonella enterica serovar Typhimurium (S. enterica) population (log10 CFU) in air and MA65 packed applesauce is as a function of treatment time during HVACP treatment. (b) SEM image of S. enterica in control (1), HVACP treated sample packed with air (2) and MA65 (3) with direct exposure.

Inactivation of *S. enterica* by HVACP in semi-solid food was investigated, using applesauce as an example food. The population of *S. enterica* in applesauce decreased with increasing treatment time. Approximately 1 $\log_{10}$ reduction occurred for both air and MA65 packed applesauce within 4 min HVACP treatment at 90 kV. However, after a subsequent 24-h storage

(incubating applesauce at 5 °C without opening the package) of these HVACP treated samples, a more than 6 log reduction was observed (Figure 3.6c). This indicates that HVACP-generated RGS remain in the package and can inactivate *S. enterica* after removing the electric field, which is consistent with a previous report [1]. The more effective inactivation of *S. enterica* by MA65 plasma than air plasma may correspond to the high concentration of RGS generated by MA65 during HVACP (Figure 3.4).

The SEM images of *S. enterica* collected from filtered from applesauce (Figure 3.6b and 3.6c) show that HVACP treatment changes the morphology of the *S. enterica*. Rather than having smooth bacterial cell walls (Figure 3.6b), HVACP treated *S. enterica* (Figure 3.7c) had cell surface wrinkles, perforation and cell lyses.

3.5   Discussion

3.5.1   Proposed Model for Plasma/PRS Penetration into Semi-solid Material
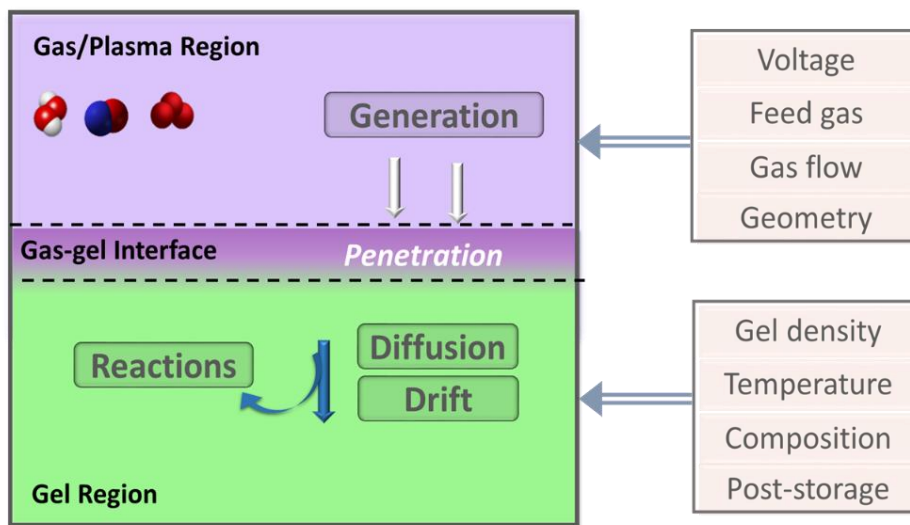
Figure 3.7 (a) Proposed mechanism for PRS penetrating into semi-solid material with a diffusion-drift-reaction model.

The plasma-gel interaction during HVACP treatment is consists of three regions, including the gaseous plasma generation region (gas region), the gas-gel interface region, and the gel region,

shown in Figure 3.7a. Regarding a long-time scale (up to 1.5 h) of this study, the efficacy of short-living species was neglected in this model. The penetration of PRS in the semi-solid material was driven by the molecular motion created by the concentration gradient-diffusion effect, and by the electrical static motion-drift effect. The PRS can also react with the media, including the microorganisms and the agarose, as it traveled in the gel. By including the interaction of the plasma species with the microorganisms, one can modify the drift-diffusion-reaction model based on Chen *et al.* and Jiang *et al.*'s model [267, 269] to obtain

$$\Gamma_{i,j} = \Gamma_{i,diff} + \Gamma_{i,drift} - \Gamma_{i,reac} = -D_{i,j}\frac{\partial C_{i,j}}{\partial x} + z_i\mu_{i,j}C_{i,j}E - k_iC_{i,j}C_x \qquad (3.10)$$

where the subscripts i and j denote the element (species) and gel, respectively, $C_{i,j}$ is the concentration of the PRS in the gel region, $D_{i,j}$ is the diffusion coefficient. The flux $\Gamma_{i,j}$ of the element i is given by

$$\Gamma_{i,j} = -D_{i,g}\frac{\partial C_{i,j}}{\partial x}. \qquad (3.11)$$

The electric field set up by all the charged elements in the gel region is given by

$$\Gamma_{i,drift} = z_i\mu_{i,j}C_{i,j}E \qquad (3.12)$$

where z_i is the ion charge number, $\mu_{i,j}$ is the drift mobility of a charged species, and E is the electrostatic field established by the charged elements. One can calculate $\mu_{i,j}$ using the Nernst-Einstein equation and E from the Poisson's equation [267]. The reaction between PRS and gel phase is given by

$$-\Gamma_{i,reac} = -k_iC_{i,j}C_x \qquad (3.13)$$

where C_x represents the concentration of reactant that might react with PRS in the gel phase, including H_2O, agarose, microorganism, and/or PRS derivatives. One of the major challenges with applying this model to the current study is that the reactions within the gel phase are not understood. For instance, when plasma interacts with a liquid, it induces 83 liquid phase species and 448 liquid reactions, which increase the challenge to predict k_i. Furthermore, PRS react with the microorganism at some reaction rate, which further modifies the differential equations as studied elsewhere for liquid [285].

While we currently cannot fully address the model proposed directly above, it does provide some insight into critical operating and device parameters that will likely impact plasma generation and, ultimately, treatment efficacy, including electric field, exposure model (direct/indirect), fill gas (air, MA65 or argon), and treatment time [9]. A high density/concentration of PRS ($C_{i,g}$) is preferable for its following penetration progress. Based on the model in equation (1), an increased electric field (voltage) - E can generate higher density/concentration of PRS due to the increase in power deposition, which the high E also facilitates the ionized species penetration into the gel through drift effect [266, 267, 286]. Lietz and Kushner reported that the densities of ROS and RNS increased roughly linearly with an increasing voltage over a certain voltage range [273]. A direct exposure system is preferable for PRS to penetrate into the gel to achieve fast penetration and an efficient microbial inactivation, shown in Figure 3.3d, which is consistent with previous reports [1, 43, 63]. Direct exposure to electric field will facilitate the reactive short-lived species (such as charge species, radicals, metastable, and electrons) to transfer into the gas-gel interface by bombardment [146]. The density of PRS ($C_{i,g}$) and E are both higher for direct exposure, which corresponds to an efficient penetration process. The penetration is very similar to electrophoresis: electrophoretic velocity (v_{ep}) of migration of charged molecules is proportional to the applied electric field E, $v_{ep} = \mu_{ep}E$, where μ_{ep} is the solute's electrophoretic mobility [287]. However, for PRS penetration, both neutral and charged species traveled into the gel, meaning that both diffusion and drift motion drive PRS migration in the gel.

The penetration capacity of PRS generated by HVACP into the semisolid material is also related to characters of semi-solid materials, including concentration/density, porosity, temperature, and chemical composition [288, 289]. PRS generated by HVACP traveled faster in low-density gel, shown in Figs. 2 and 3. Based on Smoluchowski's theory [290], $\mu_{ep} = \varepsilon_r \varepsilon_0 \zeta / \eta$, where ε_r is the permittivity of the dispersion medium, ε_0 is the permittivity of free space ($C^2\,N^{-1}\,m^{-2}$), η is dynamic viscosity of the dispersion medium (Pa s), and ζ is zeta potential, ε_r in gel of 0.5% agathe rose is higher than ε_r of 2% agarose. In other words, more free/void space was available for PRS to travel in 0.5% gel. This might correspond to a high $[D_{i,j}]$ in Eq. 1, hence a high $\Gamma_{i,diff}$ diffusion motion. Temperature is another important parameter for $\Gamma_{i,diff}$ (by affecting $[D_{i,j}]$) as well as $\Gamma_{i,reac}$ (by affecting k_i). A long treatment time (1.5 h) caused a 5~10 °C increase of sample temperature. Therefore, the proposed penetration model can be further

modified by adding a ΔH to correct the matrix temperature fluctuation. Within the electric field there was also a temperature gradient [156] and this relationship between the electron temperature and the electric field can be characterized using Boltzmann equation. The temperature dependence of liquid phase diffusion coefficients was constructed using the Stokes-Einstein equation [155] and the reaction rate coefficients (k_i) and their temperature dependence was analyzed by Lindsay *et al.*,[155]. PRS will also react with the media and its solute substance as it penetrates. In this study, agarose was chosen due to its inert and stable property, but PRS will undergo a series reactions under aqueous conditions (109 chemical reactions among 33 species) [156, 273] while also inactivating the microorganism (*S. enterica*, and biolumencent cells) [1, 208].

3.5.2 PRS Penetration and Microbial Inactivation in Semi-solid Material

The synergy between the PRS that penetrate the sample and the products derived from interactions with the sample play the key role in microbial inactivation during HVACP treatment [208, 273, 282]. The plasma complex consists of electrons, ions, radicals, metastables, and photons. Among all the PRS, the final concentration and its microbiocidal efficacy in gel region were determined by its generated concentration, stability, solubility/dissolution, and diffusivity, both in gas and gel phase [156]. During treatment, the most short-lived species, such as NO, OH, O, HO_2, and $O_2(a^1\Delta)$, could not survive with adequate concentrations much more than 5×10^{-3} m and the diffusion reach reduces progressively with increasing time suggesting strong loss mechanisms through plasma chemistry in the air gap [156]. The reactions and their respective reaction rates can be found from the NDRL/NIST Solution Kinetics Database [51]. After a series of physiochemical reactions, the most prevalent plasma produced species in the aqueous region are H_2O_2, O_{3aq}, HNO_{3aq} and HNO_{2aq} [155, 156, 273]. The concentrations of long-lived ROS/RNS are in general comparable to those reported and are known to have strong biological effects [208]. Several antibacterial mechanisms related to long-lived reactive species have been proposed [44, 268, 273, 282]. The concentration of H_2O_{2aq} is always threefold to fivefold higher than that of O_{3aq}, and this concentration ratio is similar to the experimental results reported by Shibata *et al* [208]. A 2-3 log microbial reduction was observed in the zone of 0.25 cm beyond critical line (Figure 6), which was caused by non-pH related PRS, primarily H_2O_2. This was due to the high solubility of H_2O_{2aq} (Henry's coefficient at 25°C, 2.1×10^6 H^{CC}) [291], and a high diffusivity in water (1.0×10^{-9} m^2s^-

[1]) [292]. Figure 3.4d and 3.4e showed that concentration of O_3 and NO_X in MA65 was much higher than air. However, we did not observe a faster microbial inactivation as PRS penetrates into the gel. This indicates the penetration of PRS is diffusion limited during HVACP treatment of semi-solid food rather than solubility or concentration limited. As the PRS penetrate into the gel, the generated RNS, primarily nitric acid and nitrous acid, cause the pH to decrease from 7 to 3. The resulting nitrogen radicals $NO^{\bullet}$ and $NO_2^{\bullet}$ possess strong cytotoxic properties [75]. PRS and its derived species will interact with bacterial cell membranes, interior DNA, RNA, and proteins to cause cell lysis [1, 281]. This provides a promising method for the biomedical industry. Compared with previous studies [265, 293, 294] investigating the penetration capacity of ACP using agarose as a model for wound healing, our study assesses longer treatment times (up to 1.5 h) with an increased penetration depth of up to 1.6 cm. This offers a promising model for PRS penetration into semi-solid material.

3.6   Conclusion

This study investigated the penetration of plasma/PRS generated by HVACP into the semi-solid material and the resulting microbial inactivation efficacy during this penetration. Using agarose gel of various concentrations to represent semi-solid material, the results indicate the impact of using air and MA65 as fill gas for HVACP treatment. A one-dimensional drift-diffusion-reaction model proposed in this study may ultimately be expanded to account for diffusion motion, drift motion, and the interaction between PRS and microorganisms/agar gel. The PRS has a faster penetration in the gel of low agarose concentration, with direct exposure, and approximately equal penetration rate with air or MA65 as the fill gas. A complete microbial inactivation has been achieved in the color/pH-changed zone, which corresponds to the penetration of PRS into the gel. This indicates that PRS generated by HVACP can penetrate into the semi-solid material and it can inactivate microbes as it penetrating. Our approach can be readily adapted to other plasma sources; it can accommodate more complex biological materials, and may potentially provide new insights into plasma-induced phenomena for medical treatment or in semi-solid food.

CHAPTER 4.   PHYSIOCHEMICAL INTERACTIONS BETWEEN HIGH VOLTAGE ATMOSPHERIC COLD PLASMA AND PROTEINS

4.1   Abstract

Atmospheric cold plasma as a novel, non-thermal, and highly efficient approach has been successfully used to inactivate biohazardous proteinaceous molecules (enzyme, prions, and allergen), or modify proteins with improved functionalities. Few studies have elucidated the mechanism of plasma-protein interactions. This study investigates the physicochemical interactions and structural alteration of bovine serum albumin (BSA) and its reaction mechanism when subjected to high voltage atmospheric cold plasma (HVACP) treatment. HVACP was generated by dielectric barrier discharge in sealed bags packed with air or modified air (MA65, with 65% O_2, 30% N_2, 5% CO_2). After treating 10 mL of BSA solution (50 mg/mL) at 90 kV for 20, 40, or 60 min, we characterized its structural alterations and side-group modifications. Treating BSA solution with HVACP for 60 min changed the sample color from transparent to yellow and induced protein precipitation. FTIR spectroscopy, Raman spectroscopy, and circular dichroism analysis demonstrated protein unfolding and decreased secondary structure (27% loss of α-helix) and increased disorder structure (10% increase of random coil) in HVACP treated BSA. The average particle size of treated protein increased from 10 nm to 113 µm, with a broader distribution after 60 min HVACP treatment. SDS-PAGE and mass spectrometer analysis observed a formation of new peptides from 1 to 10 kDa, indicating plasma-triggered peptide bond cleavage. Chemical analysis and mass spectrometry results demonstrated side-group modifications, predominantly oxidation and deamidation in plasma tread samples. This study illustrates that HVACP treatment may effectively introduce structural alteration, peptide cleavage, and side-group modification to proteins in aqueous conditions, through numerous physicochemical interactions between plasma reactive species and proteins.

4.2   Introduction

Atmospheric cold plasma (ACP) had been broadly investigated with various ***biological applications*** in clinical studies [152, 295], including wound healing [296], bleeding cessation [261], cancer treatment, as well as ***food processing*** [13], such as sterilization [1, 16], seed

germination [297, 298], enzyme inactivation [209]. The advantages of ACP in energy saving, flexible operation, and production of highly reactive species, promote ACP to a broader application as a non-thermal technique to substitute conventional treatment [261].

The recent studies illuminate that ACP treatment efficacy on biological, biomedical relevant applications, corresponds to the plasma modifications on protein [299, 300], DNA [301, 302], and amino acids [164], which can stimulate cell proliferation or death [303-305], or alter its biological functionality (enzyme activity, techno-functional property) [234, 306, 307]. Among various macromolecules, interactions between plasma and protein are notably important to elucidate when applying plasma as a biomedical tool, due to its biological functionalities and prevalence [294]. Protein structure (primary, secondary, tertiary, and quaternary structure) and its molecular mechanism play an important role in biological processes. Lackmann *et al.* [308] reported that ACP inactivated DNA nucleobases and modified protein in cellular milieu to stimulate the bacteria inactivation. ACP has also successfully inactivated prion proteins [309], surface proteins in bacteria [310], or enzymes, such as lactate dehydrogenase [209], alkaline phosphatase [311], or peroxidase [38].

Results from CHAPTER 2 illustrated that HVACP can be applied into enzyme inactivation of Pectin Methylesterase (PME) for orange juice. A recent study used HVACP to inactivate Pectin Methylesterase (PME) during orange juice processing [1]. A 2 min HVACP treatment at 90 kV using modified air (MA65) reduced PME enzyme activity by up to 85%. The mechanism for this high enzyme inactivation effectiveness of MA65 compared to air is unclear. Previous reports illustrated that plasma generated by low-frequency plasma jet (13.9 kHz, at 5 kV), using helium gas as operation gas, can interact with 14 amino acids and cause hydroxylation and nitration of aromatic rings in Tyr, Phe and Try; sulfonation and disulfide linkage formation of thiol groups in Cys; sulfoxidation of Met; and amidation and ring-opening of His and Pro [164]. Zhou *et al.*, [165] claimed that plasma may introduce a series of oxidation of amino acid side chains, including hydroxylation, nitration, dehydrogenation, and dimerization. Applying microwave plasma to Arginine Vasotocin with microwave plasma [312, 313] altered the conformation and destroyed the disulfide bond (S-S) of the peptides. However, few studies have assessed the mechanism of ACP treatment on protein structure or physicochemical reactions between plasma reactive species (RS) and proteins in aqueous condition. Therefore, understanding the modification efficacy and

mechanism of ACP on protein is critically important for optimizing ACP for medicine and facilitate its broad application in other areas [14].

In this study, bovine serum albumin (BSA) is selected as a model protein, which has been well studied and applied in research of food, medicine, nutrition and other areas [314-316]. BSA consists 607 amino acids (AAs), with seventeen S-S bounds and 1 free thiol group (SH). The *objective* of this study is using BSA as a model protein, to study the modification mechanisms using high voltage atmospheric cold plasma (HVACP) in aqueous condition. BSA solution (in a phosphate buffer) was treated by various durations of HVACP at 90 kV, packed with air or MA65 (65% O_2, 30% N_2, 5% CO_2) in sealed bags. The modification of HVACP on BSA was evaluated by characterizing its conformational and chemical alterations.

4.3 Materials and methods

Sample Preparation and Packages

BSA (Sigma-Aldrich, US), solutions (50 mg/mL) were prepared in 10 mM phosphate-buffered saline (PBS) solution with Milli-Q water, with an initial pH of 7. Protein concentrations were verified by Lowry method [317]. All BSA solutions were stirred thoroughly to ensure proper hydration of proteins and stored at 4 °C.

The 10 mL BSA solution in a Petri dish (diameter: 3.5 cm) was placed in a storage box and flushed with either dry air (<5% relative humidity) or MA65 (65% O_2, 30% N_2, 5% CO_2, <5% relative humidity) for 3 min using a Cryovac® B2630T (Sealed Air, North Carolina, USA) high barrier film to retain the plasma and reactive gas species (RGS). The gas composition in the box was analyzed using detector tubes (Dräger-Tubes®, Houston, TX) to confirm the purity of the fill gas (air or MA65).

High Voltage Atmospheric Cold Plasma (HVACP) Treatment

The HVACP device (Figure 4.1) is an ACP generator employed for in-package plasma treatment [16]. The HVACP system used a transformer (Phenix Technologies, MD, USA) to deliver a maximum output voltage of 120 kV (AC) at 60 Hz. A combination of dielectric barriers was assembled to achieve maximum PRS generation for each gas-package combination. The

package was placed in between two 15.24 cm diameter aluminum electrodes (with a gap of 4 cm), and the two acrylic layers (315 x 380 x 6 mm) above and below the package as additional dielectric barriers. BSA solutions were exposed directly and indirectly to 90 kV for 20, 40, and 60 min, respectively.
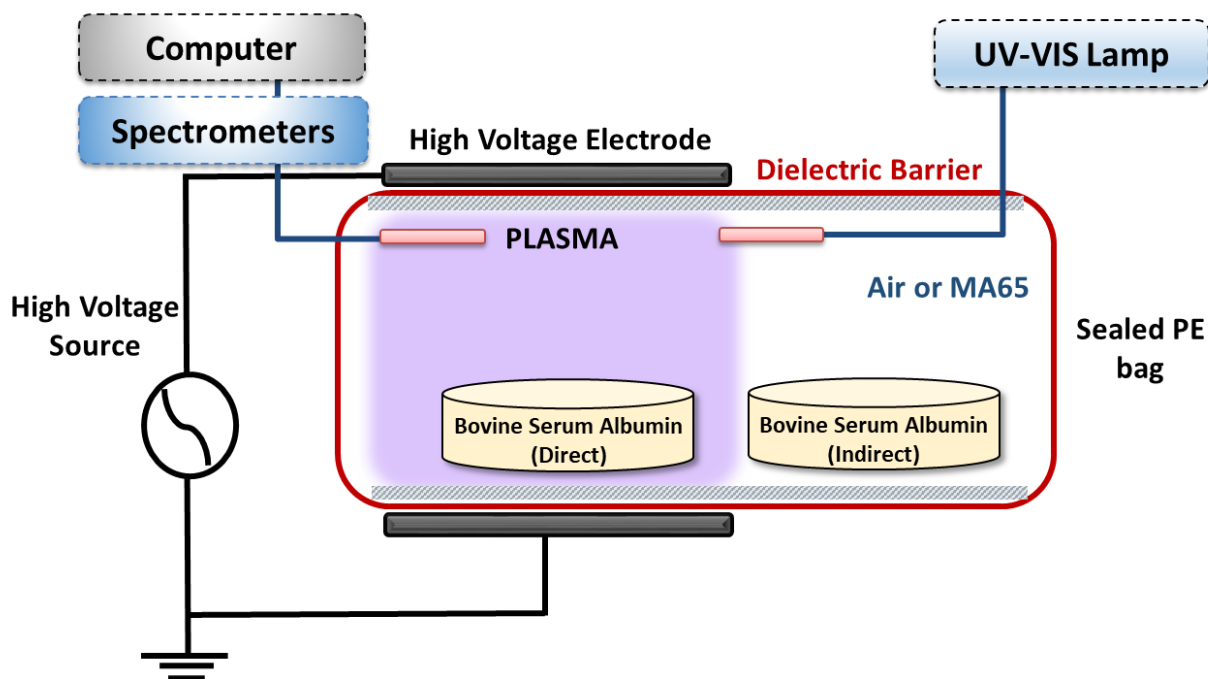
Figure 4.1 Schematic of the experimental setup employed for high voltage atmospheric cold plasma (HVACP) treatment of bovine serum albumin (BSA) solution samples (in Petri dishes) with both direct and indirect exposure, in a sealed polyethylene (PE) bag captaining air or MA65.

Characterization of Color, pH, and Temperature

Solution color was measured using a HunterLab colorimeter (ColorFlex model A60-1010-615, Hunter Associates Inc., Reston, VA) at 20 ± 1 °C. The instrument (65°/0° geometry, D25 optical sensor, 10° observer) was calibrated using white ($L = 92.8$; $a = -0.8$, $b = 0.1$) and black reference tiles. The $b*$ (yellowness/blueness) value was recorded.

The pH values of BSA solutions were recorded by a digital pH meter (Orion model 420A, Allometrics Inc., Seabrook, TX). Continually stirred samples (10 mL) were measured right after the plasma treatment (0 h) and after 24 h post-storage. Upon complete the plasma treatment, we

measured the temperature of each plasma-treated solution and compared it to the nontreated samples.

Particle Size Determination

The particle size distribution of samples was determined using Static Light Scattering Mastersizer 2000 equipped with a Hydro 2000 MU dispersion unit (Malvern Instruments Ltd., Worcestershire, UK) and Dynamic Light Scattering Zeta-sizer (Nano ZS, Malvern Instruments Ltd., Worcestershire, UK) [318]. We set the refractive index (RI) of the fluid phase (1.33), disperse phase (1.45) and absorption parameter (0.001) [315]. The particle sizes are reported as the average of six measurements of cycles of 10 s [319].

Far-UV-Circular Dichroism (CD)

The far-UV CD spectrum (190-250 nm) of the BSA (control and HVACP treated), measured by the Jasco Model J-810 spectropolarimeter (Japan Spectroscopic Company, Tokyo, Japan) was characterized to analyze the secondary structure of proteins [320]. The samples were measured at room temperature in a 1.0 mm optical path length quartz cell with a continuous flow of nitrogen. The BSA solutions were analyzed in 0.1mg/mL dilutions. Each CD spectrum was the accumulation of five scans at 50 nm/min with a 0.5 nm slit width. Using phosphate buffer as a blank, the spectrum was subtracted from the average of three spectra to obtain a corrected spectrum expressed as CD (mdeg) for each sample. We recorded the spectra in triplicate and analyzed them using Spectra Manager (JASCO Co., Ltd). The percentages of α-helix, β-sheet, β-turn and random coil structures were determined using the protein secondary structure estimation program (Yang's method [321]) provided by the Jasco J-810 spectropolarimeter [320].

Sodium Dodecyl Sulfate-Polyacrylamide Gel Electrophoresis (SDS-PAGE)

SDS-PAGE was performed on native and HVACP treated BSA to characterize molecular weight (Mw) distributions. SDS-PAGE analyses were carried out on a mini-Protein 3 cell from BioRad Laboratories (Hercules, CA) based on the method of Laemmli [322]. The samples were diluted with Laemmli sample buffer (1:2) containing 5% (v/v) β-mercaptoethanol (in reducing gel) and heated at 100 °C for 3 min. The samples were loaded onto 10 well Mini-PROTEAN TGX Precast Gel (Tris-HCl, 4-15%) with a loading concentration of 3 mg/mL (on a protein basis) and

loading volume of 15 mL. The running buffer (25 M Tris-HCl buffer pH 8.3) included 0.192 M glycine and 0.1% w/w SDS. Gels were stained for protein with Coomassie Brilliant Blue G-250 (Bio-Red Laboratories). The gels were destained with 10% acetic acid (v/v), washed with Milli-Q water, and then quantified using a gel analyzer (Syngene Europe, Cambridge, United Kingdom).

Fourier-transform infrared (FTIR) spectroscopy

FTIR spectra were collected to characterize the structure of untreated and plasma treated BSA [323]. FTIR spectroscopy (Travel IR, SensIR Technologies, United States) equipped with a temperature-stabilized deuterated triglycine sulfate detector was used to collect spectra of lyophilized powder of untreated and plasma treated BSA, with 4 cm^{-1} resolution over a wavenumber range of 4000-650 cm^{-1}, accumulating 256 scans per spectrum. The cell was cleaned after each sample measurement with water and detergent. A blank spectrum was registered to avoid any cross-contamination. The data were analyzed by *OMNIC* (Thermo Fisher Scientific, Waltham, MA), normalized at 1645 cm^{-1} (Amide I band). Bands were assigned based on a previous report [324].

FT-Raman

The FT-Raman spectrum of BSA was obtained using a Bruker IFS 66 spectrophotometer equipped with the FRA-106 Raman module and a cooled Ge-diode detector (Bruker Optic Inc., Billerica, MA, United States). The lyophilized sample was placed into the tiny hole of a stainless steel holder for the Raman measurement. Spectra were collected for each sample over a wavenumber range of 600–2000 cm^{-1}. The Raman had a spectral resolution of 4 cm^{-1} with 4000 scans. The spectral data processing included smoothing, baseline correction, and normalization to the intensity of 1450 cm^{-1}. The following bands were analyzed within spectral ranges: disulfide bridges (500-550 cm^{-1}), Amide I (1620-1720 cm^{-1}), Amide III (1230-1350 cm^{-1}) and Phe (1003-1005 cm^{-1}) [325].

Sulfhydryl (S-H) Groups and Disulfide Bonds (S-S)

The total and reactive SH were characterized by the colorimetric method based on *Ellman*'s method [326]. A 40 mg of 5, 5'-dithio-bis-2-nitrobenzoic acid (Sigma Aldrich, MO, USA) and 20 mL of 0.05 M Tris-Glycine buffer were mixed to prepare Ellman's reagent. Protein samples (0.4

mL) were diluted in buffer (2 mL) containing 85 mM Tris Base, 100 mM Glycine, 4 mM EDTA with or without 8 M Urea to determine free SH group or total SH group. Prepared solutions were incubated at room temperature for 30 min followed by adding 240 µL of Ellman's reagent. After incubating for another 1 h at room temperature (darkness), the subsequent absorbance was measured at 412 nm by a UV-visible spectrophotometer (Beckman, CA, USA). Sample blanks contained 2.4 mL buffer with or without urea in 240 µL Ellman's reagent for free or total SH group.

We also characterized the S-S bonds content [327, 328]. A 2-nitro-5-thiosulfobenzoate (NTSB) solution was prepared by adding 5, 5'-dithio-bis-2-nitrobenzoic acid (Sigma Aldrich, MO, USA) (0.1 g) into Na_2CO_3 buffer solution (10 mL, 1M, pH 7.5) followed by continually flowing O_2 into the solution at 38 °C until it turned orange. The stock solution (1 mL) was diluted 100-fold with buffer containing 0.2 M Tris, 0.1 M sodium sulfite, 3 mM EDTA and 3 M guanidine thiocyanate and then adjusted pH to 9.5 (assay solution). BSA samples (200 µL) were added into the assay solution (1.5 mL) and incubated in darkness for 25 min. The sample blank contained 200 µL assay solution and 1.5 mL buffer. The absorbance of the mixture was then determined at 412 nm by the UV-visible spectrophotometer. Amount of SH groups and S-S bonds were calculated as M/M protein µmol/g protein using the molar absorptivity of 13, 600 M^{-1} cm^{-1} [329].

Mass Spectrometry (MS)

MALDI-TOF Mass Spectrometry (MALDI). The samples were diluted with dH_2O to a protein concentration of 1 mg/mL. An aliquot (0.5 µL) of diluted sample and 0.5 µL of matrix (10 mg/mL a-cyano-4-hydroxycinnamic acid in 50% acetonitrile and 0.1% trifluoroacetic acid) were successively placed onto a MALDI-TOF sample plate. The mass spectra were acquired using an Applied Biosystems 4700 Proteomics Analyzer (Framingham, MA, USA), in the linear mode with an acceleration voltage of 25 kV. Mass-to-charge ratio (m/z) of control and HVACP treated BSA was obtained.

Side group modification was performed by analyzing tryptic digested samples using MS and tandem mass spectrometry (MS/MS) [164]. Native and HVACP treated BSA samples were dissolved in the assay of 6 M guanidine HCl, 50mM Tris-HCl (pH=8.0), 4mM DTT, to reach a final concentration of 0.5 mg/mL, and incubated at 37 °C for 60 min, before adding trypsin (20:1, w/w) [330]. After incubating at 37 °C overnight, samples were quenched by freezing. The

lyophilized samples were characterized by MS and MS/MS. The collected peptide mass spectra were analyzed by Mascot (Matrix Science) software and GPS Explorer software (Applied Biosystems, Framingham, MA) to match their peptide mass fingerprints. For the setup parameters, we included up to two missed cleavage sites, and oxidative-related modifications and we excluded peaks corresponding to the matrix and trypsin [331].

4.4   Results

4.4.1   Plasma Characterization

We used OES [214] and gas detector tubes (ozone-Dragger, CH21001 and NOX-Dragger, CH31001) to characterize plasma species and its concentration during HVACP treatment . Figure 4.2 shows that the recorded HVACP spectra consist of various molecular and atomic nitrogen and/or oxygen species during HVACP treatment. The major peaks in the spectra corresponded to the emissions of excited species of atomic nitrogen and atomic oxygen, including the nitrogen second positive system N_2(C-B) [224, 280], the first negative system N_2^+ (B-X) (at 336, 357, 380, 390, 405, 426 nm), and optical transitions of the O atom, including 616 nm, 777 nm and 844.6 nm. MA65 plasmas (line 2) contain primarily reactive oxygen species (ROS: such as $OH^{\cdot}$, $O^{\cdot-}$, $O_2^{\cdot-}$, H_2O_2) while air plasmas (line 1) consist primarily reactive nitrogen species (RNS, such as $NO^{\cdot}$, $ONOO^-$, and NO_2^-) (Figure 4.2a), which predetermines the RGS categories, indicates their distinct reactions rate and treatment effeteness on treated targets [1], will be discussed in the later section.
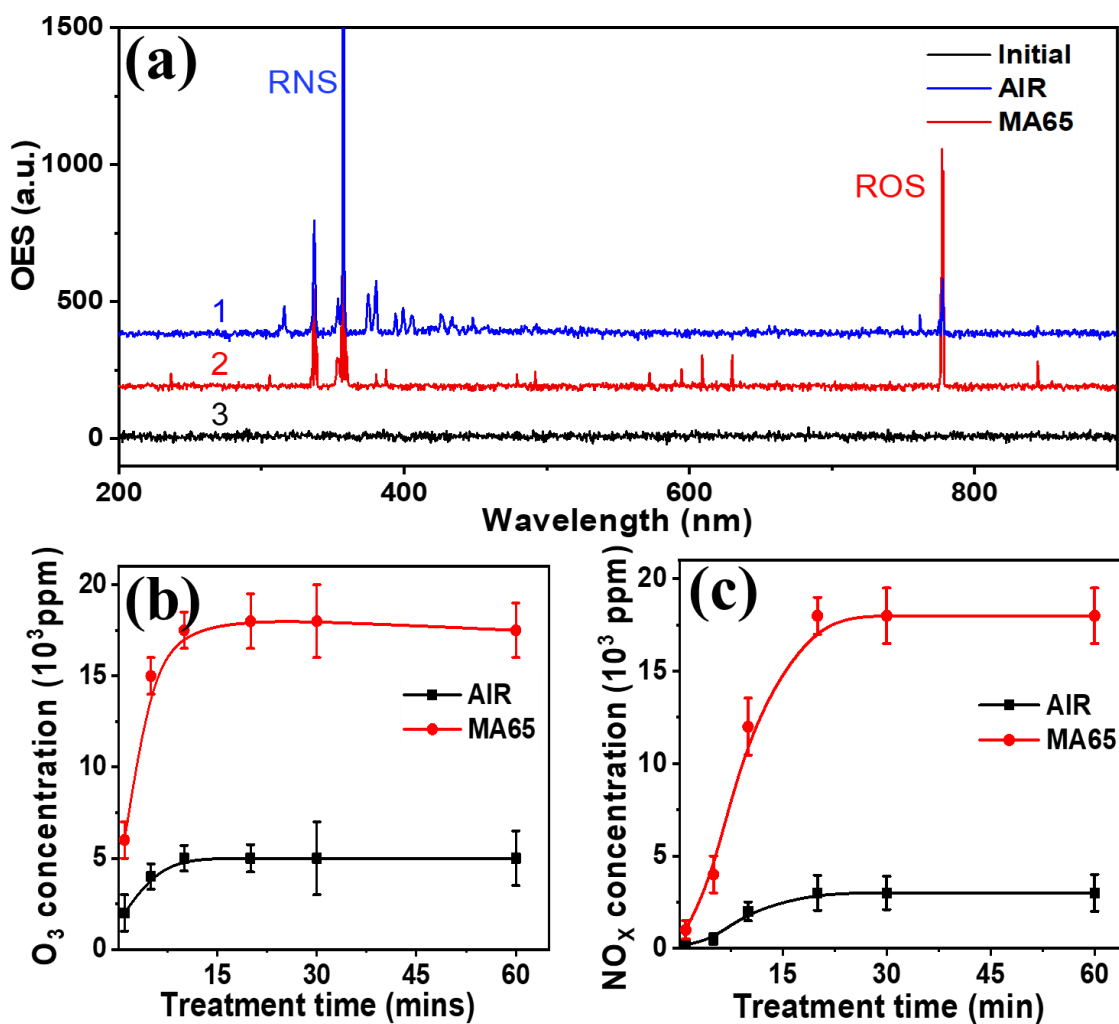
Figure 4.2 (a) Optical emission spectroscopy spectra for Air (a1) and MA65 (a2) packed BSA samples during (the steady state) HVACP treatment (direct) at 90 kV for 10 min. (a3) Optical emission spectroscopy of initial state. (c) O3 concentration (d) NOX concentration results from text strips analysis.

MA65 is feasible to generate a highly concentrated ROS species than air, as confirmed by strip test. Ozone concentrations increased up to 17,500 ppm in MA65 and 5000 ppm in air within 10 min HVACP treatment and remained at saturation concentrations for up to 60 min (Figure 4.2b and 2c), consistent with previous report [46]. Both the concentrations of ozone and NO_X were higher in the MA65 packaged sample than in air. This may be associated with the 3.1× higher concentration of oxygen in MA65 than air, which generates more ROS, confirmed by OES (Figure 4.2b). The nitrogen oxides (NO and NO_2) formed by gas-phase reactions can dissolve in water rapidly,

forming nitrous acid (HNO$_2$), nitric acid (HNO$_3$), or peroxynitrous acid (ONOOH), which induced the pH decrease and other physicochemical effects in the aqueous phase [332]. The decrease of pH may highly affect the surrounding environment of proteins and hinder its electrostatic balance, which will be discussed in the following section.

4.4.2 Protein-protein Interaction and Aggregation

HVACP treatment of BSA solution induced protein precipitation and change the sample color from transparent to yellow, shown in Figure 3a. The *b** value increased from 0.5 to 2.7 for air, and 3.1 for MA65 after 60 min treatment. This yellow color formation may primarily arise due to the protein oxidation, consistent with previous reports [333]. Protein aggregation and precipitation were first observed after BSA subject 40 min treatment (Figure 4.3a). More precipitation was generated in 60 min samples (60-D and 60-IN), which may be primarily triggered by the decrease of pH (associated with RNS) along with the protein unfolding. The pH decreased from 7 to 4.49 (MA-D-40) and 4.26 (MA-D-60), which was below the isoelectric point (PI) 4.75 of BSA control. This decrease of pH was predominantly due to the generation of nitrate and nitrite as confirmed by nitrate/nitrite acid test strips (data not shown). This mechanism was previously described [278, 279]. The nitrogen oxides (NO$_x$) formed by the gas-phase reactions (Figure 4.2c) of dissociated N$_2$ and O$_2$, can dissolve rapidly in water, to form nitrite NO^{2-} and nitrate NO^{3-} by the following reactions [280, 332]:

$$NO_{(aq)} + NO_{2\,(aq)} \longleftrightarrow 2\,HNO_2 \tag{4.1}$$

$$HNO_2 + H_2O \longleftrightarrow H_3O+ + NO_2^- \tag{4.2}$$

$$2HNO_2 \longleftrightarrow H_2O + N_2O_3 \tag{4.3}$$

$$2NO_2 + H_2O \longleftrightarrow HNO_2 + HNO_3 \tag{4.4}$$

The decreased pH consequently lowered the electrostatic repulsion between protein molecules, due to the reduction of net charge [334]. The subsequent attractive forces exceeded the repulsive forces, leading to an increased protein precipitation as time proceeding. Additionally, conformation alteration of BSA may be another reason for protein precipitation. The unfolding of BSA globular proteins prompted the hydrophobic group exposure to the surface, which facilitated protein-protein interaction and aggregation. Therefore, the synergetic effect of pH decrease and protein unfolding caused the disruption of some Van der Waals interactions, hydrogen bonds, and

electrostatic interactions, which may correspond to increased protein-protein interaction and derived aggregation [335].

Consequently, the average partial size in BSA solution/suspension increased from 10 nm (control) to 50 µm (MA-40min) and 113 µm (MA-60min), as shown in Figure 4.2d and 4.2e. The result is consistent with the observation in Figure 2a which confirmed that particle size of proteins increased as HVACP treatment time proceeding, accelerating the protein-protein interaction/aggregation and deriving protein precipitation.
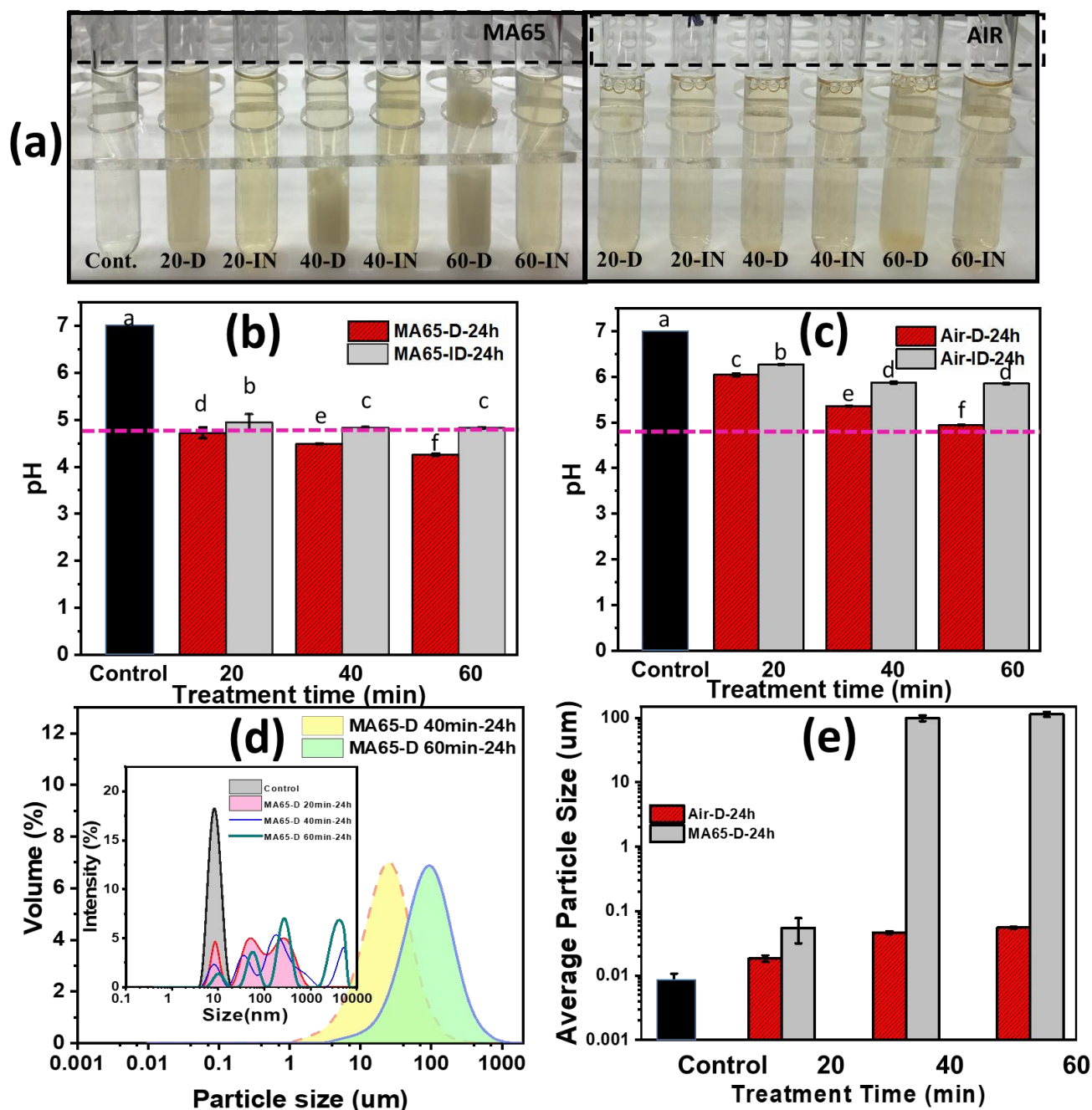
Figure 4.3 (a) Color and precipitation captures of BSA samples packed with MA65 and air subjected to direct and indirect HVACP treatment (with 24-h post-storage). (b) and (c) are pH of control and BSA sample subjected to 20, 40 and 60 min direct/indirect HVACP treatments (with 24-h post-storage) packed with MA65 (b) and Air (c). The pink line is the PI value (4.75) of native BSA. The different letters (a-f) represent statistically significant differences ($p < 0.05$). (d) Particle size distributions of control and HVACP treated BSA packed with MA65 subjected to 20, 40, 60 min direct HVACP treatments after 24-h post-storage. (e) The average particle size of control and HVACP treated BSA packed with MA65 and air subjected to 20, 40, 60 min direct HVACP treatments after 24-h post-storage.

4.4.3 Protein Unfolding and Secondary Structural Alteration

In general, protein unfolding and secondary structural alteration of BSA subjected HVACP treatment were characterized by CD (in solution), FTIR and Raman (solid).

CD. HVACP treatment induced BSA unfolding and a loss of secondary structure. Far-UV CD results characterized the secondary structure alteration of plasma treated BSA samples at various time with direct and indirect exposure model, shown in Figure 4.4. Table 4.1 summarized the results of α-helix, β-sheet, β-turn and random coil. Compared with the untreated sample of 46% α-helix, plasma treated BSA sample has a decreased α-helix 19% (MA-D-60min-24h) and increased disorder structure (β-turn and random coil). Figure 4.4b and Table 4.1 demonstrated that BSA underwent sever unfolding and structure alteration as HVACP treatment proceeded. Moreover, a loss of α-helix from 38% (D-60min -0h) to 19% (D-60min -24h) indicated that plasma RGS would continue interacting with proteins during the post-storage stage, which may cause additional modifications. This was primarily attributed to that the physiochemical reactions between reactive gas species (ROS and RNS) and BSA molecules. RGS and its derived species may interact with BSA directly (gas phase) and indirectly (liquid phase) [163, 234, 336], which leads to a conformational alteration of protein (mechanism will be discussed later).
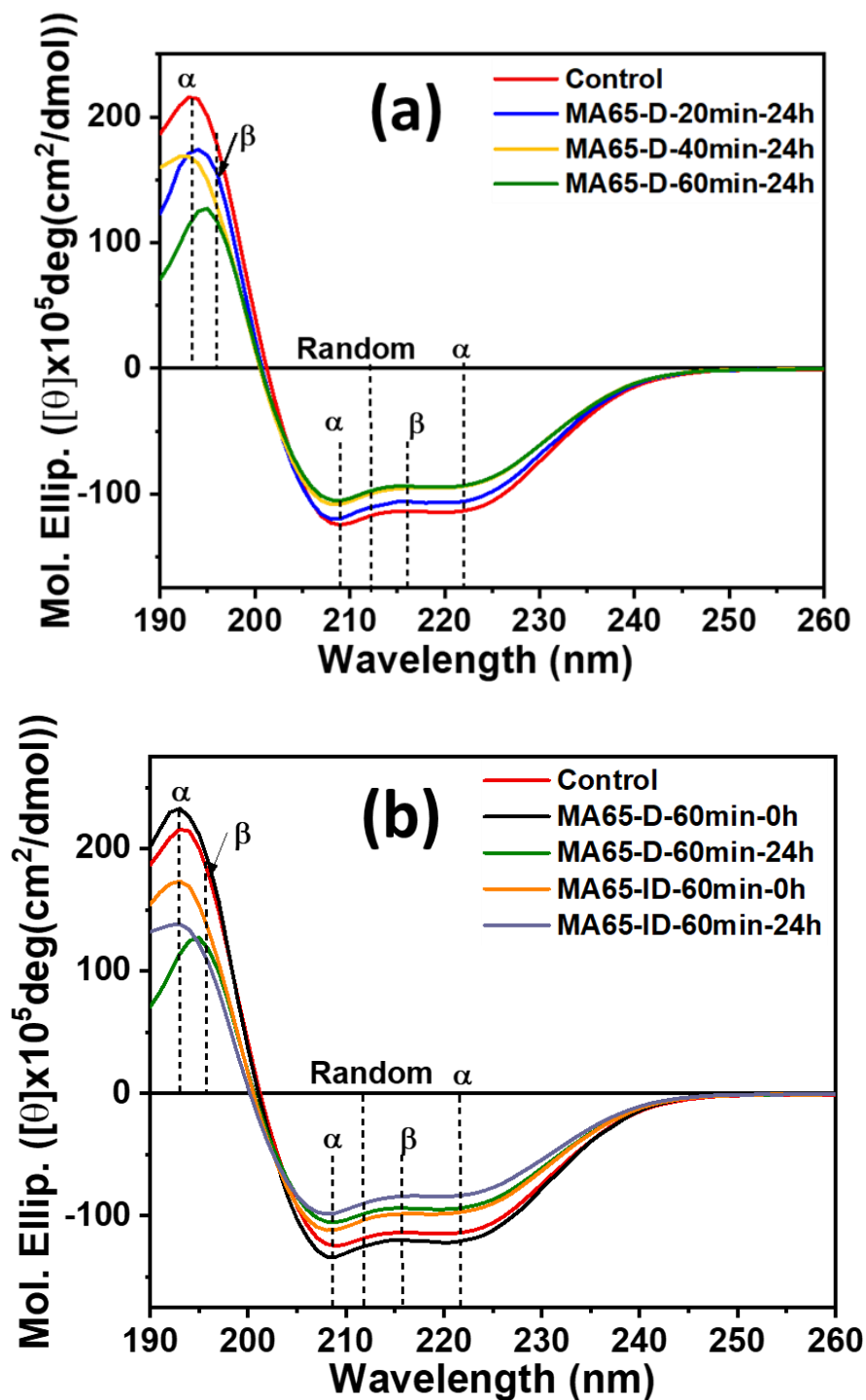
Figure 4.4 Circular dichroism spectra results. (a) Circular dichroism spectra of BSA control (red), and BSA samples packed with MA65 subjected to 20 min (blue), 40 min (yellow) and 60 min (green) of direct HVACP treatment, with 24 h post storage. (b) Circular dichroism spectra of BSA control (red), and BSA samples packed with MA65 subjected to 60 min HVACP treatment: with direct exposure at 0 h (black) and 24 h post-storage (green) storage, with indirect exposure at 0 h (orange) and 24 hours (purple).

Table 4.1 Calculated secondary structure (α-helix, β-sheet, β-turn and Random coil) based on circular dichroism spectra results in Figure 4.4, with D=direct and IN=indirect of 20, 40 or 60 min treatment at 0 h or 24 h post-storage.

Sample	Control	D-20min-24h	D-40min-24h	D-60min-24h	D-60min-0h	ID-60 min-24h	ID-60 min-0h
α-helix (%)	46	40	34	19	38	20	31
β-sheet (%)	31	37	34	34	35	36	37
β-turn (%)	8	4	6	15	7	10	4
Random (%)	15	19	26	32	20	34	28

FTIR. Figure 4.5 shows the structural change characterized by FTIR. The spectra of BSA was collected from 900 to 4000 cm^{-1}. The FTIR spectrum of natural BSA is dominated by bands of amide I (mainly C=O stretching vibration), amide II (coupling of the N-H bending and C-N stretching modes) and 3300 cm^{-1} (N–H stretch) [337, 338].A comparison between the native and plasma treated BSA samples showed that the maximum of the amide II band shifted from 1518 cm^{-1} to 1532 cm^{-1}in air/MA65 packed samples, indicating a conformational change (Figure 4.4a-I). The S$_2$O$_3$$^{2-}$ group had two characteristic peaks at about 995 cm^{-1} and 1115 cm^{-1}, whereas the SO$_4$$^{2-}$group had one characteristic peak at about 1100 cm^{-1} [339, 340]. The generation of a new peak at 1046 cm^{-1} and loss of the peak at 1103 cm^{-1} in the region of 950-1125 cm^{-1} indicate the diversification of sulfur-containing groups (Figure 4.4a-II). The single thiol, Cys34, is vulnerable for oxidization into intermediate sulfenic acid [341]. Additionally, the sulfenic acid may be able to further react with thiols to form mixed disulfides, or is further oxidation to sulfinic and sulfonic acids [341], leading to a shift/differential of characteristic peaks in the region of 950-1125 cm^{-1} [342]. All these changes of amide II, III, and sulfur-containing groups were observed in both air and MA65 packed samples (Figure 4.6a), as well as in direct and indirect exposure samples (Figure 4.6b), which confirmed our former hypothesis of plasma modification on protein structure.
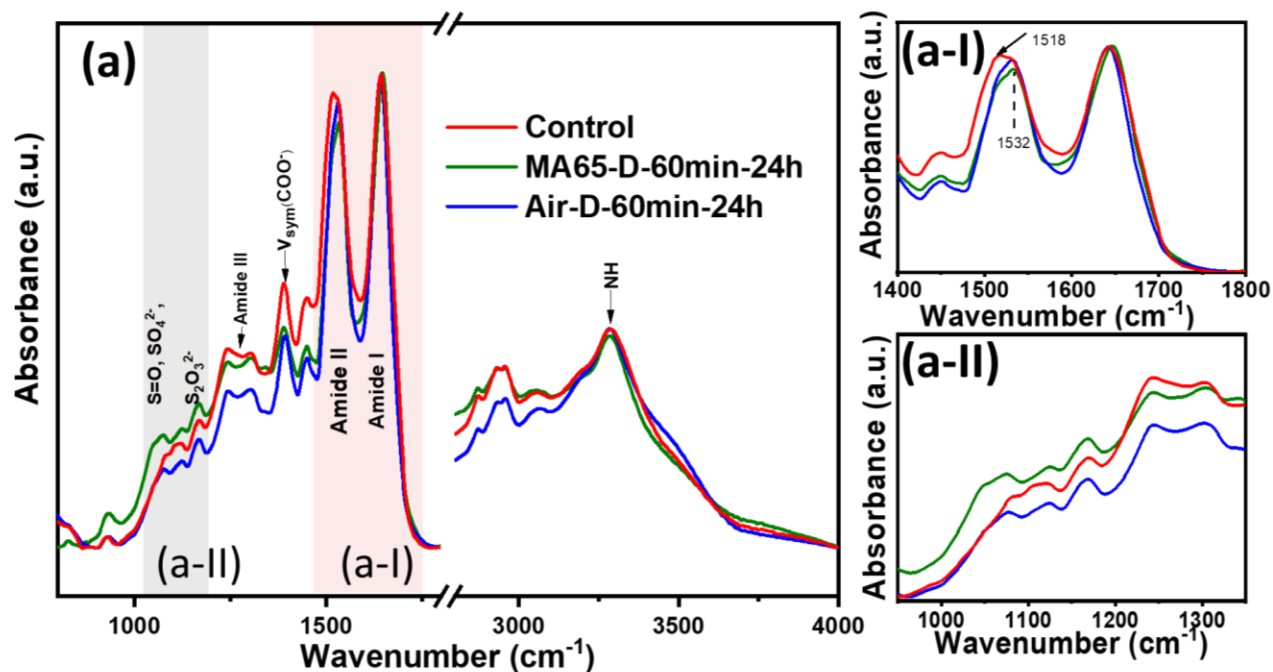
Figure 4.5 Fourier-transform infrared spectroscopy (FTIR) spectra of BSA control and HVACP treated samples. Panel (a) corresponds to FTIR spectra measured in the spectra range from 650 to 4000 cm⁻¹. BSA control (red), and BSA samples subject to 60 min direct treatment and 24 hours storage in MA65 (olive) and normal air (blue). Panel (a-I) shows Amide I and Amide II in the spectral range from 1400 to 1800 cm⁻¹. Panel (a-II) shows Amide III in the spectra range from 950 to 1350 cm⁻¹. Panel (b) corresponds to BSA control (red), and BSA samples subject 40 min direct treatment (gray) and indirect treatment (magenta) and 24 h storage in normal air. Panel (b-I) shows Amide I and Amide II in the spectral range from 1400 to 1800 cm⁻¹. Panel (b-II) illustrates Amide III in the spectral range from 950 to 1350 cm⁻¹.

Figure 4.5 continued
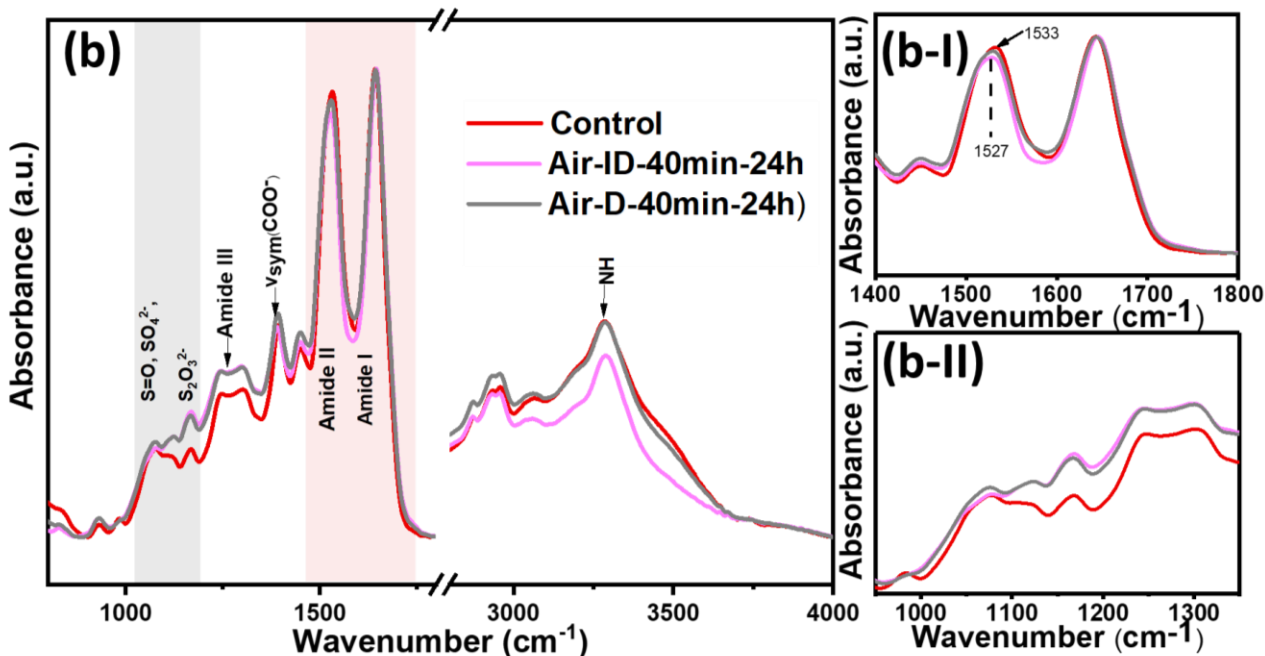
RAMAN. The secondary structure change was also characterized by FT-Raman spectroscopy, show in Figure 4.6. The Raman spectrum is dominated by bands correspond to the **amide I** (around 1650 cm^{-1}, mainly by υ-C=O vibration), C–H$_3$ and C–H$_2$ deformation vibration from side chains of different amino acids (in the range of 1440–1480 cm^{-1}), the symmetry stretching of –COO$^-$ group (around 1420 cm^{-1}), and **amide III** band from in-plane δ-NH group and υ-C–N (1230–1350 cm^{-1}), the contribution from different amino acids; Phe (1003 cm^{-1}), cysteine (505 cm^{-1}) [324]. In the zoomed spectra (Figure 4.6b), dual peak of 1300-1350 cm^{-1} (corresponds to α-helix) loss its shape, and spectra of 1250$\pm$5 cm^{-1} (corresponds to random coil) has increased signal, indicating a shift of α-helix towards disordered structure in plasma treated BSA. The shift of amide I from 1651 cm^{-1} to 1660cm^{-1} in Figure 4.6c, Phe peak from 1003 cm^{-1} to 1005 cm^{-1} in Figure 4.6d, Cys peak from 505 cm^{-1} to 513 cm^{-1} in Figure 4.6e, highly exhibited the structure alteration in plasma treated BSA samples, which is consistent with CD and FTIR results.
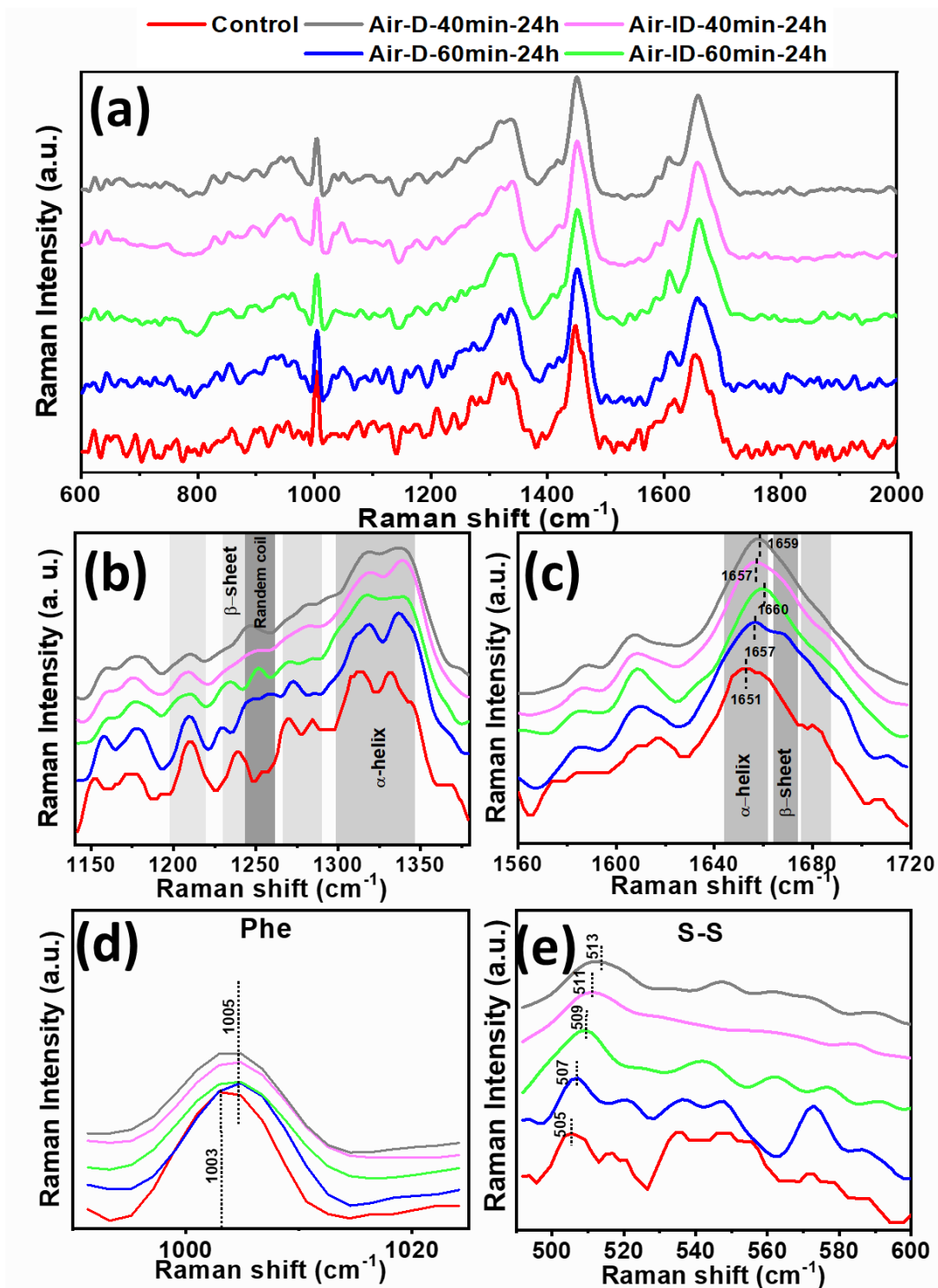
Figure 4.6 Raman spectra of BSA control (red) and BSA samples subject direct treatment in air for 40 min (gray) and 60 min (blue), indirect treatment in air for 40 min (magenta) and 60 min (green). (a) Raman spectra are shown in the whole range from 600 to 2000 cm-1. Raman spectra are shown in various ranges, corresponding (b) Amide III (1228 to 1340 cm-1). (c) Amide I (1649 to 1700 cm-1). (d) Phenylalanine (1003 cm-1). (e) Disulfide bond (500 to 550 cm-1).

4.4.4 Peptide-bond Cleavage

HVACP treatment can cleave the peptide-bond of BSA. Protein Mw distributions of native and plasma treated BSA were characterized by SDS-PAGE and MALDI, shown in Figure 4.7. The major protein in BSA has an Mw of 66 kDa. After HVACP treatment, smear bands appeared in the gel region corresponding to a lower Mw (10-50 kDa) in the gel running under non-reducing and reducing conditions. The formation of new bands suggested that plasma treatment caused peptide-bond cleavage to BSA, generating new peptides with a smaller Mw shown in the SDS-PAGE gel. Figure 4.7 shows the application of MALDI mass spectrometry to characterize the molecular distributions to further confirm the peptide-bond cleavage of plasma treated BSA. The major peaks in the control (Figure 4.7b) correspond to singly charged (66.56 km/z) and doubly charged (33.28 km/z) BSA. The new peaks with m/z of 8.1. 9.6, 10.5×10^3 in Figure 4.7c validated that new peptides (in a lower mass range, less than 66 kDa) were generated in plasma treated BSA samples, which is consistent with the observation in SDS-PAGE. Furthermore, the peak pattern of the MS spectra broadened and shifted to higher m/z, which may indicate the protein crosslinking or side-group modifications.
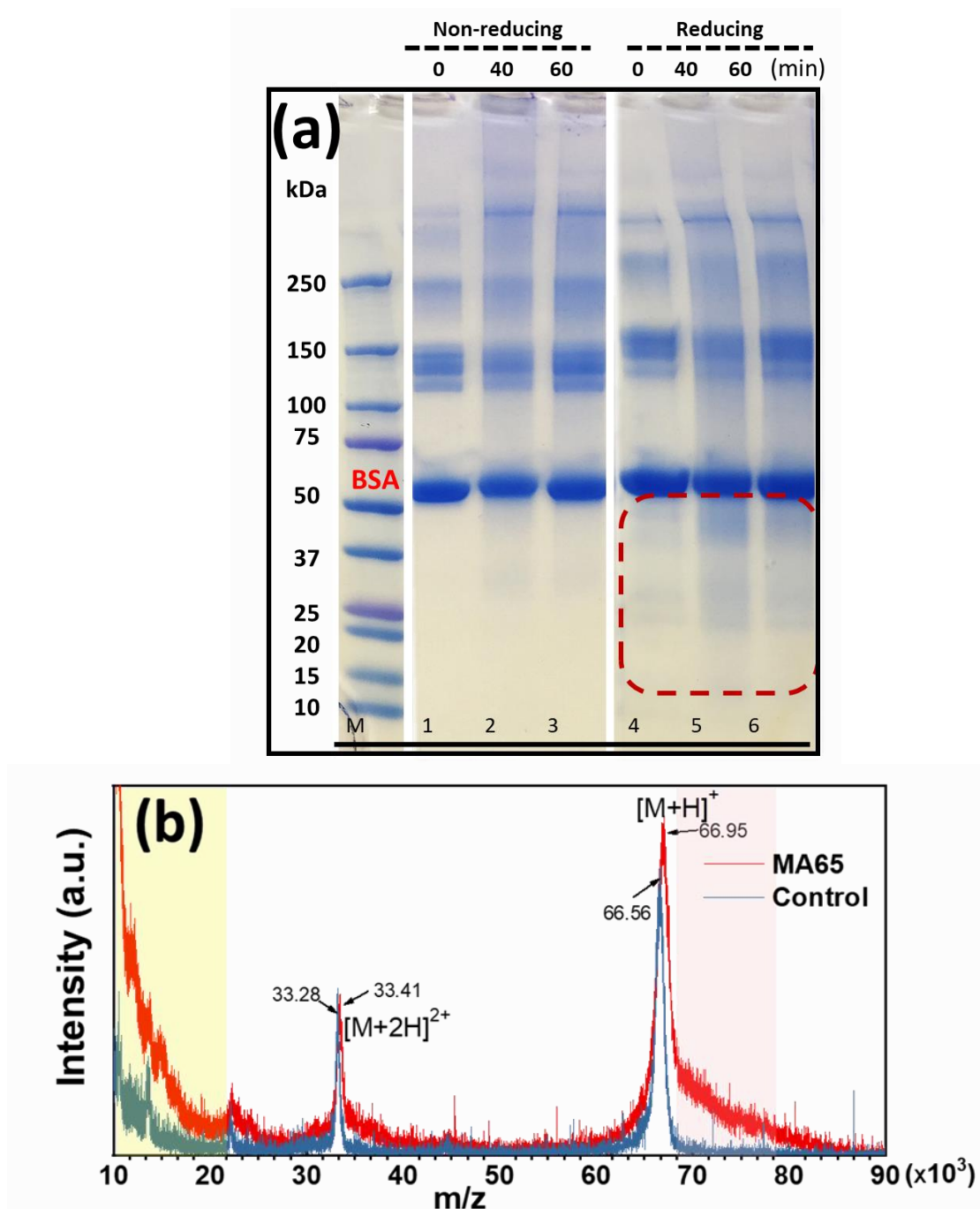
Figure 4.7 (a) SDS-PAGE electrophoresis image (non-reducing/reducing) of BSA control, and BSA samples (MA65) subjected to 40, 60 min HVACP treatments with direct exposure. (b) MALDI-TOF mass spectrometry analysis of BSA control (blue), BSA protein packed with modified air subjected to direct HVACP treatments after 24-h post-storage (red) in the range of $10 \sim 90$ ($\times 10^3$). (c) MALDI-TOF mass spectrometry analysis of BSA control (blue), and BSA samples packed with MA65 subjected to direct HVACP treatments after 24-h post-storage (red) in the range of $6 \sim 20$ ($\times 10^3$); (d) hydrolyzed BSA control (red), hydrolyzed BSA protein packed with MA65 (red) subjected to direct HVACP treatments after 24-h post-storage.

Figure 4.7 continued
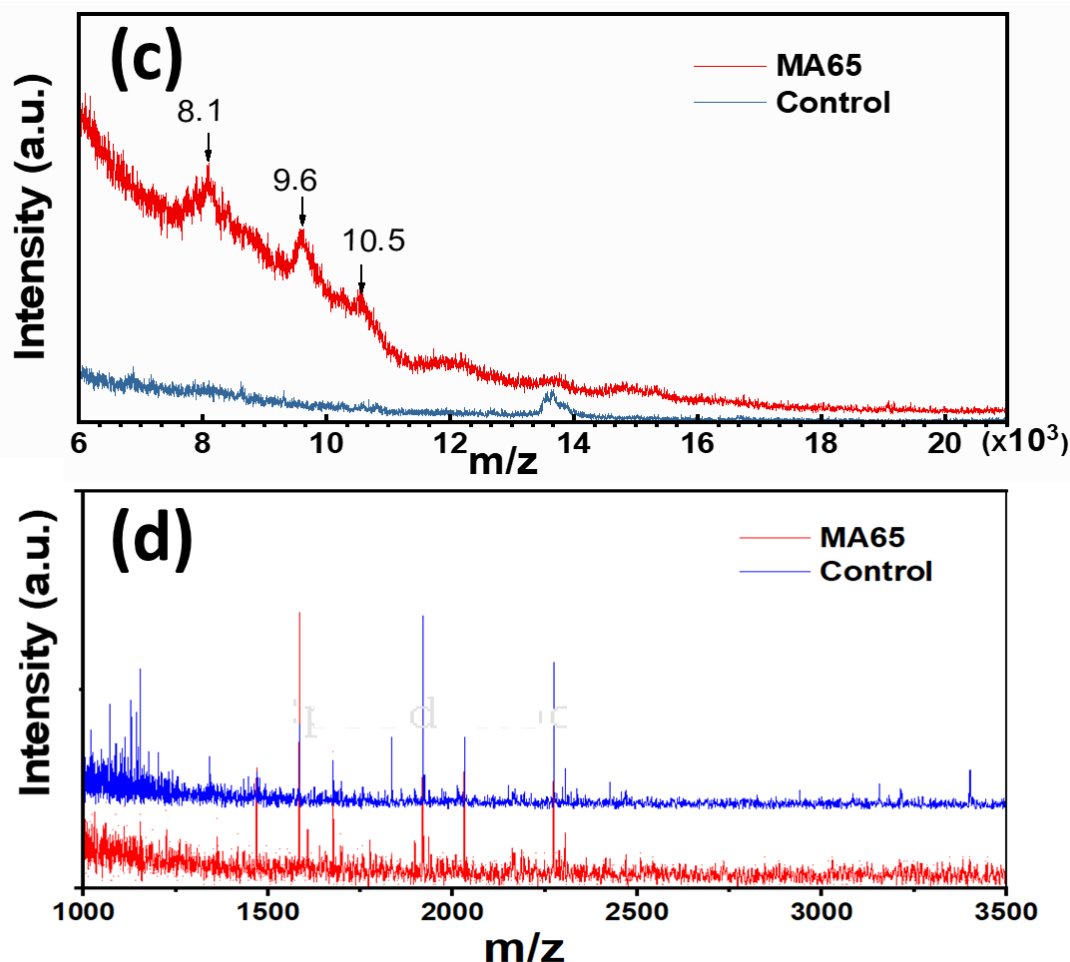
This peptides cleavage may be caused by the electric field (photochemical and photophysical reactions) during plasma treatment, as well as by RGS (oxidation cleavage) [312]. HVACP contains numerous radicals, including superoxide ($O_2^{\bullet-}$) and hydroxyl radicals ($^{\bullet}OH$), atomic oxygen (O), nitric oxide ($^{\bullet}NO$). Throughout the plasma-liquid interactions, several moderately long lifetime PRS are generated, including nitrites (NO_2^-), nitrates (NO_3^-), ozone (O_3) and hydrogen peroxide (H_2O_2) [343]. The photochemical, photophysical, and electrochemical oxidation may have synergetic efficacy on proteins, including cleavage of a covalent bond, interaction with amino acid/modification of side group. Motrescu *et al.* [312] reported that plasma will generate ions with high energy that can cleave disulfide bonds more efficiently than the ion kinetic energy [312].

4.4.5   Amino Acid Modification

Plasma can introduce side chain modification of amino acids during HVACP treatment, demonstrated by mass spectrometry. The physicochemical reactions were activated by the plasma and its derived PRS that can oxidize amino acids side chains, including sulfur-containing and aromatic amino acids. Results of Raman spectra shift of Cys (from 505 cm^{-1} to 513 cm^{-1}) in Figure 4.6e, and peak alteration in FTIR results in Figure 4.5 (generation of a new peak at 1046 cm^{-1}, loss of a peak at 1103 cm^{-1} in the region from 950 to 1125 cm^{-1}), highly demonstrated the modification of sulfur-containing groups in plasma treated BSA samples. The native BSA contains 35 half-cysteines, comprised 17 disulfide bridges and 1 free sulfhydryl group [316]. Chemical analysis in Figure 4.8a characterized that the free sulfhydryl group content for native BSA was 0.93 M/M protein. Less free sulfhydryl groups in BSA was found with increasing HVACP treatment time; 0.41, 0.32, 0.21 M/M protein after 20, 40, 60 min treatment, respectively, with direct exposure packed with air. Up to 96% reduction of free sulfhydryl group was observed in MA65-Direct exposure for 60 min, indicating the majority of free sulfhydryl group has reacted with PRS and transfer to sulfinic/sulfonic acids. Plasma may preferentially react with sulfur-containing amino acids [344], which are associated with the highly reactive thiol group in Cys and Met. The thiol groups can oxidize to sulfonic acid (R-SO$_2$-OH) *via* the intermediates sulfenic acid (R-S-OH) and sulfinic acid (R-SO-OH) [342, 345].
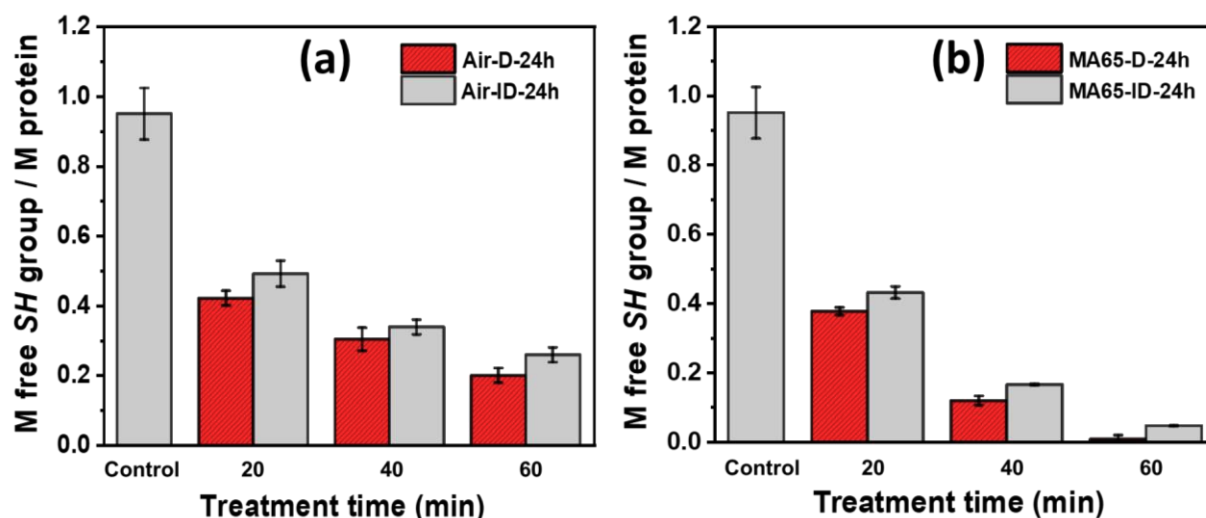
Figure 4.8 Free SH group contents of control BSA protein, BSA samples packed with air (a) MA65 (b) subjected to 20 min, 40 min, and 60 min direct/indirect HVACP treatments followed by a 24-h post-storage.

A combined analysis using MALDI and MS/MS, shown in Figure 4.8 (c) and (d), validated that the plasma treatment triggered multiple modifications of BSA samples, predominantly oxidation. In addition to oxidation, hydroxylation and deamination also occured in both air and MA65 packed samples (Figure 4.9a, 4.9b), which is consistent with previous studies [164, 165]. A mass spectrometry analysis identified methionine sulfoxide as the first and most abundant modification in RNase A subjected to plasma treatment [161]. Moreover, the observed modifications of amino acids corresponded to the chemical reactions with the plasma reactive species, rather than chemical degradation by acidic pH [344]. Figure 4.10 summarized all the modified spot on the whole BSA sequence, which served as a reference for future studies of plasma-protein interactions.
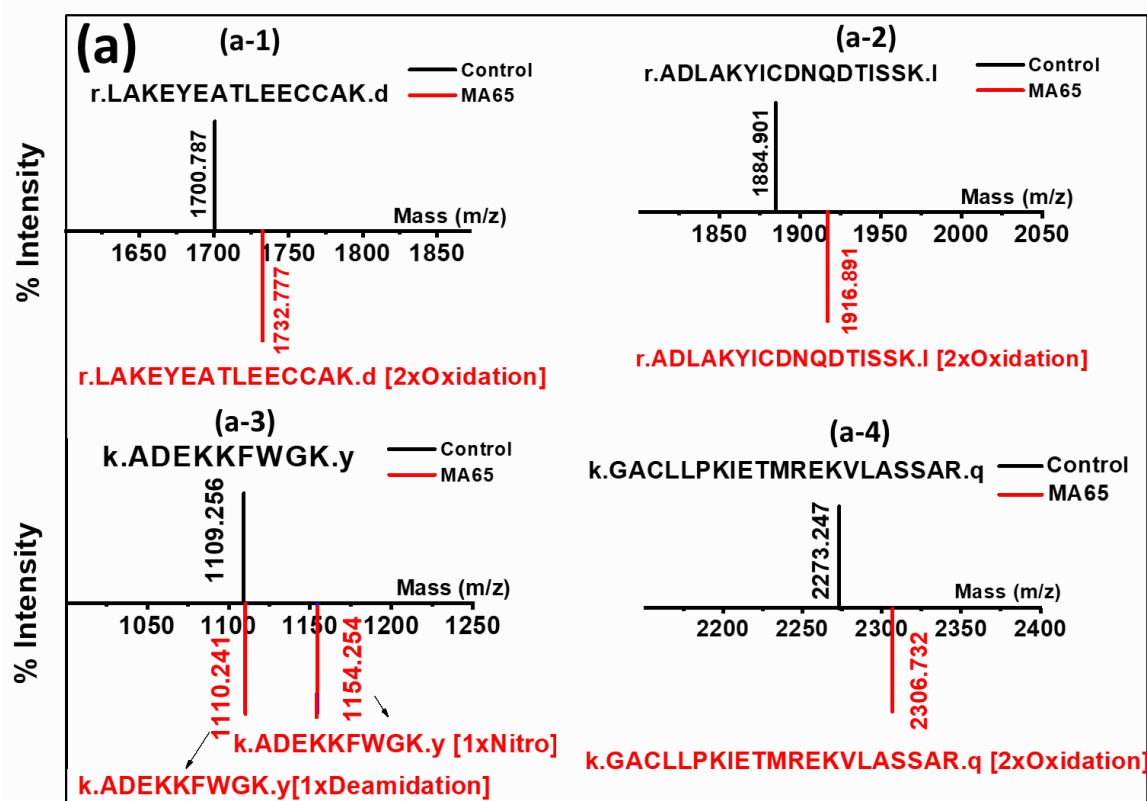
Figure 4.9 (a) Mass spectrum analysis of control BSA protein (black) and BSA proteins packed with MA65 (red) subjected to direct HVACP treatment; (b) Mass spectrum of control BSA protein (black) and BSA proteins packed with air (red) subjected to direct HVACP treatment.

Figure 4.9 continued

(b) **(b-1)** k.LVTDLTKVHK.e — Control — Air

1153.694

Mass (m/z)

1100 1150 1200 1250 1300

1170.381

k.LVTDLTKVHK.e [1xOxidation]

(b-2) k.ADEKKFWGK.y — Control — Air

1108.579

Mass (m/z)

1050 1100 1150 1200 1250

1125.256

k.ADEKKFWGK.y [1xOxidation]

(b-3) k.KFWGKYLYEIARR.h — Control — Air

1729.954

Mass (m/z)

1650 1700 1750 1800 1850

1733.986

k.KFWGKYLYEIARR.h [3xDeamidation]

(b-4) k.ADEKKFWGK.y — Control — Air

1109.256

Mass (m/z)

1050 1100 1150 1200 1250

1110.241

k.ADEKKFWGK.y [1xDeamidation]

% Intensity

Figure 4.10 Summary of ACP modified amino acid (color) and peptide sequence (identified through MS/MS).

In addition to the oxidation of methionine and cysteine, several other modifications were characterized by the mass spectrometry data (Figure 4.8). A mass spectrometry analysis identified methionine sulfoxide as the first and most abundant modification in RNase A [161]. The amino acid observed chemical modification in this study resulted from the chemical reaction with the active species generated by APCP, rather than chemical degradation by acidic pH [344].

4.5   Discussion

In this study, HVACP has caused protein-protein aggregation, protein unfolding, and secondary structural alteration, peptide-bond cleavage, as well as amino acid modification, shown in Figure 4.11. The proposed mechanism for these changes is that plasma and its derived PRS will interact with protein through physiochemical reactions (photochemical, photophysical,

electrochemical reactions) directly and indirectly. The ions, neutrals, UV radiation, electrons, photons, and other reactive species have synergetic effects on proteins and its surrounding environment (pH). PRS plays a primary role in these modifications. Previous studies reported that plasma can generate various chemically-active species, especially in discharges with high oxygen or nitrogen content [161]. OES and chemical analysis verified that HVACP treatment creates ROS and RNS, which have biological reactivity and can interact with DNA, proteinase, other bioactive components [308]. In this study, the interactions between the PRS and proteins initiated protein denaturation, which changed its surrounding environment that led to a loss of secondary and tertiary structure (Figure 4.4, 4.5 and 4.6). Additionally, protein unfolding accelerated the protein-protein interaction and aggregation (Figure 4.3). Oxidative stress from ROS can also yield side-chain and backbone fragmentation (Figure 4.7), aggregation via covalent cross-linking or hydrophobic interactions, protein unfolding and altered conformation [346]. This is consistent with previous reports that plasma treatment may alter the protein physical (Mw) and chemical properties (the primary and the secondary structure), which has been prevalently applied for surface cleaning or enzyme inactivation [234, 347].
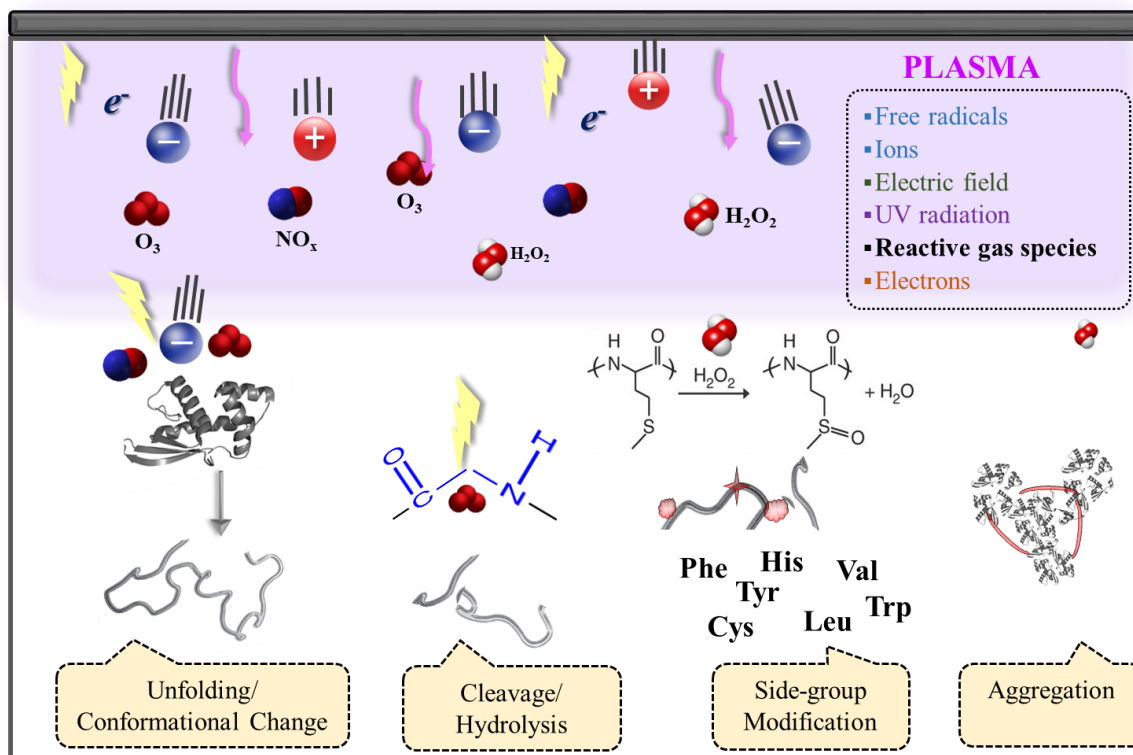
Figure 4.11 Schematic of the proposed mechanism for plasma-protein interactions.

The modification efficacy of HVACP treatment on BSA is primarily affected by the treatment parameters, including treatment time, plasma generation gas (air/MA65), and exposure model (direct/indirect exposure). A substantial denaturation occurred with increasing HVACP treatment time, which was associated with the high concentration of PRS in the long-time treated BSA samples (Figure 4.2). Consequently, using MA65 as plasma generation gas was more effective in introducing protein aggregation and oxidation (Figure 4.3), which was associated with the high concentrations of ROS (Figure 4.2b) [346]. Subjecting a series of physiochemical reactions, the most prevalent plasma derived species in the aqueous region include H_2O_2, O_{3aq}, HNO_{3aq} and HNO_{2aq} [155, 156, 273], which obtaining strong biological reactivity [208] and is feasible to interact directly or indirectly with proteins. From an energy perspective, though peptides bond (330-380 KJ/mol) is relatively stable, compared with hydrogen bond (4-12 KJ/mol) or electrostatic interaction (42-84 KJ/mol), which has a high energy barrier for chemical or physical reactions [335], HVACP is capable to modify protein, altering its structure, modifying side chain of amino acid and even triggering peptide bond cleavage through physiochemical reactions, which is rarely found in non-thermal processing. Therefore, various degrees of physicochemical modifications to proteins can be achieved by plasma with adjusting the HVACP treatment parameters.

4.6   Conclusion

In summary, this study investigated the modifications of HVACP on BSA in aqueous solution. We used air and MA65 as plasma generation gas, treating BSA at 90 kV up to 60 min. The treated samples were characterized by FTIR, Raman, CD, and MALDI to evaluate its physical and chemical alterations. The observed loss of α-helix (19%), and increased disorder structure (β-turn and random coil) revealed the protein unfolding. The derived particle size increased from 10 nm (control) to 50 µm (MA-40-min) and 113 µm (MA-60-min). The synergetic effects of electric filed and PRS generated by plasma led to peptide bond cleavage and side-group modifications of BSA, which was rarely reported in other non-thermal treatment (high pressure, UV light, ultrasound, and irradiation) [116]. The novelty of this study addressed using a high voltage (up to 90 kV) cold plasma to treat protein, which provides an effective way to modify protein by physicochemical reactions, introducing protein structural alteration, peptide-bond cleavage and side-group modifications by plasma treatment. The results and proposed mechanism may be

readily applied into explaining the observed phenomena of plasma-medicinal treatment, sterilization, and enzyme inactivation, as well as expanding its application into thermal sensitive surface.

CHAPTER 5.   SUMMARY AND PERSPECTIVES

5.1   Summary

This dissertation has investigated the interactions of HVACP with microorganism and protein in the food system. CHAPTER 1 has reviewed the roadmap of ACP development and its applications in agriculture (microbial inactivation, food modifications, and waste management) and biology. Numerous studies of ACP in food system have been reported, especially with its effectiveness in food decontamination and food modifications. With respect to these broad applications and limited understanding of the reaction mechanism with the food system, this study has:

1) evaluated the interactions between HVACP and microorganism in liquid and semi-solid food;

2) identified plasma penetration and mechanism of microbial inactivation in semi-solid food;

3) explored the interactions and its mechanism between plasma and proteins.

Results from CHAPTER 2 indicated that both direct and indirect HVACP treatment of 25 mL OJ induce greater than a 5 log reduction of *S. enterica*, demonstrating that HVACP can effectively inactivate *Salmonella* in OJ. Food qualities, for instance, color, vitamin C, pH, Brix were also evaluated in OJ subjected HVACP treatment. Additional enzyme inactivation (>82% PME) was achieved by HVACP treatment, revealing its potential applications in enzyme inactivation and protein modification.

CHAPTER 3 initialized the study of HVACP treatment in semi-solid food. The study examined penetration capacity and plasma transport mechanism in the semi-solid material; identified the close relationship between plasma penetration and microbial inactivation in semi-solid food. A complete microbial inactivation has been achieved in the color/pH-changed zone, which corresponds to the penetration of plasma reactive species into the gel. This indicates that plasma reactive species generated by HVACP can penetrate into the semi-solid material and it can inactivate microbes as the penetrating proceeding.

With regards to the observation of enzyme inactivation by HVACP in CHAPTER 2 and previous reports of ACP treatment on proteins, CHAPTER 4 investigated the interactions between plasma and proteins, using BSA as a model protein. This study illustrates that HVACP treatment may effectively introduce structural alteration, peptide cleavage, and side-group modification to

proteins in aqueous conditions, through numerous physicochemical interactions between plasma reactive species and proteins.

5.2   Proposed Mechanism

5.2.1   Plasma-Microorganism Interactions

Plasma-cell surface interactions. Firstly, RGS may interact with the cell surface, both physically and chemically, as well as directly and indirectly, leading to the disruption of cell walls. The physical process includes electroporation, etching, charge deposition, UV radiation, etc., and the chemical process refers to the oxidation, surface electrolysis, hydrolysis, and other interactions between RGS and cell membrane. For example, the surface of *E. Coli* is formed by lipopolysaccharide, proteins and lipoproteins on the outer membrane. Using air as plasma generation gas, ACP treatment will generates numerous RGS, such as ROS (e.g. hydrogen peroxide, ozone, superoxide anion, hydroperoxyl, alkoxyl, peroxyl, singlet oxygen, hydroxyl radical, and carbonate anion radical) and RNS (e.g. nitric oxide, nitrogen dioxide radical, peroxynitrite, peroxynitrous acid , and alkylperoxynitrite). These RGS may interact with lipopolysaccharide, proteins and lipoproteins directly, by breaking of the chemical bond, etching due to bombardment by radicals, causing cell lesions and perforations on the membrane. At the same time, the negatively charged surface can also be neutralized by the H^+ ions, which is generated after RGS diffused into water, resulting in simultaneous disturbance in bacterial physiological system and molecular changes [230]. This indirect interactions between RGS and microorganism membrane result in the perturbation in membrane potential, causing either the change of membrane tension or the production of ROS inside the cell. Both these direct and indirect interactions between RGS and cell surface lead to the loss of cell integrity, which facilitate the diffusion of PRS into the cell and cause the subsequent damage interior the cell, DNA/RNA damage and protein inactivation.

Plasma cause DNA and protein degradation inside the cell. Singh et al. reported that generated plasma caused oxidative damage of bacterial DNA and proteins. The ROS and RNS interacted with DNA and damage its backbone structure, by the single or double strand break and directly affecting the sugar and base moiety [230]. RGS will also interact with side groups of the proteins, such as sulfhydryl groups, reducing the number of disulphides. These oxidation of the amino acid side

group on the protein will also lead to the structure of the proteins, as well as it functionalities. Plasma can even breakdown the peptide bound, hence reducing the molecular weight of the proteins. Smaller peptides are easier to be leaked out of the cell and facilitate this apoptosis process.

The mechanism of plasma-cell interactions has been proposed in numerous studies [110], demonstrated in Figure 5.2. Charged species generated by ACP are identified as playing the predominant biological efficacy on the cells. Revealing the mechanism of plasma-cell interactions is critical for employing ACP into food pathogen inactivation, cancer treatment and wound healing (Figure 5.2). Results from CHAPTER 2, HVACP operation parameters on microbial inactivation, and CHAPTER 3, the close relationship between plasma transfer and microbiocidal effect, facilitate the understanding of plasma-cell interactions and broaden its applications as an advance non-thermal treatment techniques.
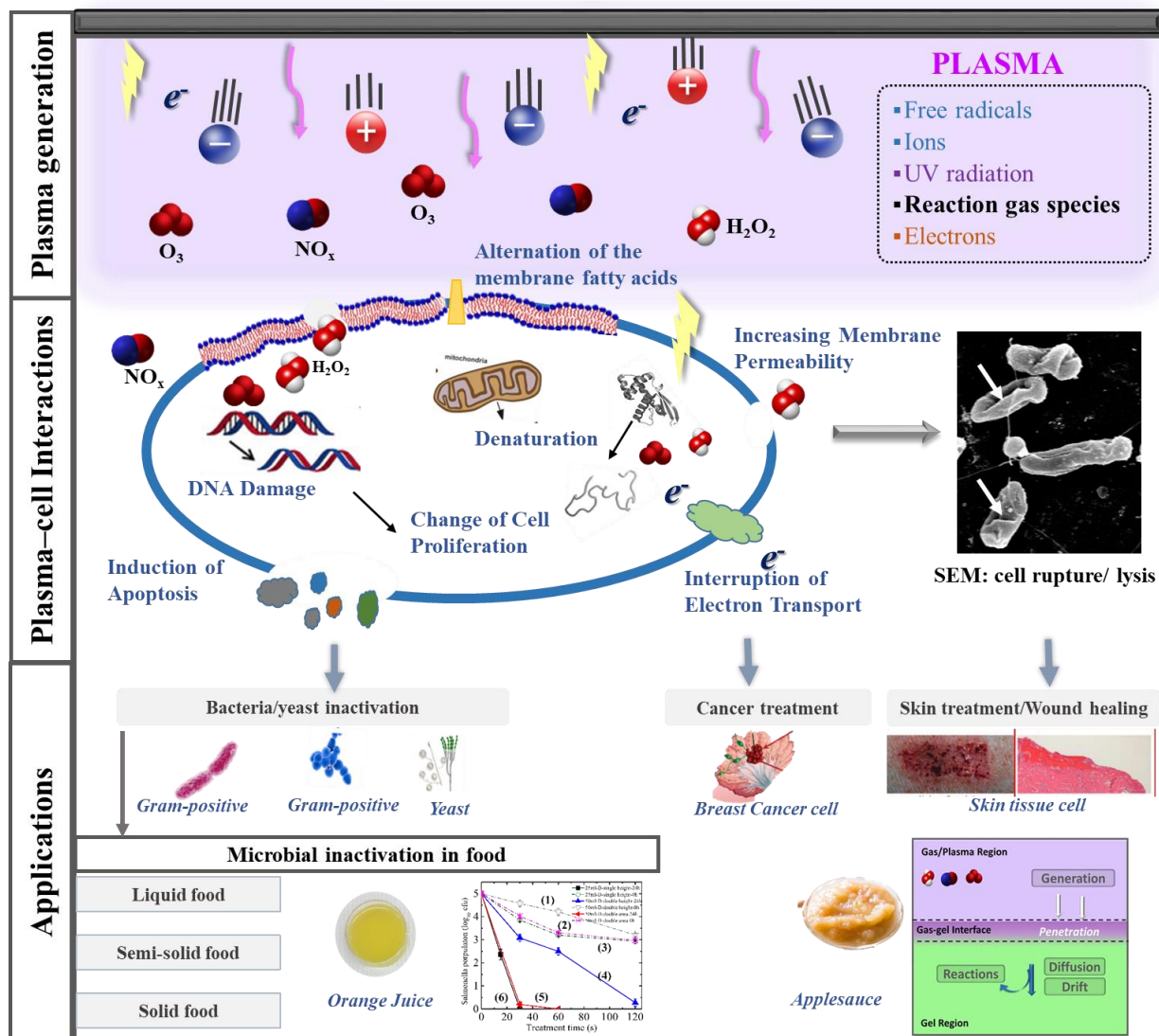
Figure 5.1 Schematic diagram of the plasma-cell interaction and its applications.

5.3 Implications

5.3.1 Plasma Generation, Transfer, and Interactions

Plasma Generation	Plasma Transfer	Interactions with Food Matrix
Voltage	Drift effect	Proteins
Time	Diffusion	Lipids
Operation gas	Media density	Carbohydrates
Exposure model	Transfer capacity	Vitamins and others
Post treatment storage	Relationship with interactions	

Solid Food	Liquid Food	Semi-solid Food
Peanut	Fruits juice	Sauce
Milk powder	Milk	Cookie dough
Vegetables	Coffee	Semi-solid cheese
Meats products	Liquid flavoring	Baby food
Cheese		

Figure 5.2 Schematic diagram of the relationship between plasma generation, transfer, and interactions in food processing.

In general, treatment efficacy of ACP into food processing (solid, liquid and semi-solid foods), is closely associated with plasma generation, plasma transfer, and plasma interactions with food components, shown in Figure 5.1. Plasma and its derived species, along with other physicochemical reactions, play the dominant role during HVACP treatment. Plasma generation process has been demonstrated to be associated with the HVACP operation parameters, such as operation voltage, treatment time, packaging gas, direct/indirect exposure model, demonstrated in Figure 5.1. A substantially microbial/enzyme inactivation (CHAPTER 2, 3) and protein modification (CHAPTER 4) were observed as HVACP treatment time proceeding, which was closely associated with the high concentration of PRS in the long-time treated samples. Lietz and Kushner reported that the densities of ROS and RNS increased roughly linearly with an increasing voltage over a certain voltage range [273]. Packaging gas will predetermine the reactions when

employing HVACP into food processing. Observed results in this study, using MA65 as plasma generation gas was more effective in introducing microbial inactivation, or protein aggregation and oxidation, which was associated with the high concentrations of ROS and RNS generated in MA65. Compared with indirect exposure, direct exposure is feasible to generate additional reactive species (such as charge species, radicals, metastable, and electrons) which has higher biological reactivity. Additionally, the treatment efficacy of HVACP is also related to characters of the treatment target, including chemical compositions/concentrations, surface topography/structure, temperature, and other factors, which will be interesting to investigate in the future studies.

In addition, CHAPTER 3 has illustrated that the penetration of plasma in semi-solid is driven by the molecular motion created by the concentration gradient-diffusion effect, and by the electrical static motion-drift effect. Therefore, a direct exposure system is preferable for plasma penetrating into treatment target to achieve fast penetration and an efficient microbial inactivation. Plasma transfer has been invested in CHAPTER 3 with a proposed model including drift, diffusion and reaction effect. This model can be readily applied adapted to other plasma sources; it can accommodate more complex biological materials, and may potentially provide new insights into plasma-induced phenomena for medical treatment or in semi-solid food, such as cookie dough, or baby foods (Figure 5.1).

5.3.2   Microbial Inactivation, Food Quality, and Food Nutrition Retention

Applying ACP treatment into inactivation of foodborne pathogens provides an alternative non-thermal technique for food processing. On the other hand, food qualities, such as viscosity, color/appearance, flavor, and texture, as well as food nutrition are critical for food consumers, which are less investigated in food subjected plasma treatment. In this study, CHAPTER 2 evaluated both microbial inactivation and quality alterations in HVACP treated OJ, providing a reference for future studies that combined microbes and quality evaluations are necessary to achieve an optimized food processing condition. The food processing conditions are predominantly determined by the achievement of food pathogen or enzyme inactivation [348]. In the typical thermal processing, the extended treatment time or increased processing temperature may affect food qualities and cause undesirable quality loss. The plasma treatment may also introduce quality alterations to food through interactions between plasma and food components, proteins, lipids, carbohydrates, and vitamins. In CHAPTER 2, we investigated the color, vitamin

C, PEM activity, and pH in OJ subjected HVACP treatment, providing necessary information for the future industrial production of HVACP commercialization in fruits juice processing. The optimum plasma processing condition need to balance the operation conditions (treatment time, voltage, operation gas, etc.) to achieve a desirable foodborne pathogen lethality as well as maximum quality and nutrient retention. Therefore, the future studies are suggested to verify the microbial, enzymatic, nutritional, and sensory quality and stability of food during the ACP process control.

5.3.3   Selective Modification by ACP

RGS plays a primary role in protein modification during HVACP treatment. CHAPTER 4 has investigated that using a high voltage (up to 90 kV) cold plasma to treat protein, which provides an effective way to modify protein by physicochemical reactions, introducing protein structural alteration, peptide-bond cleavage and side-group modifications by plasma treatment. The ions, neutrals, UV radiation, electrons, photons, and other reactive species have synergetic effects on proteins and its surrounding environment (pH). OES and chemical analysis verified that both ROS and RNS was generated during HVACP treatment, of which have biological reactivity and can interact with DNA, proteinase, other bioactive components [308]. The interactions between the RGS and proteins, initiated protein denaturation and the change of its surround environment, leading a loss of secondary and tertiary structure. Oxidative stress from ROS can also yield side-chain and backbone fragmentation, aggregation via covalent cross-linking or hydrophobic interactions, protein unfolding and altered conformation [346]. The results and proposed mechanism may be readily applied into explaining the observed phenomena of plasma-medicinal treatment, sterilization, and enzyme inactivation, as well as expanding its application into the thermal sensitive surface.

Regarding the predominant role of RGS during plasma-protein interactions, ACP operation process should be further investigated to elucidate the reactions between specific species and proteins. This will facilitate the development of a selective modification by ACP treatment. This requires a better understanding of controlling plasma generation, plasma transfer, and plasma-target interactions. The treatment efficiency will be tremendously increased by generating a controlled specific RGS of selective reactions with the treatment media. In addition to the generation control, employing modelling techniques to track and estimate plasma transfer process

will also increase the selectivity of modifications. CHAPTER 3 tracks the plasma transfer process by adding pH indicator into the gel to provide a reference for future studies of modelling plasma transfer process. A better understanding of the transfer rate, transfer capacity and limitations of RGS in liquid and the semi-solid material is necessary for estimating the treatment efficiency as well as increasing the treatment selectivity. Therefore, ACP can be applied to the broader area by generating a controlled RGS with selective reactions/modifications with the treating target.

5.4   Suggestion for future works

Table 5.1 summarizes the application prospects for ACP in the food industry. Results of this work can be readily applied into various studies of plasma processing, for instance, in beverage processing, shelf-life extensions of ready to eat food, allergen cleaning or modifications, and combining with other exiting food process (plasma-drying process).

Table 5.1   Summary of the application prospects on ACP in the food industry.

Applications	Applications	Potential applications
Food processing	Beverage processing	Microorganism, enzyme inactivation in fruits/vegetable juices; Milk/protein rich sports beverages;
	Shelf-life extensions	Ready to eat meats/seafood/cheese; Dipping sauce,
	Food Allergy	Allergen modification in foods
	Combined with other food processing	Plasma-drying process: powder foods/ingredients (milk powder, spices, carbohydrate powder)
	Environmental sterilization/cleaning	Equipment; Packaging; Residual cleaning;
	Ingredient modifications	
Challenges	(i) Interactions with vitamins and other phenolic compounds in fruits and vegetables; (ii) Lipid oxidation/hydrogenation of meats; (iii) Penetration limitation; (iv) Scale-up factors; (v) Incomplete understanding of plasma-food interactions (vi) Limited studies on sensory profile of plasma treated foods (vii) Lack of nutritional analysis, etc.	

Further investigation should analyze of the interaction between plasma and vitamins and other phenolic compounds that would benefit from its application and operation control in fruits and vegetable products. It remains challenging to maintain the products quality and nutritional value, operation optimization of plasma treatment. ACP, its non-thermal nature, provides its privilege in processing thermal sensitive foods (fresh-cut products, ready to eat foods) to extend their shelf-life by microbial decontamination or enzyme inactivation. However, few studies

evaluated the browning reactions (plasma-carbohydrate), polymerization (plasma-lipid), and discoloration (plasma-phenolic) reactions that plasma may introduce to the food system.

Besides chemistry issues (plasma-food interaction), engineering aspects, such as scale-up factors, equipment adaptability, processing design, ACP discharge configurations/capacity, and operation efficiency should also be evaluated and optimized before adapting ACP into industry scale of food processing. Though ACP may offer an operation of improved suitability by reducing input energy, or adding value to the byproducts, along with extending shelf-life of ended products, the capital of switching exiting equipment and adapting new ACP system is another concern. Therefore, a subsequent model analysis on processing capacity and operation cost will complement the integrity this area and promote the integration of ACP into existing pilot plant.

Beyond a scaled-up processing design, a portable plasma sterilizer for home or office would of great interest for costumers, demonstrated in Figure 5.3. The design consists combined applications in food preservation, air purification, and peroneal care products serializations. The portable plasma-sterilizer idea is inspired by microwave, with convincing in carrying and operation. The design includes a tray by putting foods into the chamber for direct sterilization. An extended tube on the side of the chamber is designed for treating foods in a package, by flowing plasma species into the package and sealing the bag during the storage. The species in the sealed bags will continue to react with the food to inactivate the foodborne pathogens during the post-storage, demonstrated in CHAPTER 2. On the top of the design is a control panel (time, temperature and flow) and a fan for air purification (similar to an air purifier).

Figure 5.3 Schematic diagram of portable plasma-sterilizer for home or office.

Regulation of ACP into food system is another concern. Authorizations of introducing new technology into food processing require a few reviews and approvals from federal agencies, Food and Drug Administration (FDA), United States Department of Agriculture (USDA) and Environmental Protection Agency (EPA). Application of ACP in food and food packages is associated with the regulations of the US EPA as a pesticide and then US FDA, as a food contact substance (FCS), additionally, US Department of Agriculture's Food Safety Inspection Service (USDA-FSIS) for poultry, and egg products [88]. The approval requires substantial evaluations and documents to justify the safety, quality, nutrition, chemical residual/ food additive, or other marketable benefit of the new technology compared with the controlled studies [88].

Applications of plasma in the food system are rapidly expanding and create many interdisciplinary research areas to investigate, along with providing an innovative technique to substitute conventional food process, which maintains or improves the qualities or functionalities of foods.

REFERENCES

1. Xu, L., Garner, A. L., Tao, B., & Keener, K. M. (2017). Microbial inactivation and quality changes in orange juice treated by high voltage atmospheric cold plasma. *Food and Bioprocess Technology, 10*(10), 1778-1791.

2. Keener, K. M., & Misra, N. N. (2016). Chapter 14-future of cold plasma in food processing *Cold plasma in food and agriculture* (pp. 343-360). San Diego: Academic Press.

3. Adamovich, I., Baalrud, S. D., Bogaerts, A., Bruggeman, P. J., Cappelli, M., Colombo, V. et al. (2017). The 2017 plasma roadmap: Low temperature plasma science and technology. *Journal of Physics D: Applied Physics, 50*(32), 323001.

4. Graves, D. B., & Brault, P. (2009). Molecular dynamics for low temperature plasma–surface interaction studies. *Journal of Physics D: Applied Physics, 42*(19), 194011.

5. Fitzpatrick, R. (2014). *Plasma physics: An introduction*: CRC Press.

6. Ulbin-Figlewicz, N., Jarmoluk, A., & Marycz, K. (2015). Antimicrobial activity of low-pressure plasma treatment against selected foodborne bacteria and meat microbiota. *Annals of microbiology, 65*(3), 1537-1546.

7. Fricke, K. (2012). *Influence of non-thermal plasma-based biological decontamination processes on the surface properties of plasma-exposed polymers.* Universitätsbibliothek, Dissertation.

8. Piel, A. (2017). *Plasma physics: An introduction to laboratory, space, and fusion plasmas*: Springer.

9. Peter, B., & Ronny, B. (2013). Atmospheric pressure discharge filaments and microplasmas: Physics, chemistry and diagnostics. *Journal of Physics D: Applied Physics, 46*(46), 464001.

10. Goldston, R. J., & Rutherford, P. H. (1995). *Introduction to plasma physics*: CRC Press.

11. Shukla, P. K., & Mamun, A. (2015). *Introduction to dusty plasma physics*: CRC Press.

12. Szili, E. J., Hong, S.-H., Oh, J.-S., Gaur, N., & Short, R. D. (2017). Tracking the penetration of plasma reactive species in tissue models. *Trends in Biotechnology*.

13. Pankaj, S., Wan, Z., & Keener, K. (2018). Effects of cold plasma on food quality: A review. *Foods, 7*(1), 4.

14. Kong, M. G., Kroesen, G., Morfill, G., Nosenko, T., Shimizu, T., Van Dijk, J. et al. (2009). Plasma medicine: An introductory review. *new Journal of Physics, 11*(11), 115012.

15. Misra, N. N., Tiwari, B. K., Raghavarao, K. S. M. S., & Cullen, P. J. (2011). Nonthermal plasma inactivation of food-borne pathogens. *Food Engineering Reviews, 3*(3), 159-170.

16. Pankaj, S. K., Bueno-Ferrer, C., Misra, N., Milosavljević, V., O'Donnell, C., Bourke, P. et al. (2014). Applications of cold plasma technology in food packaging. *Trends in Food Science & Technology, 35*(1), 5-17.

17. Sarangapani, C., Misra, N. N., Milosavljevic, V., Bourke, P., O'Regan, F., & Cullen, P. J. (2016). Pesticide degradation in water using atmospheric air cold plasma. *Journal of Water Process Engineering, 9*, 225-232.

18. Bermúdez-Aguirre, D., Wemlinger, E., Pedrow, P., Barbosa-Cánovas, G., & Garcia-Perez, M. (2013). Effect of atmospheric pressure cold plasma (apcp) on the inactivation of escherichia coli in fresh produce. *Food Control, 34*(1), 149-157.

19. Kim, J. S., Lee, E. J., Choi, E. H., & Kim, Y. J. (2014). Inactivation of staphylococcus aureus on the beef jerky by radio-frequency atmospheric pressure plasma discharge treatment. *Innovative Food Science & Emerging Technologies, 22*, 124-130.

20. Chen, Y. (2014). *High voltage atmospheric cold plasma treatment of refrigerated chicken eggs for control of salmonella enteritidis on external surfaces.* Purdue University, Dissertation.

21. Raizer, Y. P. (1991). Gas discharge physics. Springer.

22. Ehlbeck, J., Schnabel, U., Polak, M., Winter, J., Von Woedtke, T., Brandenburg, R. et al. (2010). Low temperature atmospheric pressure plasma sources for microbial decontamination. *Journal of Physics D: Applied Physics, 44*(1), 013002.

23. Shin, G. A., & Sobsey, M. D. (2003). Reduction of norwalk virus, poliovirus 1, and bacteriophage ms2 by ozone disinfection of water. *Applied and environmental microbiology, 69*(7), 3975-3978.

24. Scholtz, V., Julák, J., & Kříha, V. (2010). The microbicidal effect of low- temperature plasma generated by corona discharge: Comparison of various microorganisms on an agar surface or in aqueous suspension. *Plasma Processes and Polymers, 7*(3- 4), 237-243.

25. Fridman, A., Chirokov, A., & Gutsol, A. (2005). Non-thermal atmospheric pressure discharges. *Journal of Physics D: Applied Physics, 38*(2), R1.

26. Boisseau, S., Despesse, G., & Seddik, B. A. (2012). Electrostatic conversion for vibration energy harvesting. In M. Lallart (Ed.), *Small-scale energy harvesting* (pp. Ch. 05). Rijeka: InTech.

27. Konuma, M. (1992). Generation of cold plasma *Film deposition by plasma techniques* (pp. 49-73). Berlin, Heidelberg: Springer Berlin Heidelberg.

28. Prysiazhnyi, V. (2012). *Atmospheric pressure plasma treatment of metal surfaces by dcsbd plasma source: Effects of plasma treatment and aging effect of plasma treated surfaces.* Masarykova univerzita, Přírodovědecká fakulta, Dissertation.

29. Nassour, K., Brahami, M., Nemmich, S., Hammadi, N., Zouzou, N., & Tilmatine, A. (2017). New hybrid surface–volume dielectric barrier discharge reactor for ozone generation. *IEEE Transactions on Industry Applications, 53*(3), 2477-2484.

30. Brandt, S., Schütz, A., Klute, F. D., Kratzer, J., & Franzke, J. (2016). Dielectric barrier discharges applied for optical spectrometry. *Spectrochimica Acta Part B: Atomic Spectroscopy, 123*, 6-32.

31. Conrads, H., & Schmidt, M. (2000). Plasma generation and plasma sources. *Plasma Sources Science and Technology, 9*(4), 441.

32. Borcia, G., Anderson, C. A., & Brown, N. M. D. (2003). Dielectric barrier discharge for surface treatment: Application to selected polymers in film and fibre form. *Plasma Sources Science and Technology, 12*(3), 335.

33. Surowsky, B., Schlüter, O., & Knorr, D. (2015). Interactions of non-thermal atmospheric pressure plasma with solid and liquid food systems: A review. *Food Engineering Reviews, 7*(2), 82-108.

34. Haertel, B., von Woedtke, T., Weltmann, K.-D., & Lindequist, U. (2014). Non-thermal atmospheric-pressure plasma possible application in wound healing. *Biomolecules & Therapeutics, 22*(6), 477-490.

35. Walsh, J. L., Iza, F., Janson, N. B., Law, V. J., & Kong, M. G. (2010). Three distinct modes in a cold atmospheric pressure plasma jet. *Journal of Physics D: Applied Physics, 43*(7), 075201.

36. Pan, J., Sun, K., Liang, Y., Sun, P., Yang, X., Wang, J. et al. (2013). Cold plasma therapy of a tooth root canal infected with enterococcus faecalis biofilms in vitro. *Journal of endodontics, 39*(1), 105-110.

37. Keener, K. M., & Jensen, J. L. (2015). Generation of microbiocide inside a package utilizing a controlled gas composition: U.S. Patent 8,961,894.

38. Surowsky, B., Fischer, A., Schlueter, O., & Knorr, D. (2013). Cold plasma effects on enzyme activity in a model food system. *Innovative Food Science & Emerging Technologies, 19*, 146-152.

39. Bruggeman, P. J., Kushner, M. J., Locke, B. R., Gardeniers, J. G. E., Graham, W. G., Graves, D. B. et al. (2016). Plasma–liquid interactions: A review and roadmap. *Plasma Sources Science and Technology, 25*(5), 053002.

40. Lu, X., Naidis, G., Laroussi, M., Reuter, S., Graves, D., & Ostrikov, K. (2016). Reactive species in non-equilibrium atmospheric-pressure plasmas: Generation, transport, and biological effects. *Physics Reports, 630*, 1-84.

41. Patil, S., Moiseev, T., Misra, N. N., Cullen, P. J., Mosnier, J. P., Keener, K. M. et al. (2014). Influence of high voltage atmospheric cold plasma process parameters and role of relative humidity on inactivation of bacillus atrophaeus spores inside a sealed package. *Journal of Hospital Infection, 88*(3), 162-169.

42. Misra, N. N., Patil, S., Moiseev, T., Bourke, P., Mosnier, J. P., Keener, K. M. et al. (2014). In-package atmospheric pressure cold plasma treatment of strawberries. *Journal of Food Engineering, 125*(Supplement C), 131-138.

43. Misra, N. N., Zuizina, D., Cullen, P. J., & Keener, K. M. (2013). Characterization of a novel atmospheric air cold plasma system for treatment of packaged biomaterials. *Transactions of the ASABE, 56*(3), 1011-1016.

44. Moiseev, T., Misra, N., Patil, S., Cullen, P., Bourke, P., Keener, K. et al. (2014). Post-discharge gas composition of a large-gap dbd in humid air by uv–vis absorption spectroscopy. *Plasma Sources Science and Technology, 23*(6), 065033.

45. Wan, Z., Chen, Y., Pankaj, S. K., & Keener, K. M. (2017). High voltage atmospheric cold plasma treatment of refrigerated chicken eggs for control of salmonella enteritidis contamination on egg shell. *LWT - Food Science and Technology, 76*, 124-130.

46. Shi, H., Ileleji, K., Stroshine, R. L., Keener, K., & Jensen, J. L. (2017). Reduction of aflatoxin in corn by high voltage atmospheric cold plasma. *Food and Bioprocess Technology, 10*(6), 1042-1052.

47. Tabarés, F. L., Tafalla, D., Tanarro, I., Herrero, V. J., & Islyaikin, A. M. (2004). Mass spectrometric studies of the mechanism of film inhibition in hydrogen/methane plasmas in the presence of nitrogen. *Vacuum, 73*(2), 161-167.

48. Tanişli, M., Rafatov, I., Şahin, N., Mertadam, S., & Demir, S. (2016). Spectroscopic study and numerical simulation of low-pressure radio-frequency capacitive discharge with argon downstream. *Canadian Journal of Physics, 95*(2), 190-200.

49. Tanışlı, M., & Şahin, N. (2016). Optical characteristics for capacitively and inductively radio frequency discharge and post-discharge of helium. *Physics of Plasmas, 23*(1), 013513.

50. Tanarro, I., Herrero, V. J., Carrasco, E., & Jiménez-Redondo, M. (2011). Cold plasma chemistry and diagnostics. *Vacuum, 85*(12), 1120-1124.

51. Fantz, U. (2006). Basics of plasma spectroscopy. *Plasma Sources Science and Technology, 15*(4), S137.

52. Kunze, H. J. (2009). *Introduction to plasma spectroscopy* (Vol. 56): Springer Science & Business Media.

53.   Boffard, J. B., Jung, R., Lin, C. C., & Wendt, A. (2009). Measurement of metastable and resonance level densities in rare-gas plasmas by optical emission spectroscopy. *Plasma Sources Science and Technology, 18*(3), 035017.

54.   Boffard, J. B., Jung, R., Lin, C. C., & Wendt, A. (2010). Optical emission measurements of electron energy distributions in low-pressure argon inductively coupled plasmas. *Plasma Sources Science and Technology, 19*(6), 065001.

55.   Zhu, X. M., & Pu, Y. K. (2008). Using OES to determine electron temperature and density in low-pressure nitrogen and argon plasmas. *Plasma Sources Science and Technology, 17*(2), 024002.

56.   Sarani, A., Nikiforov, A. Y., & Leys, C. (2010). Atmospheric pressure plasma jet in ar and ar/h2o mixtures: Optical emission spectroscopy and temperature measurements. *Physics of Plasmas, 17*(6), 063504.

57.   Ochkin, V. N. (2009). *Spectroscopy of low temperature plasma*: John Wiley & Sons.

58.   Kinsey, J. L. (1977). Laser-induced fluorescence. *Annual Review of Physical Chemistry, 28*(1), 349-372.

59.   Crimaldi, J. (2008). Planar laser induced fluorescence in aqueous flows. *Experiments in fluids, 44*(6), 851-863.

60.   Stoffels, E., Gonzalvo, Y. A., Whitmore, T., Seymour, D., & Rees, J. (2007). Mass spectrometric detection of short-living radicals produced by a plasma needle. *Plasma Sources Science and Technology, 16*(3), 549.

61.   Belikov, A., Sakhapov, S., Smith, M., & Tikhonov, G. (2011). Mass spectrometry of molecules and radicals in glow discharge plasma. *Journal of Engineering Thermophysics, 20*(1), 42-54.

62.   Skalny, J. D., Orszagh, J., Mason, N. J., Rees, J. A., Aranda-Gonzalvo, Y., & Whitmore, T. D. (2008). Mass spectrometric study of negative ions extracted from point to plane negative corona discharge in ambient air at atmospheric pressure. *International Journal of Mass Spectrometry, 272*(1), 12-21.

63.   Stoffels, E., Sakiyama, Y., & Graves, D. B. (2008). Cold atmospheric plasma: Charged species and their interactions with cells and tissues. *IEEE Transactions on Plasma Science, 36*(4), 1441-1457.

64.   Stoffels, E., Kieft, I., Sladek, R., Van den Bedem, L., Van der Laan, E., & Steinbuch, M. (2006). Plasma needle for in vivo medical treatment: Recent developments and perspectives. *Plasma Sources Science and Technology, 15*(4), S169.

65.   Pankaj, S. K., & Keener, K. M. (2018). Chapter 26 - cold plasma processing of fruit juices a2-rajauria, gaurav. In B. K. Tiwari (Ed.), *Fruit juices* (pp. 529-537). San Diego: Academic Press.

66.   Wagenaars, E. (2006). Plasma breakdown of low-pressure gas discharges (Vol. 68).

67.   Bárdos, L., & Baránková, H. (2008). Plasma processes at atmospheric and low pressures. *Vacuum, 83*(3), 522-527.

68.   Ziuzina, D., Patil, S., Cullen, P. J., Keener, K. M., & Bourke, P. (2013). Atmospheric cold plasma inactivation of escherichia coli in liquid media inside a sealed package. *Journal of Applied Microbiology, 114*(3), 778-787.

69.   Keener, K. M., Jensen, J., Valdramidis, V., Byrne, E., Connolly, J., Mosnier, J. et al. (2012). Decontamination of bacillus subtilis spores in a sealed package using a non-thermal plasma system *Plasma for bio-decontamination, medicine and food security* (pp. 445-455): Springer.

70.   Noriega, E., Shama, G., Laca, A., Díaz, M., & Kong, M. G. (2011). Cold atmospheric gas plasma disinfection of chicken meat and chicken skin contaminated with listeria innocua. *Food Microbiology, 28*(7), 1293-1300.

71.   Pankaj, S. K., Bueno-Ferrer, C., Misra, N., O'Neill, L., Jiménez, A., Bourke, P. et al. (2014). Characterization of polylactic acid films for food packaging as affected by dielectric barrier discharge atmospheric plasma. *Innovative Food Science & Emerging Technologies, 21*, 107-113.

72.   Pankaj, S. K., Bueno- Ferrer, C., Misra, N., Bourke, P., & Cullen, P. (2014). Zein film: Effects of dielectric barrier discharge atmospheric cold plasma. *Journal of Applied Polymer Science, 131*(18).

73.   Misra, N., Pankaj, S., Walsh, T., O'Regan, F., Bourke, P., & Cullen, P. (2014). In-package nonthermal plasma degradation of pesticides on fresh produce. *Journal of hazardous materials, 271*, 33-40.

74.   Sarangapani, C., Dixit, Y., Milosavljevic, V., Bourke, P., Sullivan, C., & Cullen, P. (2017). Optimization of atmospheric air plasma for degradation of organic dyes in wastewater. *Water Science and Technology, 75*(1), 207-219.

75.   Machala, Z., Hensel, K., & Akishev, Y. (2012). *Plasma for bio-decontamination, medicine and food security*: Springer Science & Business Media.

76.   Lee, K., Paek, K. h., Ju, W. T., & Lee, Y. (2006). Sterilization of bacteria, yeast, and bacterial endospores by atmospheric-pressure cold plasma using helium and oxygen. *The Journal of Microbiology, 44*(3), 269-275.

77.   Takamatsu, T., Uehara, K., Sasaki, Y., Miyahara, H., Matsumura, Y., Iwasawa, A. et al. (2014). Investigation of reactive species using various gas plasmas. *RSC Advances, 4*(75), 39901-39905.

78. Chizoba Ekezie, F.-G., Sun, D.-W., & Cheng, J.-H. (2017). A review on recent advances in cold plasma technology for the food industry: Current applications and future trends. *Trends in Food Science & Technology, 69*, 46-58.

79. Bußler, S. (2017). *Cold atmospheric pressure plasma treatment of food matrices: Tailored modification of product properties along value-added chains of plant and animal related products: Dissertation*: Leibniz-Institut für Agrartechnik und Bioökonomie eV.

80. Gadri, R. B., Roth, J. R., Montie, T. C., Kelly-Wintenberg, K., Tsai, P. P.-Y., Helfritch, D. J. et al. (2000). Sterilization and plasma processing of room temperature surfaces with a one atmosphere uniform glow discharge plasma (oaugdp). *Surface and Coatings Technology, 131*(1-3), 528-541.

81. Shi, X. M., Zhang, G. J., Wu, X. L., Li, Y. X., Ma, Y., & Shao, X. J. (2011). Effect of low-temperature plasma on microorganism inactivation and quality of freshly squeezed orange juice. *IEEE Transactions on Plasma Science, 39*(7), 1591-1597.

82. Ziuzina, D., Han, L., Cullen, P. J., & Bourke, P. (2015). Cold plasma inactivation of internalised bacteria and biofilms for salmonella enterica serovar typhimurium, listeria monocytogenes and escherichia coli. *International journal of food microbiology, 210*, 53-61.

83. Shi, H., Cooper, B., Stroshine, R. L., Ileleji, K. E., & Keener, K. M. (2017). Structures of degradation products and degradation pathways of aflatoxin b1 by high-voltage atmospheric cold plasma (hvacp) treatment. *Journal of Agricultural and Food Chemistry, 65*(30), 6222-6230.

84. Fathollah, S., Mirpour, S., Mansouri, P., Dehpour, A. R., Ghoranneviss, M., Rahimi, N. et al. (2016). Investigation on the effects of the atmospheric pressure plasma on wound healing in diabetic rats. *Scientific Reports, 6*, 19144.

85. Park, G., Park, S., Choi, M., Koo, I., Byun, J., Hong, J. et al. (2012). Atmospheric-pressure plasma sources for biomedical applications. *Plasma Sources Science and Technology, 21*(4), 043001.

86. Laroussi, M. (2015). Low-temperature plasma jet for biomedical applications: A review. *IEEE Transactions on Plasma Science, 43*(3), 703-712.

87. Misra, N., Schlüter, O., & Cullen, P. J. (2016). *Cold plasma in food and agriculture: Fundamentals and applications*: Academic Press.

88. Bourke, P., Ziuzina, D., Boehm, D., Cullen, P. J., & Keener, K. (2018). The potential of cold plasma for safe and sustainable food production. *Trends in Biotechnology*.

89. Won, M. Y., Lee, S. J., & Min, S. C. (2017). Mandarin preservation by microwave-powered cold plasma treatment. *Innovative Food Science & Emerging Technologies, 39*, 25-32.

90. Laroussi, M. (2002). Nonthermal decontamination of biological media by atmospheric-pressure plasmas: Review, analysis, and prospects. *IEEE Transactions on Plasma Science, 30*(4), 1409-1415.

91. Hertrich, S. M., Boyd, G., Sites, J., & Niemira, B. A. (2017). Cold plasma inactivation of salmonella in prepackaged, mixed salads is influenced by cross-contamination sequence. *Journal of Food Protection, 80*(12), 2132-2136.

92. Min, S. C., Roh, S. H., Niemira, B. A., Boyd, G., Sites, J. E., Uknalis, J. et al. (2017). In-package inhibition of e. coli o157:H7 on bulk romaine lettuce using cold plasma. *Food Microbiology, 65*, 1-6.

93. Tappi, S., Berardinelli, A., Ragni, L., Dalla Rosa, M., Guarnieri, A., & Rocculi, P. (2014). Atmospheric gas plasma treatment of fresh-cut apples. *Innovative Food Science & Emerging Technologies, 21*, 114-122.

94. Jiang, Y., Sokorai, K., Pyrgiotakis, G., Demokritou, P., Li, X., Mukhopadhyay, S. et al. (2017). Cold plasma-activated hydrogen peroxide aerosol inactivates escherichia coli o157: H7, salmonella typhimurium, and listeria innocua and maintains quality of grape tomato, spinach and cantaloupe. *International Journal of Food Microbiology, 249*, 53-60.

95. Misra, N. N., Keener, K. M., Bourke, P., Mosnier, J.-P., & Cullen, P. J. (2014). In-package atmospheric pressure cold plasma treatment of cherry tomatoes. *Journal of Bioscience and Bioengineering, 118*(2), 177-182.

96. Niemira, B. A. (2012). Cold plasma decontamination of foods. *Annual Review of Food Science and Technology, 3*, 125-142.

97. Ziuzina, D., Patil, S., Cullen, P. J., Keener, K., & Bourke, P. (2014). Atmospheric cold plasma inactivation of escherichia coli, salmonella enterica serovar typhimurium and listeria monocytogenes inoculated on fresh produce. *Food Microbiology, 42*, 109-116.

98. Ölmez, H., & Kretzschmar, U. (2009). Potential alternative disinfection methods for organic fresh-cut industry for minimizing water consumption and environmental impact. *LWT-Food Science and Technology, 42*(3), 686-693.

99. Jayasena, D. D., Kim, H. J., Yong, H. I., Park, S., Kim, K., Choe, W. et al. (2015). Flexible thin-layer dielectric barrier discharge plasma treatment of pork butt and beef loin: Effects on pathogen inactivation and meat-quality attributes. *Food Microbiology, 46*, 51-57.

100. Deng, S., Ruan, R., Mok, C. K., Huang, G., Lin, X., & Chen, P. (2007). Inactivation of escherichia coli on almonds using nonthermal plasma. *Journal of Food Science, 72*(2).

101. Kim, H.-J., Yong, H. I., Park, S., Kim, K., Choe, W., & Jo, C. (2015). Microbial safety and quality attributes of milk following treatment with atmospheric pressure encapsulated dielectric barrier discharge plasma. *Food Control, 47*, 451-456.

102. Xiang, Q., Liu, X., Li, J., Liu, S., Zhang, H., & Bai, Y. (2018). Effects of dielectric barrier discharge plasma on the inactivation of zygosaccharomyces rouxii and quality of apple juice. *Food Chemistry, 254*, 201-207.

103. Patange, A., Boehm, D., Bueno-Ferrer, C., Cullen, P. J., & Bourke, P. (2017). Controlling brochothrix thermosphacta as a spoilage risk using in-package atmospheric cold plasma. *Food Microbiology, 66*, 48-54.

104. Moritz, M., Wiacek, C., Koethe, M., & Braun, P. G. (2017). Atmospheric pressure plasma jet treatment of salmonella enteritidis inoculated eggshells. *International Journal of Food Microbiology, 245*, 22-28.

105. Georgescu, N., Apostol, L., & Gherendi, F. (2017). Inactivation of salmonella enterica serovar typhimurium on egg surface, by direct and indirect treatments with cold atmospheric plasma. *Food Control, 76*, 52-61.

106. Bauer, A., Ni, Y., Bauer, S., Paulsen, P., Modic, M., Walsh, J. L. et al. (2017). The effects of atmospheric pressure cold plasma treatment on microbiological, physical-chemical and sensory characteristics of vacuum packaged beef loin. *Meat Science, 128*, 77-87.

107. Sarangapani, C., O'Toole, G., Cullen, P. J., & Bourke, P. (2017). Atmospheric cold plasma dissipation efficiency of agrochemicals on blueberries. *Innovative Food Science & Emerging Technologies, 44*, 235-241.

108. Albertos, I., Martín-Diana, A. B., Cullen, P. J., Tiwari, B. K., Ojha, S. K., Bourke, P. et al. (2017). Effects of dielectric barrier discharge (dbd) generated plasma on microbial reduction and quality parameters of fresh mackerel (scomber scombrus) fillets. *Innovative Food Science & Emerging Technologies, 44*, 117-122.

109. McClurkin-Moore, J. D., Ileleji, K. E., & Keener, K. M. (2017). The effect of high-voltage atmospheric cold plasma treatment on the shelf-life of distillers wet grains. *Food and Bioprocess Technology, 10*(8), 1431-1440.

110. Liao, X., Liu, D., Xiang, Q., Ahn, J., Chen, S., Ye, X. et al. (2017). Inactivation mechanisms of non-thermal plasma on microbes: A review. *Food Control, 75*, 83-91.

111. Misra, N. N., & Jo, C. (2017). Applications of cold plasma technology for microbiological safety in meat industry. *Trends in Food Science & Technology, 64*, 74-86.

112. Critzer, F. J., Kelly-Wintenberg, K., South, S. L., & Golden, D. A. (2007). Atmospheric plasma inactivation of foodborne pathogens on fresh produce surfaces. *Journal of Food Protection, 70*(10), 2290-2296.

113. Lunov, O., Zablotskii, V., Churpita, O., Jäger, A., Polívka, L., Syková, E. et al. (2016). The interplay between biological and physical scenarios of bacterial death induced by non-thermal plasma. *Biomaterials, 82*, 71-83.

114. Bußler, S., Steins, V., Ehlbeck, J., & Schlüter, O. (2015). Impact of thermal treatment versus cold atmospheric plasma processing on the techno-functional protein properties from pisum sativum 'salamanca'. *Journal of Food Engineering, 167*, 166-174.

115. Bahrami, N., Bayliss, D., Chope, G., Penson, S., Perehinec, T., & Fisk, I. D. (2016). Cold plasma: A new technology to modify wheat flour functionality. *Food Chemistry, 202*, 247-253.

116. Tolouie, H., Mohammadifar, M. A., Ghomi, H., & Hashemi, M. (2017). Cold atmospheric plasma manipulation of proteins in food systems. *Critical Reviews in Food Science and Nutrition*, 1-15.

117. Thirumdas, R., Trimukhe, A., Deshmukh, R. R., & Annapure, U. S. (2017). Functional and rheological properties of cold plasma treated rice starch. *Carbohydrate Polymers, 157*, 1723-1731.

118. Thirumdas, R., Kadam, D., & Annapure, U. S. (2017). Cold plasma: An alternative technology for the starch modification. *Food Biophysics, 12*(1), 129-139.

119. Wongsagonsup, R., Deeyai, P., Chaiwat, W., Horrungsiwat, S., Leejariensuk, K., Suphantharika, M. et al. (2014). Modification of tapioca starch by non-chemical route using jet atmospheric argon plasma. *Carbohydrate Polymers, 102*, 790-798.

120. Wu, T. Y., Sun, N. N., & Chau, C. F. (2018). Application of corona electrical discharge plasma on modifying the physicochemical properties of banana starch indigenous to taiwan. *Journal of Food and Drug Analysis, 26*(1), 244-251.

121. Dong, S., Wang, J. M., Cheng, L. M., Lu, Y. L., Li, S. H., & Chen, Y. (2017). Behavior of zein in aqueous ethanol under atmospheric pressure cold plasma treatment. *Journal of Agricultural and Food Chemistry, 65*(34), 7352-7360.

122. Dong, S., Gao, A., Xu, H., & Chen, Y. (2017). Effects of dielectric barrier discharges (dbd) cold plasma treatment on physicochemical and structural properties of zein powders. *Food and Bioprocess Technology, 10*(3), 434-444.

123. Ji, H., Dong, S., Han, F., Li, Y., Chen, G., Li, L. et al. (2017). Effects of dielectric barrier discharge (DBD) cold plasma treatment on physicochemical and functional properties of peanut protein. *Food and Bioprocess Technology, 23*(1), 24-25.

124. Lee, K. H., Kim, H. J., Woo, K. S., Jo, C., Kim, J. K., Kim, S. H. et al. (2016). Evaluation of cold plasma treatments for improved microbial and physicochemical qualities of brown rice. *LWT - Food Science and Technology, 73*, 442-447.

125. Thirumdas, R., Kadam, D., & Annapure, U. (2017). Cold plasma: An alternative technology for the starch modification. *Food Biophysics, 12*(1), 129-139.

126. Thirumdas, R., Deshmukh, R., & Annapure, U. (2016). Effect of low temperature plasma on the functional properties of basmati rice flour. *Journal of food science and technology, 53*(6), 2742-2751.

127. Thirumdas, R., Deshmukh, R. R., & Annapure, U. S. (2016). Effect of low temperature plasma on the functional properties of basmati rice flour. *Journal of Food Science and Technology, 53*(6), 2742-2751.

128. Sarangapani, C., Devi, Y., Thirundas, R., Annapure, U. S., & Deshmukh, R. R. (2015). Effect of low-pressure plasma on physico-chemical properties of parboiled rice. *LWT - Food Science and Technology, 63*(1), 452-460.

129. Yepez, X. V., & Keener, K. M. (2016). High-voltage atmospheric cold plasma (hvacp) hydrogenation of soybean oil without trans-fatty acids. *Innovative Food Science & Emerging Technologies, 38*, 169-174.

130. Sicherer, S. H., & Sampson, H. A. (2014). Food allergy: Epidemiology, pathogenesis, diagnosis, and treatment. *Journal of Allergy and Clinical Immunology, 133*(2), 291-307.e295.

131. Meinlschmidt, P., Ueberham, E., Lehmann, J., Reineke, K., Schlüter, O., Schweiggert-Weisz, U. et al. (2016). The effects of pulsed ultraviolet light, cold atmospheric pressure plasma, and gamma-irradiation on the immunoreactivity of soy protein isolate. *Innovative Food Science & Emerging Technologies, 38*, 374-383.

132. Shriver, S. K., & Yang, W. W. (2011). Thermal and nonthermal methods for food allergen control. *Food Engineering Reviews, 3*(1), 26-43.

133. He, L. (2011). *Molecular beam study of non-thermal plasma treatment of volatile organic compounds.* Tulane University School of Science and Engineering.

134. Malik, M. A., Ghaffar, A. and Malik, S. A. (2001). Water purification by electrical discharges. *Plasma Sources Science and Technology, 10*(1), 82.

135. Leslie, M. R., Anu, R., & Priyanie, A. (2017). Wastewater treatment and reuse in urban agriculture: Exploring the food, energy, water, and health nexus in hyderabad, india. *Environmental Research Letters, 12*(7), 075005.

136. Saka, C., Şahin, Ö., Adsoy, H., & Akyel, Ş. M. (2012). Removal of methylene blue from aqueous solutions by using cold plasma, microwave radiation and formaldehyde treated acorn shell. *Separation Science and Technology, 47*(10), 1542-1551.

137. Benidris, E. B., Ghezzar, M. R., Ma, A., Ouddane, B., & Addou, A. (2017). Water purification by a new hybrid plasma-sensitization-coagulation process. *Separation and Purification Technology, 178*, 253-260.

138. Jiang, B., Zheng, J., Qiu, S., Wu, M., Zhang, Q., Yan, Z. et al. (2014). Review on electrical discharge plasma technology for wastewater remediation. *Chemical Engineering Journal, 236*, 348-368.

139. Schiorlin, M., Paradisi, C., Brandenburg, R., Schmidt, M., Marotta, E., Giardina, A. et al. (2015). Pollutant degradation in gas streams by means of non-thermal plasmas *Current air quality issues*: InTech.

140. Arena, U. (2012). Process and technological aspects of municipal solid waste gasification. A review. *Waste Management, 32*(4), 625-639.

141. Moustakas, K., Fatta, D., Malamis, S., Haralambous, K., & Loizidou, M. (2005). Demonstration plasma gasification/vitrification system for effective hazardous waste treatment. *Journal of Hazardous Materials, 123*(1), 120-126.

142. Keidar, M., & Beilis, I. (2013). *Plasma engineering: Applications from aerospace to bio and nanotechnology*: Academic Press.

143. Fridman, G., Peddinghaus, M., Balasubramanian, M., Ayan, H., Fridman, A., Gutsol, A. et al. (2006). Blood coagulation and living tissue sterilization by floating-electrode dielectric barrier discharge in air. *Plasma Chemistry and Plasma Processing, 26*(4), 425-442.

144. Fridman, G., Shereshevsky, A., Jost, M. M., Brooks, A. D., Fridman, A., Gutsol, A. et al. (2007). Floating electrode dielectric barrier discharge plasma in air promoting apoptotic behavior in melanoma skin cancer cell lines. *Plasma Chemistry and Plasma Processing, 27*(2), 163-176.

145. Bekeschus, S., Lin, A., Fridman, A., Wende, K., Weltmann, K. D., & Miller, V. (2018). A comparison of floating-electrode dbd and kinpen jet: Plasma parameters to achieve similar growth reduction in colon cancer cells under standardized conditions. *Plasma Chemistry and Plasma Processing, 38*(1), 1-12.

146. Dobrynin, D., Fridman, G., Friedman, G., & Fridman, A. (2009). Physical and biological mechanisms of direct plasma interaction with living tissue. *New Journal of Physics, 11*(11), 115020.

147. Nastuta, A. V., Topala, I., Grigoras, C., Pohoata, V., & Popa, G. (2011). Stimulation of wound healing by helium atmospheric pressure plasma treatment. *Journal of Physics D: Applied Physics, 44*(10), 105204.

148. Heinlin, J., Isbary, G., Stolz, W., Morfill, G., Landthaler, M., Shimizu, T. et al. (2011). Plasma applications in medicine with a special focus on dermatology. *Journal of the European Academy of Dermatology and Venereology, 25*(1), 1-11.

149. Mai-Prochnow, A., Murphy, A. B., McLean, K. M., Kong, M. G., & Ostrikov, K. (2014). Atmospheric pressure plasmas: Infection control and bacterial responses. *International Journal of Antimicrobial Agents, 43*(6), 508-517.

150. Isbary, G., Heinlin, J., Shimizu, T., Zimmermann, J., Morfill, G., Schmidt, H. U. et al. (2012). Successful and safe use of 2 min cold atmospheric argon plasma in chronic wounds: Results of a randomized controlled trial. *British Journal of Dermatology, 167*(2), 404-410.

151. Ginsberg, G. G., Barkun, A. N., Bosco, J. J., Burdick, J. S., Isenberg, G. A., Nakao, N. L. et al. (2002). The argon plasma coagulatorfebruary 2002. *Gastrointestinal Endoscopy, 55*(7), 807-810.

152. Fridman, G., Friedman, G., Gutsol, A., Shekhter, A. B., Vasilets, V. N., & Fridman, A. (2008). Applied plasma medicine. *Plasma Processes and Polymers, 5*(6), 503-533.

153. Kalghatgi, S. U., Fridman, G., Cooper, M., Nagaraj, G., Peddinghaus, M., Balasubramanian, M. et al. (2007). Mechanism of blood coagulation by nonthermal atmospheric pressure dielectric barrier discharge plasma. *IEEE Transactions on Plasma Science, 35*(5), 1559-1566.

154. Williams, P. F. (2013). *Plasma processing of semiconductors* (Vol. 336): Springer Science & Business Media.

155. Alexander, L., Carly, A., Elmar, S., Steven, S., & David, G. (2015). Momentum, heat, and neutral mass transport in convective atmospheric pressure plasma-liquid systems and implications for aqueous targets. *Journal of Physics D: Applied Physics, 48*(42), 424007.

156. Liu, Z. C., Liu, D. X., Chen, C., Li, D., Yang, A. J., Rong, M. Z. et al. (2015). Physicochemical processes in the indirect interaction between surface air plasma and deionized water. *Journal of Physics D: Applied Physics, 48*(49), 495201.

157. Anderson, C. E. (2016). *Interactions of non-thermal air plasmas with aqueous solutions*. PhD Dissertation: University of California, Berkeley.

158. Gordillo-Vázquez, F. (2008). Air plasma kinetics under the influence of sprites. *Journal of Physics D: Applied Physics, 41*(23), 234016.

159. Ke, Z., Huang, Q., Dang, B., Lu, Y., Yuan, H., Zhang, S. et al. (2010). A study of low-energy ion induced radiolysis of thiol-containing amino acid cysteine in the solid and aqueous solution states. *Nuclear Instruments and Methods in Physics Research Section B: Beam Interactions with Materials and Atoms, 268*(17), 2729-2734.

160. Misra, N. N., Kaur, S., Tiwari, B. K., Kaur, A., Singh, N., & Cullen, P. J. (2015). Atmospheric pressure cold plasma (acp) treatment of wheat flour. *Food Hydrocolloids, 44*, 115-121.

161. Lackmann, J. W., Baldus, S., Steinborn, E., Edengeiser, E., Kogelheide, F., Langklotz, S. et al. (2015). A dielectric barrier discharge terminally inactivates rnase a by oxidizing sulfur-containing amino acids and breaking structural disulfide bonds. *Journal of Physics D: Applied Physics, 48*(49), 494003.

162. Gisuke, M., Kotaro, S., Atsuko, M., Hiroshi, S., & Yoshiharu, S. (1964). Radiolysis of solid glycine. *Bulletin of the Chemical Society of Japan, 37*(7), 928-930.

163. Segat, A., Misra, N. N., Cullen, P. J., & Innocente, N. (2015). Atmospheric pressure cold plasma (acp) treatment of whey protein isolate model solution. *Innovative Food Science & Emerging Technologies, 29*, 247-254.

164. Eisuke, T., Tsuyoshi, K., Junpei, K., Satoshi, I., Shunsuke, Y., Kentaro, S. et al. (2014). Chemical modification of amino acids by atmospheric-pressure cold plasma in aqueous solution. *Journal of Physics D: Applied Physics, 47*(28), 285403.

165. Zhou, R., Zhou, R., Zhuang, J., Zong, Z., Zhang, X., Liu, D. et al. (2016). Interaction of atmospheric-pressure air microplasmas with amino acids as fundamental processes in aqueous solution. *PLOS ONE, 11*(5), e0155584.

166. Pankaj, S. K., Bueno-Ferrer, C., Misra, N. N., O'Neill, L., Tiwari, B. K., Bourke, P. et al. (2014). Physicochemical characterization of plasma-treated sodium caseinate film. *Food Research International, 66*, 438-444.

167. Vasilieva, T. M. (2010). A beam-plasma source for protein modification technology. *IEEE Transactions on Plasma Science, 38*(8), 1903-1907.

168. Li, H. P., Wang, L. Y., Li, G., Jin, L. H., Le, P. S., Zhao, H. X. et al. (2011). Manipulation of lipase activity by the helium radio-frequency, atmospheric-pressure glow discharge plasma jet. *Plasma Processes and Polymers, 8*(3), 224-229.

169. Halfmann, H. D. B. W. A., Denis, B., Bibinov, N., Wunderlich, J., & Awakowicz, P. (2007). Identification of the most efficient vuv/uv radiation for plasma based inactivation of bacillus atrophaeus spores. *J. Phys. D: Appl. Phys., 40*(19), 5907.

170. Bernard, C., Leduc, A., Barbeau, J., Saoudi, B., Yahia, L. H., & De Crescenzo, G. (2006). Validation of cold plasma treatment for protein inactivation: A surface plasmon resonance-based biosensor study. *J. Phys. D: Appl. Phys., 39*(16), 3470.

171. Choe, E., & Min, D. (2006). Mechanisms and factors for edible oil oxidation. *Comprehensive reviews in food science and food safety, 5*.

172. Carocho, M., & Ferreira, I. C. (2013). A review on antioxidants, prooxidants and related controversy: Natural and synthetic compounds, screening and analysis methodologies and future perspectives. *Food Chem Toxicol, 51*, 15-25.

173. Labuza, T. P., & Dugan, L. R. (2009). Kinetics of lipid oxidation in foods. *C R C Critical Reviews in Food Technology, 2*(3), 355-405.

174. Frankel, E. N. (2014). *Lipid oxidation*: Elsevier.

175. Slezak, J., Zion, B., & Sibener, S. (1999). Enhanced oxidation rate of ni by atomic oxygen. *Surface science, 442*.

176. Sarangapani, C., Ryan Keogh, D., Dunne, J., Bourke, P., & Cullen, P. J. (2017). Characterisation of cold plasma treated beef and dairy lipids using spectroscopic and chromatographic methods. *Food Chem, 235*, 324-333.

177. Van Durme, J., Nikiforov, A., Vandamme, J., Leys, C., & De Winne, A. (2014). Accelerated lipid oxidation using non-thermal plasma technology: Evaluation of volatile compounds. *Food Research International, 62*, 868-876.

178. Van Durme, J., & Vandamme, J. (2016). Non-thermal plasma as preparative technique to evaluate olive oil adulteration. *Food Chem, 208*, 185-191.

179. Vandamme, J., Nikiforov, A., De Roose, M., Leys, C., De Cooman, L., & Van Durme, J. (2016). Controlled accelerated oxidation of oleic acid using a dbd plasma: Determination of volatile oxidation compounds. *Food Research International, 79*, 54-63.

180. Vandamme, J., Nikiforov, A., Dujardin, K., Leys, C., De Cooman, L., & Van Durme, J. (2015). Critical evaluation of non-thermal plasma as an innovative accelerated lipid oxidation technique in fish oil. *Food Research International, 72*, 115-125.

181. Zhao, X., Yang, J., Tao, D., & Xu, X. (2013). Tribological study of nitrogen plasma polymerized soybean oil with nitrogen heterocyclic structures. *Industrial Crops and Products, 51*, 236-243.

182. Zhao, X., Yang, J., Tao, D., & Xu, X. (2014). Synthesis and tribological properties of air plasma polymerized soybean oil with n-containing structures. *Journal of the American Oil Chemists' Society, 91*(5), 827-837.

183. Esteves, M., Girio, F., Amaral Collaco, M., Andrade, M., & Empis, J. (1997). Characterization of starch from white and black pepper treated by ionizing radiation. *Sciences des Aliments (France)*.

184. Morent, R., De Geyter, N., Desmet, T., Dubruel, P., & Leys, C. (2011). Plasma surface modification of biodegradable polymers: A review. *Plasma Processes and Polymers, 8*(3), 171-190.

185. Bhat, R., & Karim, A. (2009). Ultraviolet irradiation improves gel strength of fish gelatin. *Food chemistry, 113*(4), 1160-1164.

186. Lii, C. y., Liao, C. d., Stobinski, L., & Tomasik, P. (2002). Exposure of granular starches to low-pressure glow ethylene plasma. *European Polymer Journal, 38*(8), 1601-1606.

187. Misra, N., Pankaj, S., Segat, A., & Ishikawa, K. (2016). Cold plasma interactions with enzymes in foods and model systems. *Trends in Food Science & Technology, 55*, 39-47.

188. Thirumdas, R., Sarangapani, C., & Annapure, U. S. (2015). Cold plasma: A novel non-thermal technology for food processing. *Food Biophysics, 10*(1), 1-11.

189.   Chen, H. H., Chen, Y. K., & Chang, H. C. (2012). Evaluation of physicochemical properties of plasma treated brown rice. *Food Chemistry, 135*(1), 74-79.

190.   Scallan, E., Hoekstra, R. M., Angulo, F. J., Tauxe, R. V., Widdowson, M.-A., Roy, S. L. et al. (2011). Foodborne illness acquired in the united states—major pathogens. *Emerging Infectious Diseases, 17*(1), 7-15.

191.   Control, C. f. D., & Prevention. (2013). National enteric disease surveillance: Salmonella annual report, 2011. *Centers for Disease Control and Prevention, Atlanta, GA.*

192.   Eagerman, B. A., & Rouse, A. H. (1976). Heat inactivation temperature-time relationships for pectinesterase inactivation in citrus juices. *Journal of Food Science, 41*(6), 1396-1397.

193.   Arreola, A. G., Balaban, M. O., Marshall, M. R., Peplow, A. J., Wei, C. I., & Cornell, J. A. (1991). Supercritical carbon dioxide effects on some quality attributes of single strength orange juice. *Journal of Food Science, 56*(4), 1030-1033.

194.   Vikram, V. B., Ramesh, M. N., & Prapulla, S. G. (2005). Thermal degradation kinetics of nutrients in orange juice heated by electromagnetic and conventional methods. *Journal of Food Engineering, 69*(1), 31-40.

195.   Lee, J. Y., Kim, S. S., & Kang, D. H. (2015). Effect of ph for inactivation of escherichia coli o157:H7, salmonella typhimurium and listeria monocytogenes in orange juice by ohmic heating. *LWT - Food Science and Technology, 62*(1, Part 1), 83-88.

196.   Tiwari, B. K., O'Donnell, C. P., & Cullen, P. J. (2009). Effect of non thermal processing technologies on the anthocyanin content of fruit juices. *Trends in Food Science & Technology, 20*(3), 137-145.

197.   Sampedro, F., McAloon, A., Yee, W., Fan, X., & Geveke, D. J. (2014). Cost analysis and environmental impact of pulsed electric fields and high pressure processing in comparison with thermal pasteurization. *Food and Bioprocess Technology, 7*(7), 1928-1937.

198.   Deng, X., Shi, J., & Kong, M. G. (2006). Physical mechanisms of inactivation of bacillus subtilis spores using cold atmospheric plasmas. *IEEE Transactions on Plasma Science, 34*(4), 1310-1316.

199.   Napartovich, A. P. (2001). Overview of atmospheric pressure discharges producing nonthermal plasma. *Plasmas and Polymers, 6*(1), 1-14.

200.   Fernández, A., Noriega, E., & Thompson, A. (2013). Inactivation of salmonella enterica serovar typhimurium on fresh produce by cold atmospheric gas plasma technology. *Food Microbiology, 33*(1), 24-29.

201.   Wan, J., Coventry, J., Swiergon, P., Sanguansri, P., & Versteeg, C. (2009). Advances in innovative processing technologies for microbial inactivation and enhancement of food safety – pulsed electric field and low-temperature plasma. *Trends in Food Science & Technology, 20*(9), 414-424.

202. Lu, X., Ye, T., Cao, Y., Sun, Z., Xiong, Q., Tang, Z. et al. (2008). The roles of the various plasma agents in the inactivation of bacteria. *Journal of Applied Physics, 104*(5), 053309.

203. Ikawa, S., Kitano, K., & Hamaguchi, S. (2010). Effects of ph on bacterial inactivation in aqueous solutions due to low-temperature atmospheric pressure plasma application. *Plasma Processes and Polymers, 7*(1), 33-42.

204. Xu, L., Sanders, S. M., Tao, B., Garner, A. L., & Keener, K. M. (2016, 19-23 June 2016). *Assessment of efficacy and reactive gas species generation for orange juice decontamination using high voltage atmospheric cold plasma.* Paper presented at the 2016 IEEE International Conference on Plasma Science (ICOPS).

205. Gallagher, L. A., Ramage, E., Jacobs, M. A., Kaul, R., Brittnacher, M., & Manoil, C. (2007). A comprehensive transposon mutant library of Francisella novicida, a bioweapon surrogate. *Proceedings of the National Academy of Sciences, 104*(3), 1009-1014.

206. Cooper, M., Fridman, G., Fridman, A., & Joshi, S. G. (2010). Biological responses of bacillus stratosphericus to floating electrode-dielectric barrier discharge plasma treatment. *Journal of Applied Microbiology, 109*(6), 2039-2048.

207. Kvam, E., Davis, B., Mondello, F., & Garner, A. L. (2012). Nonthermal atmospheric plasma rapidly disinfects multidrug-resistant microbes by inducing cell surface damage. *Antimicrobial Agents and Chemotherapy, 56*(4), 2028-2036.

208. Gils, C. A. J. v., Hofmann, S., Boekema, B. K. H. L., Brandenburg, R., & Bruggeman, P. J. (2013). Mechanisms of bacterial inactivation in the liquid phase induced by a remote rf cold atmospheric pressure plasma jet. *Journal of Physics D: Applied Physics, 46*(17), 175203.

209. Zhang, H., Xu, Z., Shen, J., Li, X., Ding, L., Ma, J. et al. (2015). Effects and mechanism of atmospheric-pressure dielectric barrier discharge cold plasma on lactate dehydrogenase (ldh) enzyme. *Scientific Reports, 5*, 10031.

210. Fröhling, A., Durek, J., Schnabel, U., Ehlbeck, J., Bolling, J., & Schlüter, O. (2012). Indirect plasma treatment of fresh pork: Decontamination efficiency and effects on quality attributes. *Innovative Food Science & Emerging Technologies, 16*, 381-390.

211. Alkawareek, M. Y., Gorman, S. P., Graham, W. G., & Gilmore, B. F. (2014). Potential cellular targets and antibacterial efficacy of atmospheric pressure non-thermal plasma. *International Journal of Antimicrobial Agents, 43*(2), 154-160.

212. Han, L., Patil, S., Boehm, D., Milosavljević, V., Cullen, P. J., & Bourke, P. (2016). Mechanisms of inactivation by high-voltage atmospheric cold plasma differ for escherichia coli and staphylococcus aureus. *Applied and Environmental Microbiology, 82*(2), 450-458.

213. Fernández, A., Shearer, N., Wilson, D. R., & Thompson, A. (2012). Effect of microbial loading on the efficiency of cold atmospheric gas plasma inactivation of salmonella enterica serovar typhimurium. *International Journal of Food Microbiology, 152*(3), 175-180.

214. Brayfield, R. S., Jassem, A., Lauria, M. V., Fairbanks, A. J., Keener, K. M., & Garner, A. L. (2018). Characterization of high voltage cold atmospheric plasma generation in sealed packages as a function of container material and fill gas. *Plasma Chemistry and Plasma Processing, 38*(2), 379-395.

215. Cserhalmi, Z., Sass-Kiss, Á., Tóth-Markus, M., & Lechner, N. (2006). Study of pulsed electric field treated citrus juices. *Innovative Food Science & Emerging Technologies, 7*(1), 49-54.

216. Ayhan, Z., Yeom, H. W., Zhang, Q. H., & Min, D. B. (2001). Flavor, color, and vitamin c retention of pulsed electric field processed orange juice in different packaging materials. *Journal of Agricultural and Food Chemistry, 49*(2), 669-674.

217. Rouse, A. H., & Atkins, C. D. (1955). *Pectinesterase and pectin in commercial citrus juices as determined by methods used at the citrus experiment station*.

218. Ulmer, H. M., Gänzle, M. G., & Vogel, R. F. (2000). Effects of high pressure on survival and metabolic activity of lactobacillus plantarum tmw1.460. *Applied and Environmental Microbiology, 66*(9), 3966-3973.

219. Corrales, M., Toepfl, S., Butz, P., Knorr, D., & Tauscher, B. (2008). Extraction of anthocyanins from grape by-products assisted by ultrasonics, high hydrostatic pressure or pulsed electric fields: A comparison. *Innovative Food Science & Emerging Technologies, 9*(1), 85-91.

220. Oehmigen, K., Hähnel, M., Brandenburg, R., Wilke, C., Weltmann, K. D., & von Woedtke, T. (2010). The role of acidification for antimicrobial activity of atmospheric pressure plasma in liquids. *Plasma Processes and Polymers, 7*(3-4), 250-257.

221. Kim, Y. H., Hong, Y. J., Baik, K. Y., Kwon, G. C., Choi, J. J., Cho, G. S. et al. (2014). Measurement of reactive hydroxyl radical species inside the biosolutions during non-thermal atmospheric pressure plasma jet bombardment onto the solution. *Plasma Chemistry and Plasma Processing, 34*(3), 457-472.

222. Patil, S., Bourke, P., & Cullen, P. J. (2016). Chapter 6 - principles of nonthermal plasma decontamination *Cold plasma in food and agriculture* (pp. 143-177). San Diego: Academic Press.

223. Surowsky, B., Bußler, S., & Schlüter, O. K. (2016). Chapter 7 - cold plasma interactions with food constituents in liquid and solid food matrices *Cold plasma in food and agriculture* (pp. 179-203). San Diego: Academic Press.

224. Ricard, A., Oh, S. G., & Guerra, V. (2013). Line-ratio determination of atomic oxygen and metastable absolute densities in an RF nitrogen late afterglow. *Plasma Sources Science and Technology, 22*(3), 035009.

225. Choi, Y.-H., Kim, J.-H., Paek, K.-H., Ju, W.-T., & Hwang, Y. S. (2005). Characteristics of atmospheric pressure n2 cold plasma torch using 60-hz ac power and its application to polymer surface modification. *Surface and Coatings Technology, 193*(1), 319-324.

226. Machala, Z., Janda, M., Hensel, K., Jedlovský, I., Leštinská, L., Foltin, V. et al. (2007). Emission spectroscopy of atmospheric pressure plasmas for bio-medical and environmental applications. *Journal of Molecular Spectroscopy, 243*(2), 194-201.

227. Arjunan, K. P., Friedman, G., Fridman, A., & Clyne, A. M. (2012). Non-thermal dielectric barrier discharge plasma induces angiogenesis through reactive oxygen species. *Journal of The Royal Society Interface, 9*(66), 147-157.

228. Ishikawa, K. (2016). Chapter 5 - plasma diagnostics *Cold plasma in food and agriculture* (pp. 117-141). San Diego: Academic Press.

229. Sureshkumar, A., Sankar, R., Mandal, M., & Neogi, S. (2010). Effective bacterial inactivation using low temperature radio frequency plasma. *International Journal of Pharmaceutics, 396*(1), 17-22.

230. Spencer, P. K., Olga, T., Said, N., Assya, B., & Kalle, L. (2006). Plasma effects on bacterial spores in a wet environment. *New Journal of Physics, 8*(3), 41.

231. Sadler, G. D., Parish, M. E., & Wicker, L. (1992). Microbial, enzymatic, and chemical changes during storage of fresh and processed orange juice. *Journal of Food Science, 57*(5), 1187-1197.

232. Yin, M., Huang, M., Ma, B., & Ma, T. (2005). Stimulating effects of seed treatment by magnetized plasma on tomato growth and yield. *Plasma Science and Technology, 7*(6), 3143.

233. Henselová, M., Slováková, Ľ., Martinka, M., & Zahoranová, A. (2012). Growth, anatomy and enzyme activity changes in maize roots induced by treatment of seeds with low-temperature plasma *Biologia* (Vol. 67, pp. 490).

234. Takai, E., Kitano, K., Kuwabara, J., & Shiraki, K. (2012). Protein inactivation by low-temperature atmospheric pressure plasma in aqueous solution. *Plasma Processes and Polymers, 9*(1), 77-82.

235. Jablonowski, H., & von Woedtke, T. (2015). Research on plasma medicine-relevant plasma–liquid interaction: What happened in the past five years? *Clinical Plasma Medicine, 3*(2), 42-52.

236. Misra, N. N., Pankaj, S. K., Segat, A., & Ishikawa, K. (2016). Cold plasma interactions with enzymes in foods and model systems. *Trends in Food Science & Technology, 55*, 39-47.

237. Tiwari, B. K., O' Donnell, C. P., Muthukumarappan, K., & Cullen, P. J. (2009). Ascorbic acid degradation kinetics of sonicated orange juice during storage and comparison with thermally pasteurised juice. *LWT - Food Science and Technology, 42*(3), 700-704.

238. Polydera, A. C., Stoforos, N. G., & Taoukis, P. S. (2003). Comparative shelf life study and vitamin c loss kinetics in pasteurised and high pressure processed reconstituted orange juice. *Journal of Food Engineering, 60*(1), 21-29.

239. Sánchez-Moreno, C., Plaza, L., Elez-Martínez, P., De Ancos, B., Martín-Belloso, O., & Cano, M. P. (2005). Impact of high pressure and pulsed electric fields on bioactive compounds and antioxidant activity of orange juice in comparison with traditional thermal processing. *Journal of Agricultural and Food Chemistry, 53*(11), 4403-4409.

240. Vervoort, L., Van der Plancken, I., Grauwet, T., Timmermans, R. A. H., Mastwijk, H. C., Matser, A. M. et al. (2011). Comparing equivalent thermal, high pressure and pulsed electric field processes for mild pasteurization of orange juice: Part ii: Impact on specific chemical and biochemical quality parameters. *Innovative Food Science & Emerging Technologies, 12*(4), 466-477.

241. García-Viguera, C., & Bridle, P. (1999). Influence of structure on colour stability of anthocyanins and flavylium salts with ascorbic acid. *Food Chemistry, 64*(1), 21-26.

242. Tiwari, B. K., Muthukumarappan, K., O'Donnell, C. P., & Cullen, P. J. (2008). Kinetics of freshly squeezed orange juice quality changes during ozone processing. *Journal of Agricultural and Food Chemistry, 56*(15), 6416-6422.

243. Helmke, A., Hoffmeister, D., Berge, F., Emmert, S., Laspe, P., Mertens, N. et al. (2011). Physical and microbiological characterisation of staphylococcus epidermidis inactivation by dielectric barrier discharge plasma. *Plasma Processes and Polymers, 8*(4), 278-286.

244. Lee, H. S., & Coates, G. A. (2003). Effect of thermal pasteurization on valencia orange juice color and pigments. *LWT - Food Science and Technology, 36*(1), 153-156.

245. Meléndez-Martínez, A. J., Vicario, I. M., & Heredia, F. J. (2005). Instrumental measurement of orange juice colour: A review. *Journal of the Science of Food and Agriculture, 85*(6), 894-901.

246. Lu, H., Patil, S., Keener, K. M., Cullen, P. J., & Bourke, P. (2014). Bacterial inactivation by high-voltage atmospheric cold plasma: Influence of process parameters and effects on cell leakage and DNA. *Journal of Applied Microbiology, 116*(4), 784-794.

247. Moisan, M., Barbeau, J., Moreau, S., Pelletier, J., Tabrizian, M., & Yahia, L. H. (2001). Low-temperature sterilization using gas plasmas: A review of the experiments and an analysis of the inactivation mechanisms. *International Journal of Pharmaceutics, 226*(1), 1-21.

248. Schnabel, U., Andrasch, M., Weltmann, K.-D., & Ehlbeck, J. (2014). Inactivation of vegetative microorganisms and bacillus atrophaeus endospores by reactive nitrogen species (rns). *Plasma Processes and Polymers, 11*(2), 110-116.

249. Klockow, P. A., & Keener, K. M. (2008). *Quality and safety assessment of packaged spinach treated with a novel atmospheric, non-equilibrium plasma system.* Paper presented at the 2008 Providence, Rhode Island, June 29–July 2, 2008, St. Joseph, MI.

250. Gaunt, L. F., Beggs, C. B., & Georghiou, G. E. (2006). Bactericidal action of the reactive species produced by gas-discharge nonthermal plasma at atmospheric pressure: A review. *IEEE Transactions on Plasma Science, 34*(4), 1257-1269.

251. Schlegel, J., Köritzer, J., & Boxhammer, V. (2013). Plasma in cancer treatment. *Clinical Plasma Medicine, 1*(2), 2-7.

252. Hoffmann, C., Berganza, C., & Zhang, J. (2013). Cold atmospheric plasma: Methods of production and application in dentistry and oncology. *Medical Gas Research, 3*, 21-21.

253. Cheng, X., Sherman, J., Murphy, W., Ratovitski, E., Canady, J., & Keidar, M. (2014). The effect of tuning cold plasma composition on glioblastoma cell viability. *PLOS ONE, 9*(5), e98652.

254. Ting, K., Kao, J. Y., Hsieh, Y. S., Chen, C. C., Chang, C. C., & Wu, C. J. (2013). *The dry process of zno film deposition by atmospheric pressure plasma.* Paper presented at the Journal of Physics: Conference Series.

255. Li, L., Zhang, X., Zhang, M., Li, P., & Chu, P. K. (2014). Microporous n-doped carbon film produced by cold atmospheric plasma jet and its cell compatibility. *Vacuum, 108*, 27-34.

256. Lehmann, A., Rueppell, A., Schindler, A., Zylla, I. M., Seifert, H. J., Nothdurft, F. et al. (2013). Modification of enamel and dentin surfaces by non- thermal atmospheric plasma. *Plasma Processes and Polymers, 10*(3), 262-270.

257. Ito, Y., Sakai, O., & Tachibana, K. (2010). Study of plasma enhanced chemical vapor deposition of zno films by non-thermal plasma jet at atmospheric pressure. *Thin Solid Films, 518*(13), 3513-3516.

258. Dowling, D. P., O'Neill, F. T., Langlais, S. J., & Law, V. J. (2011). Influence of dc pulsed atmospheric pressure plasma jet processing conditions on polymer activation. *Plasma Processes and Polymers, 8*(8), 718-727.

259.   Kang, S. K., Choi, M. Y., Koo, I. G., Kim, P. Y., Kim, Y., Kim, G. J. et al. (2011). Reactive hydroxyl radical-driven oral bacterial inactivation by radio frequency atmospheric plasma. *Applied Physics Letters, 98*(14), 143702.

260.   Xu, L., Sanders, S. M., Tao, B., Garner, A. L., & Keener, K. M. (2016). *Assessment of efficacy and reactive gas species generation for orange juice decontamination using high voltage atmospheric cold plasma.* Paper presented at the IEEE International Conference on Plasma Science (ICOPS), 2016.

261.   Graves, D. B. (2014). Low temperature plasma biomedicine: A tutorial review. *Physics of Plasmas, 21*(8), 080901.

262.   Kim, J. H., Lee, M. A., Han, G. J., & Cho, B. H. (2014). Plasma in dentistry: A review of basic concepts and applications in dentistry. *Acta Odontologica Scandinavica, 72*(1), 1-12.

263.   Kusano, Y. (2014). Atmospheric pressure plasma processing for polymer adhesion: A review. *The Journal of Adhesion, 90*(9), 755-777.

264.   Penkov, O. V., Khadem, M., Lim, W.-S., & Kim, D.-E. (2015). A review of recent applications of atmospheric pressure plasma jets for materials processing. *Journal of Coatings Technology and Research, 12*(2), 225-235.

265.   Szili, E. J., Oh, J. S., Hong, S. H., Hatta, A., & Short, R. D. (2015). Probing the transport of plasma-generated rons in an agarose target as surrogate for real tissue: Dependency on time, distance and material composition. *Journal of Physics D: Applied Physics, 48*(20), 202001.

266.   Duan, J., Lu, X., & He, G. (2017). On the penetration depth of reactive oxygen and nitrogen species generated by a plasma jet through real biological tissue. *Physics of Plasmas, 24*(7), 073506.

267.   Jiang, J., Tan, Z., Shan, C., Pan, J., Pan, G., Liu, Y. et al. (2016). A new study on the penetration of reactive species in their mass transfer processes in water by increasing the electron energy in plasmas. *Physics of Plasmas, 23*(10), 103503.

268.   Wei, T., & Mark, J. K. (2014). Atmospheric pressure dielectric barrier discharges interacting with liquid covered tissue. *Journal of Physics D: Applied Physics, 47*(16), 165201.

269.   Chen, C., Liu, D. X., Liu, Z. C., Yang, A. J., Chen, H. L., Shama, G. et al. (2014). A model of plasma-biofilm and plasma-tissue interactions at ambient pressure. *Plasma Chemistry and Plasma Processing, 34*(3), 403-441.

270.   Fatin-Rouge, N., Starchev, K., & Buffle, J. (2004). Size effects on diffusion processes within agarose gels. *Biophysical Journal, 86*(5), 2710-2719.

271.   Ziuzina, D., Boehm, D., Patil, S., Cullen, P. J., & Bourke, P. (2015). Cold plasma inactivation of bacterial biofilms and reduction of quorum sensing regulated virulence factors. *PLOS ONE, 10*(9), e0138209.

272.   Delben, J. A., Zago, C. E., Tyhovych, N., Duarte, S., & Vergani, C. E. (2016). Effect of atmospheric-pressure cold plasma on pathogenic oral biofilms and in vitro reconstituted oral epithelium. *PLOS ONE, 11*(5), e0155427.

273.   ALietz, m. M., & Kushner, M. J. (2016). Air plasma treatment of liquid covered tissue: Long timescale chemistry. *Journal of Physics D: Applied Physics, 49*(42), 425204.

274.   Oehmigen, K., Hoder, T., Wilke, C., Brandenburg, R., Hahnel, M., Weltmann, K.-D. et al. (2011). Volume effects of atmospheric-pressure plasma in liquids. *IEEE Transactions on Plasma Science, 39*(11), 2646-2647.

275.   Kramida, A., Ralchenko, Yu., Reader, J. and NIST ASD Team. (2017). NIST atomic spectra database (version 5.5).

276.   Duarte-Gómez, E. E., Graham, D., Budzik, M., Paxson, B., Csonka, L., Morgan, M. et al. (2014). High hydrostatic pressure effects on bacterial bioluminescence. *LWT - Food Science and Technology, 56*(2), 484-493.

277.   Mamane-Gravetz, H., & Linden, K. G. (2005). Relationship between physiochemical properties, aggregation and U.V. Inactivation of isolated indigenous spores in water. *Journal of Applied Microbiology, 98*(2), 351-363.

278.   Orlandini, I., & Riedel, U. (2000). Chemical kinetics of no removal by pulsed corona discharges. *Journal of Physics D: Applied Physics, 33*(19), 2467.

279.   Lukes, P., Locke, B. R., & Brisset, J.-L. (2012). Aqueous-phase chemistry of electrical discharge plasma in water and in gas–liquid environments *Plasma chemistry and catalysis in gases and liquids* (pp. 243-308): Wiley-VCH Verlag GmbH & Co. KGaA.

280.   Vesna, V. K., Biljana, P. D., Milica, J., Goran, M. R., Bratislav, M. O., & Milorad, M. K. (2017). Measurement of reactive species generated by dielectric barrier discharge in direct contact with water in different atmospheres. *Journal of Physics D: Applied Physics, 50*(15), 155205.

281.   Traylor, M. J., Pavlovich, M. J., Karim, S., Hait, P., Sakiyama, Y., Clark, D. S. et al. (2011). Long-term antibacterial efficacy of air plasma-activated water. *Journal of Physics D: Applied Physics, 44*(47), 472001.

282.   Dobrynin, D., Fridman, G., Friedman, G., & Fridman, A. (2009). Physical and biological mechanisms of direct plasma interaction with living tissue. *New Journal of Physics, 11*(11), 115020.

283.   Amsden, B. (1998). Solute diffusion within hydrogels. Mechanisms and models. *Macromolecules, 31*(23), 8382-8395.

284. Liu, D. X., Liu, Z. C., Chen, C., Yang, A. J., Li, D., Rong, M. Z. et al. (2016). Aqueous reactive species induced by a surface air discharge: Heterogeneous mass transfer and liquid chemistry pathways. *6*, 23737.

285. Zhou, R., Zhang, X., Bi, Z., Zong, Z., Niu, J., Song, Y. et al. (2015). Inactivation of escherichia coli cells in aqueous solution by atmospheric-pressure N_2, He, Air, and O_2 microplasmas. *Applied and environmental microbiology, 81*(15), 5257-5265.

286. Yang, A., Wang, X., Rong, M., Liu, D., Iza, F., & Kong, M. G. (2011). 1-d fluid model of atmospheric-pressure rf he+o2 cold plasmas: Parametric study and critical evaluation. *Physics of Plasmas, 18*(11), 113503.

287. Hames, B. D. (1998). *Gel electrophoresis of proteins: A practical approach* (Vol. 197): OUP Oxford.

288. Ingham, D. B., & Pop, I. (1998). *Transport phenomena in porous media*: Elsevier.

289. Kaviany, M. (2012). *Principles of heat transfer in porous media*: Springer Science & Business Media.

290. Smoluchowski, M. V. (1903). Contribution to the theory of electro-osmosis and related phenomena. *Bull Int Acad Sci Cracovie, 3*, 184-199.

291. Zhou, X., & Lee, Y. N. (1992). Aqueous solubility and reaction kinetics of hydroxymethyl hydroperoxide. *The Journal of Physical Chemistry, 96*(1), 265-272.

292. Zhang, J., & Oloman, C. W. (2005). Electro-oxidation of carbonate in aqueous solution on a platinum rotating ring disk electrode. *Journal of Applied Electrochemistry, 35*(10), 945-953.

293. Dobrynin, D., Fridman, G., Friedman, G., & Fridman, A. A. (2012). Deep penetration into tissues of reactive oxygen species generated in floating-electrode dielectric barrier discharge (fe-dbd): An in vitro agarose gel model mimicking an open wound. *Plasma Medicine, 2*(1-3).

294. Gaur, N., Szili, E. J., Oh, J. S., Hong, S. H., Michelmore, A., Graves, D. B. et al. (2015). Combined effect of protein and oxygen on reactive oxygen and nitrogen species in the plasma treatment of tissue. *Applied Physics Letters, 107*(10), 103703.

295. Weltmann, K. D., Polak, M., Masur, K., von Woedtke, T., Winter, J., & Reuter, S. (2012). Plasma processes and plasma sources in medicine. *Contributions to Plasma Physics, 52*(7), 644-654.

296. Emmert, S., Brehmer, F., Hänßle, H., Helmke, A., Mertens, N., Ahmed, R. et al. (2013). Atmospheric pressure plasma in dermatology: Ulcus treatment and much more. *Clinical Plasma Medicine, 1*(1), 24-29.

297. Sadhu, S., Thirumdas, R., Deshmukh, R. R., & Annapure, U. S. (2017). Influence of cold plasma on the enzymatic activity in germinating mung beans (vigna radiate). *LWT - Food Science and Technology, 78*, 97-104.

298. Mitra, A., Li, Y. F., Klämpfl, T. G., Shimizu, T., Jeon, J., Morfill, G. E. et al. (2014). Inactivation of surface-borne microorganisms and increased germination of seed specimen by cold atmospheric plasma. *Food and Bioprocess Technology, 7*(3), 645-653.

299. Attri, P., Kumar, N., Park, J. H., Yadav, D. K., Choi, S., Uhm, H. S. et al. (2015). Influence of reactive species on the modification of biomolecules generated from the soft plasma. *Scientific Reports, 5*, 8221.

300. Winter, T., Bernhardt, J., Winter, J., Mäder, U., Schlüter, R., Weltmann, K.-D. et al. (2013). Common versus noble bacillus subtilis differentially responds to air and argon gas plasma. *PROTEOMICS, 13*(17), 2608-2621.

301. Antoniu, A., Nakajima, T., Kurita, H., & Mizuno, A. (2014). Safety evaluation of nonthermal atmospheric pressure plasma liquid treatment: Single DNA molecule-based method. *Journal of Electrostatics, 72*(3), 210-217.

302. Kalghatgi, S., Fridman, A., Azizkhan-Clifford, J., & Friedman, G. (2012). DNA damage in mammalian cells by non-thermal atmospheric pressure microsecond pulsed dielectric barrier discharge plasma is not mediated by ozone. *Plasma Processes and Polymers, 9*(7), 726-732.

303. Schmidt, A., Wende, K., Bekeschus, S., Bundscherer, L., Barton, A., Ottmüller, K. et al. (2013). Non-thermal plasma treatment is associated with changes in transcriptome of human epithelial skin cells. *Free Radical Research, 47*(8), 577-592.

304. Kalghatgi, S., Friedman, G., Fridman, A., & Clyne, A. M. (2010). Endothelial cell proliferation is enhanced by low dose non-thermal plasma through fibroblast growth factor-2 release. *Annals of Biomedical Engineering, 38*(3), 748-757.

305. Vandamme, M., Robert, E., Lerondel, S., Sarron, V., Ries, D., Dozias, S. et al. (2012). Ros implication in a new antitumor strategy based on non-thermal plasma. *International Journal of Cancer, 130*(9), 2185-2194.

306. Lackmann, J. W., Schneider, S., Edengeiser, E., Jarzina, F., Brinckmann, S., Steinborn, E. et al. (2013). Photons and particles emitted from cold atmospheric-pressure plasma inactivate bacteria and biomolecules independently and synergistically. *Journal of the Royal Society Interface, 10*(89).

307. Bußler, S., Ehlbeck, J., & Schlüter, O. K. (2017). Pre-drying treatment of plant related tissues using plasma processed air: Impact on enzyme activity and quality attributes of cut apple and potato. *Innovative Food Science & Emerging Technologies, 40*, 78-86.

308. Lackmann, J.-W., Schneider, S., Edengeiser, E., Jarzina, F., Brinckmann, S., Steinborn, E. et al. (2013). Photons and particles emitted from cold atmospheric-pressure plasma inactivate bacteria and biomolecules independently and synergistically. *Journal of the Royal Society Interface, 10*(89), 20130591.

309. Elmoualij, B., Thellin, O., Gofflot, S., Heinen, E., Levif, P., Séguin, J. et al. (2012). Decontamination of prions by the flowing afterglow of a reduced-pressure n2☐o2 cold-plasma. *Plasma Processes and Polymers, 9*(6), 612-618.

310. Digel, I., Artmann, A. T., Nishikawa, K., Cook, M., Kurulgan, E., & Artmann, G. M. (2005). Bactericidal effects of plasma-generated cluster ions. *Medical and Biological Engineering and Computing, 43*(6), 800-807.

311. Segat, A., Misra, N. N., Cullen, P. J., & Innocente, N. (2016). Effect of atmospheric pressure cold plasma (acp) on activity and structure of alkaline phosphatase. *Food and Bioproducts Processing, 98*, 181-188.

312. Motrescu, I., Ogino, A., Tanaka, S., Fujiwara, T., Kodani, S., Kawagishi, H. et al. (2011). Mechanism of peptide modification by low-temperature microwave plasma. *Soft Matter, 7*(10), 4845-4850.

313. Motrescu, I., Ogino, A., Tanaka, S., Fujiwara, T., Kodani, S., Kawagishi, H. et al. (2010). Modification of peptide by surface-wave plasma processing. *Thin Solid Films, 518*(13), 3585-3589.

314. Della Porta, V., Bramanti, E., Campanella, B., Tine, M. R., & Duce, C. (2016). Conformational analysis of bovine serum albumin adsorbed on halloysite nanotubes and kaolinite: A fourier transform infrared spectroscopy study. *RSC Advances, 6*(76), 72386-72398.

315. Povey, M. J., Moore, J. D., Braybrook, J., Simons, H., Belchamber, R., Raganathan, M. et al. (2011). Investigation of bovine serum albumin denaturation using ultrasonic spectroscopy. *Food Hydrocolloids, 25*(5), 1233-1241.

316. Gülseren, İ., Güzey, D., Bruce, B. D., & Weiss, J. (2007). Structural and functional changes in ultrasonicated bovine serum albumin solutions. *Ultrasonics Sonochemistry, 14*(2), 173-183.

317. Waterborg, J. H., & Matthews, H. R. (1994). The lowry method for protein quantitation. In J. M. Walker (Ed.), *Basic protein and peptide protocols* (pp. 1-4). Totowa, NJ: Humana Press.

318. Eren, N. M., Narsimhan, G., & Campanella, O. H. (2016). Protein adsorption induced bridging flocculation: The dominant entropic pathway for nano-bio complexation. *Nanoscale, 8*(6), 3326-3336.

319. Desam, G. P., Li, J., Chen, G., Campanella, O., & Narsimhan, G. (2018). A mechanistic model for swelling kinetics of waxy maize starch suspension. *Journal of Food Engineering, 222*(Supplement C), 237-249.

320. Güler, G., Vorob'ev, M. M., Vogel, V., & Mäntele, W. (2016). Proteolytically-induced changes of secondary structural protein conformation of bovine serum albumin monitored by fourier transform infrared (FT-IR) and UV-circular dichroism spectroscopy. *Spectrochimica Acta Part A: Molecular and Biomolecular Spectroscopy, 161*, 8-18.

321. Chang, C. T., Wu, C. S. C., & Yang, J. T. (1978). Circular dichroic analysis of protein conformation: Inclusion of the β-turns. *Analytical Biochemistry, 91*(1), 13-31.

322. Laemmli, U. K. (1970). Cleavage of structural proteins during the assembly of the head of bacteriophage t4. *Nature, 227*, 680.

323. Koyama, S., Ishizawa, H., Miyauchi, Y., & Dozono, T. (2012). Introduction of non-invasive measurement method by infrared application *Infrared spectroscopy-life and biomedical sciences*: InTech.

324. Wang, C. H., Huang, C. C., Lin, L. L., & Chen, W. (2016). The effect of disulfide bonds on protein folding, unfolding, and misfolding investigated by ft–raman spectroscopy. *Journal of Raman Spectroscopy, 47*(8), 940-947.

325. Nakamura, K., Era, S., Ozaki, Y., Sogami, M., Hayashi, T., & Murakami, M. (1997). Conformational changes in seventeen cystine disulfide bridges of bovine serum albumin proved by raman spectroscopy. *FEBS Letters, 417*(3), 375-378.

326. Ellman, G. L. (1959). Tissue sulfhydryl groups. *Archives of Biochemistry and Biophysics, 82*(1), 70-77.

327. Thannhauser, T. W., Konishi, Y., & Scheraga, H. A. (1984). Sensitive quantitative analysis of disulfide bonds in polypeptides and proteins. *Analytical Biochemistry, 138*(1), 181-188.

328. Damodaran, S. (1985). Estimation of disulfide bonds using 2-nitro-5-thiosulfobenzoic acid: Limitations. *Analytical Biochemistry, 145*(1), 200-204.

329. Hall, F. G., Jones, O. G., O'Haire, M. E., & Liceaga, A. M. (2017). Functional properties of tropical banded cricket (gryllodes sigillatus) protein hydrolysates. *Food Chemistry, 224*, 414-422.

330. Ledesma-Osuna, A. I., Ramos-Clamont, G., & Vázquez-Moreno, L. (2008). Characterization of bovine serum albumin glycated with glucose, galactose and lactose. *Acta Biochim Pol, 55*(3), 491-497.

331. Guedes, S., Vitorino, R., Domingues, R., Amado, F., & Domingues, P. (2009). Oxidation of bovine serum albumin: Identification of oxidation products and structural modifications. *Rapid Communications in Mass Spectrometry, 23*(15), 2307-2315.

332. Hänsch, M. A., Mann, M., Weltmann, K. D., & von Woedtke, T. (2015). Analysis of antibacterial efficacy of plasma-treated sodium chloride solutions. *Journal of Physics D: Applied Physics, 48*(45), 454001.

333. Lee, M. S., & Ji, Q. C. (2017). *Protein analysis using mass spectrometry : Accelerating protein biotherapeutics from lab to patient*: Hoboken, New Jersey : Wiley.

334. Ikeda, S., & Morris, V. J. (2002). Fine-stranded and particulate aggregates of heat-denatured whey proteins visualized by atomic force microscopy. *Biomacromolecules, 3*(2), 382-389.

335. Fersht, A. (1999). *Structure and mechanism in protein science: A guide to enzyme catalysis and protein folding*: Macmillan.

336. Terpiłowski, K., Tomczyńska-Mleko, M., Nishinari, K., & Mleko, S. (2017). Surface properties of ion-inducted whey protein gels deposited on cold plasma treated support. *Food Hydrocolloids, 71*, 17-25.

337. Mudunkotuwa, I. A., Al Minshid, A., & Grassian, V. H. (2014). Atr-ftir spectroscopy as a tool to probe surface adsorption on nanoparticles at the liquid–solid interface in environmentally and biologically relevant media. *Analyst, 139*(5), 870-881.

338. Belfer, S., Fainchtain, R., Purinson, Y., & Kedem, O. (2000). Surface characterization by ftir-atr spectroscopy of polyethersulfone membranes-unmodified, modified and protein fouled. *Journal of Membrane Science, 172*(1), 113-124.

339. Bandekarc, J., Sethna, R., & Kirschner, M. (1995). Quantitative determination of sulfur oxide species in white liquor by FT-IR. *Applied Spectroscopy, 49*(11), 1577-1582.

340. Wang, S., Taraballi, F., Tan, L. P., & Ng, K. W. (2012). Human keratin hydrogels support fibroblast attachment and proliferation in vitro. *Cell and Tissue Research, 347*(3), 795-802.

341. Turell, L., Carballal, S., Botti, H., Radi, R., & Alvarez, B. (2009). Oxidation of the albumin thiol to sulfenic acid and its implications in the intravascular compartment. *Brazilian Journal of Medical and Biological Research, 42*, 305-311.

342. Carballal, S., Radi, R., Kirk, M. C., Barnes, S., Freeman, B. A., & Alvarez, B. (2003). Sulfenic acid formation in human serum albumin by hydrogen peroxide and peroxynitrite. *Biochemistry, 42*(33), 9906-9914.

343. Attri, P., Kim, M., Choi, E. H., Cho, A. E., Koga, K., & Shiratani, M. (2017). Impact of an ionic liquid on protein thermodynamics in the presence of cold atmospheric plasma and gamma rays. *Physical Chemistry Chemical Physics, 19*(37), 25277-25288.

344. Takai, E., Kitamura, T., Kuwabara, J., Ikawa, S., Yoshizawa, S., Shiraki, K. et al. (2014). Chemical modification of amino acids by atmospheric-pressure cold plasma in aqueous solution. *Journal of Physics D: Applied Physics, 47*(28), 285403.

345. van Bergen, L. A., Roos, G., & De Proft, F. (2014). From thiol to sulfonic acid: Modeling the oxidation pathway of protein thiols by hydrogen peroxide. *The Journal of Physical Chemistry A, 118*(31), 6078-6084.

346. Davies, Michael J. (2016). Protein oxidation and peroxidation. *Biochemical Journal, 473*(Pt 7), 805-825.

347. Kylián, O., Rauscher, H., Gilliland, D., Brétagnol, F., & Rossi, F. (2008). Removal of model proteins by means of low-pressure inductively coupled plasma discharge. *Journal of Physics D: Applied Physics, 41*(9), 095201.

348. Terefe, N. S., Buckow, R., & Versteeg, C. (2014). Quality-related enzymes in fruit and vegetable products: Effects of novel food processing technologies, part 1: High-pressure processing. *Critical Reviews in Food Science and Nutrition, 54*(1), 24-63.

VITA

LEI SHELLY XU
(608)556-8813
shelly.xulei1@gmail.com

SUMMARY

'Making healthy food, feeding a happy world'. Innovative and result oriented food science professional, with R&D experiences at Dairy Farmers of America, *Nestlé, Wisconsin Dairy Research Center, Purdue,* on projects including protein modification/purification/characterization, aseptic processing, sensory evaluation, offering teamwork and critical thinking skills in product formulation, quality analysis and process control.

EDUCATION

Ph.D. Food Science, **Purdue University, Indiana, USA**
Major advisor: Dr. Bernard Tao (Indiana Soybean Board, Endowed Chair)   *Expected Mar. 2018*

M.S. Food Science, **University of Wisconsin-Madison, Wisconsin, USA**   *2012 - 2015*
Major advisor: Dr. John Lucey (Director of Wisconsin Dairy Research Center)

B.S. Food Engineering, **Shandong Agriculture University, China**   *2008 - 2012*

B.A. International Business Management, **Royal Agriculture University, UK**   *2009 - 2012*

INTERNSHIP AND RESEARCH EXPERIENCE

Food Scientist, **Dairy Farmers of America,** Springfield, Missouri   *Apr.- Present*
- Product formulation from ideation to commercialization as well as modification for ready-to-drink (shelf stable), retort processed products based on customer requirements
- Effectively work with cross-functional teams and customers
- Lead and manage projects, ensuring agreed upon timelines are consistently met and maintaining proper documentation of product formulations and specifications

Product Developer Intern, **Nestlé Product Technology Center,** Marysville, Ohio   *Jun.- Dec.2016*
- Worked as Product Development Intern at Nestlé to help design & develop a new formula prototype
- Designed **high protein concentrate** using various proteins and evaluated its quality
- Trained to understand PD Stage Gate process from *Ideation* to *Commercialization*
- Systematically trained on formula modification and aseptic processing control (mid & pilot plant scale)

Graduate Research Assistant, **Purdue University**   *Aug. 2015 - present*
"Nonthermal Processing and Packaging Using Atmospheric Cold Plasma (ACP) in Food System"
- Investigated microbial inactivation and quality alteration of ACP treatment on milk, orange juice, apple sauce
- Studied the mechanism of plasma treatment on protein structural and functional modification
- *Best Paper Award* at IFT, Poster Competition in Nonthermal Processing Tech. Division   *Jul. 2016*
- *1st Place Award* at Agriculture and Biological Engineering Industrial Symposium, Purdue   *Feb. 2017*

Course PD Projects:
- "Egg Free Angle Cake", Roquette, Chicago   *Jan.-May 2016*
- "High Protein Kefir", University of Wisconsin Madison   *Sep.-Dec. 2014*
- "Soy Protein Cheese", Shandong Agricultural University   *Sep.-Aug. 2011*

Graduate Research Assistant, **University of Wisconsin-Madison**
Wisconsin Dairy Research Center   *Sep. 2012 - Jun. 2015*
Project 1: "Access Digestion and Immunogenicity Function of Milk Proteins" -funded by USDA
- Studied "Impact of Maillard Modification on Reducing Immunogenicity of When Protein Isolate"
Project 2 "Inhibition of Ice Crystal Growth in Frozen Food (ice cream) Mix by Gelatin Hydrolysate"
- Purified and characterized antifreeze protein using chromatography (HPLC, MS, SDS-PAGE) analysis

Research Assistant, **National Key Lab in Shandong Agriculture University, China** *Sep. 2009 - May 2010*

Assistant Quality Control Technician in Tsingtao Brewery CO.,LTD., China   *May - Sep. 2009*

Dairy Product Evaluation Competition Team, **Wisconsin Dairy Research Center**   *Sep. 2014 - May 2015*

Teaching Assistant, **University of Wisconsin-Madison,**   *Sep. – Dec. 2013*
- FS: Advanced Food Processing and Manufacturing

Teaching Assistant, **Purdue University**   *Sep. 2015 - May 2016*
- FS: Food Microbiology, Food Analysis

LEADERSHIP AND VOLUNTEERING EXPERIENCE

Student Representative-Institute of Food Technologists (IFT) — *Nov. 2016- Present*

Student Committee Chair-Chinese American Food Society — *Oct. 2016- Present*

Secretary, Purdue Food Science Graduate Student Association — *2016-2017*

Product Development Competition Team, University of Wisconsin-Madison — *Sep. – Dec. 2014*
- Served as team leader to use technical knowledge to develop an innovative product for IFT product development competition

Social Chair of Food Science Club, University of Wisconsin-Madison — *Sep. 2013 - May 2014*
- Led and assisted food science club in holding social events: Valentine's Day chocolate dipping social, the Halloween pumpkin Iron Chef Competition, other celebrations and daily schedules

PRESENTATIONS AND PUBLICATION (Selected)

- *Lei Xu*, Yiwen Bao, Chumin Zhang, Hu Hou, Ximena Yepez, Brian Farkas, Kevin M. Keener, Allen L. Garner, and Bernard Tao, 2018. "Physicochemical, Structural Characteristic and Modification Mechanism of High Voltage Atmospheric Cold Plasma on Bovine Serum Albumin", 2018 Institute of Food Technologists Conference, 15th. July 2018, Chicago, IL USA
- *Lei Xu*, Y. Gong, James E. Gern, Shinya Ikeda, and John Lucey, 2018. "Glycation of Whey Protein With Dextrans of Different Molar Mass: Impact on IgE Binding Capacity with Blood Sera Obtained from Patients with Cow's Milk Protein Allergy", Journal of Dairy Science, In press.
- *Lei Xu*, A. L. Garner, B. Tao, and K. M. Keener, 2017. "Microbial Inactivation and Quality Changes in Orange Juice Treated by High Voltage Atmospheric Cold Plasma", Food and Bioprocess Technology, pp.1-14.
- *Lei Xu*, V. Borja, A. L. Garner, B. Tao, B. Applegate, K. M. Keener, "Microbial Inactivation and Diffusion Mechanism In Semi-solid Foods Treated with High Voltage Atmospheric Cold Plasma", 2017 Institute of Food Technologists Conference, Poster, 27 June 2017, Las Vegas, NV USA.
- *Lei Xu*, N. Mahot, A. L. Garner, B. Tao, and K. M. Keener, "The Effect of High Voltage Atmospheric Cold Plasma on the Microbial, Physical, and Chemical Properties of Orange Juice," 2016 Institute of Food Technologists Conference, Poster 102, 17 July 2016, Chicago, IL USA. *[2nd Place Poster Competition]*
- *Lei Xu*, A. L. Garner, B. Tao, K. M. Keener, and A. L. Garner, " Microbial Inactivation and Quality Retention in Orange Juice Treated by High Voltage Atmospheric Cold Plasma," 2017 Agriculture and Biological Engineering Industrial Symposium, Purdue University, West Lafayette IN *[1st Place Poster Competition]*
- *Lei Xu*, S. M. Sanders, B. Tao, K. M. Keener, and A. L. Garner, "Assessment of Efficacy and Reactive Gas Species Generation for Orange Juice Decontamination using High Voltage Atmospheric Cold Plasma," 2016 IEEE International Conference on Plasma Sciences, June 2016, Banff, Alberta, Canada.
- *Lei Xu*, Y.S. Gong, J.A. Lucey. "Production and Purification of Whey Protein Glycate Conjugated with Low Molecular Mass Dextrans". Oral presentation, American Dairy Science Association. July 2014, *Kansas City, MI*
- *Lei Xu*, Y.S. Gong, J.A. Lucey. "Impact of Maillard Modification on Reducing Immunogenicity of When Protein Isolate". Oral presentation, American Dairy Science Association. July 2015, *Orlando, FL*
- Q. Sun, L. Zhang, Z. Xu, *Lei Xu*, and J. Zhou. "The Recent Advance of Molecular Imprinted Online Solid Phase Extraction and Its Application in Sample Pretreatment-A Mini Review", Advanced Materials ICAMMP 2011, pp. 1799-1805, Dec. 2011

CERTIFICATIONS

Better Process Control School (Grocery Manufacturers Associations), Purdue University	*May. 2016*
Aseptic Processing Technology Workshop, Purdue University	*Jan. 2016*
HACCP (International HACCP Alliance), Chicago	*Mar. 2015*
Whistler Center for Carbohydrate Research Short Course, Purdue University	*Oct. 2017*

HONORS & AWARDS

Dairy Products Evaluation Competition: *[1st Place]* Team Award in Cheddar Cheese & *[3rd place]* Team Award in Ice Cream at Dairy Product Evaluation Competition, Chicago, IL — *Dec. 2014*

Professional Membership: IFT, ADSA, Phi Tau Sigma-Hoosier Chapter, CAFS — *2012-present*

PUBLICATIONS AND PRESENTATIONS

Lei Xu, Yiwen Bao, Chumin Zhang, Hu Hou, Ximena Yepez, Brian Farkas, Kevin M. Keener, Allen L. Garner, and Bernard Tao, 2018. "Physicochemical, Structural Characteristic and Modification Mechanism of High Voltage Atmospheric Cold Plasma on Bovine Serum Albumin", 2018 Institute of Food Technologists Conference, 15th. July 2018, Chicago, IL USA

Lei Xu, A. L. Garner, B. Tao, and K. M. Keener, 2017. "Microbial Inactivation and Quality Changes in Orange Juice Treated by High Voltage Atmospheric Cold Plasma", *Food and Bioprocess Technology*, pp.1-14.

Lei Xu, V. Borja, A. L. Garner, B. Tao, B. Applegate, K. M. Keener, "Microbial Inactivation and Diffusion Mechanism In Semi-solid Foods Treated with High Voltage Atmospheric Cold Plasma", 2017 Institute of Food Technologists Conference, Poster, 27 June 2017, Las Vegas, NV USA.

Lei Xu, N. Mahot, A. L. Garner, B. Tao, and K. M. Keener, "The Effect of High Voltage Atmospheric Cold Plasma on the Microbial, Physical, and Chemical Properties of Orange Juice", 2016 Institute of Food Technologists Conference, Poster 102, 17 July 2016, Chicago, IL USA. *[2nd Place Poster Competition]*

Lei Xu, S. M. Sanders, B. Tao, K. M. Keener, and A. L. Garner, "Assessment of Efficacy and Reactive Gas Species Generation for Orange Juice Decontamination using High Voltage Atmospheric Cold Plasma", 2016 IEEE International Conference on Plasma Sciences, June 2016, Banff, Alberta, Canada.